Semi-Transparent Photovoltaic Technology Integration in Smart Buildings

Haytham Osama Musameh

A thesis submitted in partial fulfilment of the requirements of

Sheffield Hallam University for the degree of Doctor of Philosophy

October 2023

CANDIDATE DECLARATION

I hereby declare that:

1. I have not been enrolled for another award of the University or other academic or professional organisation whilst undertaking my research degree.

2. None of the material in the thesis has been used in any other submission for an academic award.

3. I am aware of and understand the University's policy on plagiarism and certify that this thesis is my own work. The use of all published or other sources of material consulted have been properly and fully acknowledged.

4. The work undertaken towards the thesis has been conducted in accordance with the SHU Principles of Integrity in Research and the SHU Research Ethics Policy.

5. The word count of the thesis is 24,000.

Name	Haytham Osama Musameh
Date	October 2023
Award	PhD
Research Institute	Industry & Innovation
Director(s) of Studies	Dr. Walid Issa and Dr. Faris Al-Naemi

Abstract

Research conducted over the years has established that the building industry is responsible for a significant portion of the world's energy consumption, accounting for about 30% of the total electricity used. Most of this power usage is directed towards regulating the temperature of buildings, with the primary cause being the glazing systems employed in construction.

The main aim of this undertaking is to carry out a thorough analysis of the Cadmium Telluride (CdTe) Solar Cells Semi-Transparent Photovoltaic (STPV) glazing systems. This research implemented experimental testing procedures and numerical models to evaluate the system's optical, thermal, and electrical performance to accomplish this. To perform this analysis, small samples of commercially available thin-film modules that contain CdTe solar cells were utilised for indoor testing. The primary objective of this testing is to quantify the relevant optical, thermal, and electrical parameters that affect the system's performance.

This work includes a thorough literature review, which investigates the work that has been done by other researchers and is divided into two main sections. The first section covers the research done on silicon-based solar cells STPV glazing systems. The second section covers the research that has been done on STPV glazing systems with integrated CdTe solar cells.

The literature review chapter was followed by a characteristics process that quantifies the optical, thermal, and electrical attributes. This approach was based on a set of experimental tests, these experiments were developed to be carried out in a controlled lab setting and implemented on six different CdTe STPV glazing samples, as well as two clear double-glazing samples and a clear single-glazing sample. To carry out these tests, a scaled-down testbed was built based on Guarded Hot Box and Mobile Window Thermal Test, in addition to the utilising of a heat flux sensor and thermostats that measure the temperatures on both sides of the glazing surfaces, this kit was used to calculate the Heat Transfer Coefficient (U-value). As for the Solar Heat Gain Coefficient (SHGC) and optical characteristics a spectrometer was used.

A solar simulator was developed, to carry out the electrical characterisation tests. To achieve constant solar irradiance (1000 W/m^2) while maintaining a similar movement, the developed solar simulator was split into two components. First, the sun simulator, which is the stationary part, consists of nine halogen lamps bolted into a frame and the illuminations of these lamps are controlled by a transformer. The second part is the movement simulator, which is a flat plate that moves in two axes. The movement is powered by two DC motors, an Electrical linear actuator that moves vertically, helped by a spherical ball joint installed below the flat plate, and a Geared DC motor which operates in an angular manner. A control unit operated by the data logger has been installed. This unit contains two DC-Motor Drivers with an internal DC power supply and multiple potentiometers to control the speed of both motors in case the unit is operated manually.

These outcomes were later used in building the required simulation profiles to evaluate the overall energy consumption of the buildings when utilising semi-transparent photovoltaic glazing systems. The overall energy assessment will be conducted in two stages, the first stage was conducted through a numerical model developed by the EnergyPlus software tool embedded within

Designbuilder software. In the second stage, a load flow analysis on a grid level was carried out employing PowerFactory (DIgSILENT) software.

The evaluation process has indicated that utilising Argon filled double-glazing system would be the most efficient glazing system from the overall energy consumption point of view. As the Argon-filled double-glazing system has an overall energy consumption of 6477.34 kW, 6590.8 kW, and 8521.04 kW when covering 30%, 60%, and 100% of the wall area respectively. This result is caused by the fact that the heating load is the dominant load in the location of the simulation.

Published Work

- MUSAMEH, Haytham, AL-NAEMI, Faris, ISSA, Walid, and ALRASHIDI, Hameed (2023). The thermal and optical characterization of semi-transparent photovoltaics samples for buildings energy evaluations. In: *2023 58th International Universities Power Engineering Conference (UPEC).* IEEE.
- MUSAMEH, Haytham, ALRASHIDI, Hameed, AL-NEAMI, Faris and ISSA, Walid (2022). Energy performance analytical review of semi-transparent photovoltaics glazing in the United Kingdom. Journal of Building Engineering: 104686.

Acknowledgment

Looking back at my research journey, I am pleased to recognise that I had the privilege to interact and collaborate with insightful and outstanding individuals. This work could not have been completed without them, so I would like to take this chance to express my gratitude to them.

First, I would like to express my absolute gratitude to my supervisory team, Dr Walid Issa and Dr Faris Al-Naemi, for their continued guidance and supervision of this work. They have been supportive and encouraged me to think more outside the box. Furthermore, their patience and support have carried me till the end of this work.

Secondly, my sincere gratitude is also extended to the technical team at Sheffield Hallam University and especially to Ken Duty, whose expertise and experience have helped me build the testing set that made this work possible.

Finally, I would like to thank my parents for their continued support and belief in me even when I didn’t believe in myself.

Table of Contents

Table of Figures:

Table of Tables:

Abbreviation:

a-Si	Amorphous Silicon Solar Cells
BAPV	Building Adaptive Photovoltaic
BIPV	Building Integrating Photovoltaic
CCT	Colour Rendering Index
CdTe	Cadmium Telluride Solar Cells
CNN	Custom Neural Network
CRI	Correlated Colour Temperature
c-Si	Crystallin Silicon Solar Cells
DC	Direct Current
DG	Double Glazing
DSF	Double-Skin Façade
DSSC	Dye-Sensitised Solar Cells
FF	Fill Factor
GDP	Gross Domestic Product
HISG	Heat Insulation Solar Glass
HVAC	Heating, Ventilation, and Air Conditioning
IGU	Insulation Glazing Unit
MoWiTT	Mobile Window Thermal Test
MPP	Maximum Power Point
PCM	Phase-Changing Materials
p-Si	Poly-Crystallin Silicon Solar Cells
PV	Photovoltaics
PV-TEC	Photovoltaics-Thermoelectric
SG	Single Glazing
SHGC	Solar Heat Gain Coefficient

SPTV	Semi-Transparent Photovoltaic
STC	Standard Testing Conditions
UDI	Useful Daylight Illuminance
U-Value	Heat Transfer Coefficient
VLT	Visible Light Transmittance
WWR	Window-to-Wall Ratio

Mathematical Symbols:

$\boldsymbol{\eta}$	Electrical Efficiency
$\boldsymbol{Pout}$	Output Electrical Power
$\boldsymbol{Pin}$	Input Electrical Power
$\boldsymbol{P_{max}}$	Maximum Electrical Power
$\boldsymbol{V_{max}}$	Maximum Voltage
$\boldsymbol{I_{max}}$	Maximum Current
$\boldsymbol{V_{OC}}$	Open Circuit Voltage
$\boldsymbol{I_{SC}}$	Short Circuit Current
$\boldsymbol{I_D}$	The Diode Current
$\boldsymbol{I_o}$	The Diode Current at Saturation
$\boldsymbol{q}$	The Electron's Charge
$\boldsymbol{a}$	The Ideality Factor of The Diode
$\boldsymbol{k}$	The Boltzmann's Constant
$\boldsymbol{R_s}$	Series Resistance
$\boldsymbol{R_{sh}}$	Parallel Resistance
$\boldsymbol{\rho}$	The Reflected Solar Irradiance
$\boldsymbol{\tau}$	The Transmitted Solar Irradiance
$\boldsymbol{\alpha}$	The Absorbed Solar Irradiance
$\boldsymbol{\lambda}$	The Spectrum of The Solar Irradiance
$\boldsymbol{\theta}$	The Incident Angle of The Solar Irradiance
$\boldsymbol{N}$	The Inward-Flowing Fraction of The Absorbed Radiation
$\boldsymbol{h_e}$	The External Heat Transfer
$\boldsymbol{Q}$	The Heat Flux
$\boldsymbol{\Delta T}$	The Temperature Difference Between the Inner and The Outer Surface of The Glazing System

CHAPTER 1
INTRODUCTION

1. Introduction

1.1. Motivation

As the population of humankind increases, the demand for energy sources in general and electrical ones in specific increases, where most of this demand is diverted towards the building sector. The buildings sector contributes significantly to the global economy, estimated at around 20% of the total worldwide Gross Domestic Product (GDP). On the contrary, this sector [1] brings several challenges related to energy supply and resources, the environment, and the climate crisis. As a result, the movement to understand how to reduce energy consumption levels and utilise renewable energy resources has gained momentum. Many studies have indicated that the building sector consumes around 30% of the generated electricity globally. Most of the consumption is concentrated on satisfying the heating and cooling demands of the buildings. This consumption is caused mainly by the glazing systems, i.e., in the United States, around 61% of the energy consumed in commercial buildings is directed toward fulfilling heating and cooling demands. These demands are caused by the glazing systems. In 2010, more than 40% of the energy that has been generated in the United States was consumed by the building sector, and again, around half of that energy was aimed at satisfying the heating and cooling demands [2]-[5].

Establishing effective policies to tackle these problems could not occur without analysing the energy consumption sources and causes. Many researchers have identified the glazing systems as an area that could be improved since glazing systems play a crucial role in the heat transfer process that goes through the building structure and their fundamental impact on the thermal performance of any building [5], [6].

1.2. Research Background

A keen interest in photovoltaic technologies has been growing driven by the flexibility that this technology possesses; this flexibility is shown in the ability to be utilised inside the cities and the urban areas or by the method of installation, whether that was as an added feature on the roofs of the buildings or as a part of the building structure, especially after the advancement that has been achieved in the field of the used materials that the photovoltaic technologies are built from, which is represented by the innovation of the thin film technologies and their ability to be integrated into the glazing systems [7]-[10].

As stated above, glazing systems enormously affect overall energy consumption, and conventional glazing systems tend to be poor insulation tools. Therefore, integrating solar cells into the glazing systems is a possible solution to improve the overall energy consumption of the whole building. However, although the benefits of integrating solar cells into the glazing systems or using semi-transparent photovoltaic (STPV) glazing systems extend beyond the ability to generate electricity and improve the thermal performance of the building but before utilising this technology, multiple factors need to be taken into consideration such as the climate profile of the building location and the shading that is generated from the surrounding buildings [11]-[17].

Employing STPV glazing systems requires deep analysis to conclude the optimal design that will be implemented into the building. Furthermore, due to the existence of solar cells, the amount of solar radiation that enters the building is limited or at least less than the conventional glazing systems, resulting in a reduction in the natural daylight and the outdoor view and leading to an effect on the lighting demand and the thermal performance inside the building [17], [18].

Finally, utilising such technology requires an in-depth analysis to highlight the thermal, electrical, and optical characterisation and impact to reach an optimal case study that can be transferred to a real-world application. This knowledge will allow the PV and glazing industries to provide the necessary database to design high-performance STPV systems.

1.3. Research Aim and Objectives

This work aims to implement an in-depth analysis while developing an experimental testing procedure and numerical models to characterise the optical, thermal, and electrical performance of the CdTe STPV glazing systems. Small samples of unique CdTe solar cells commercially available thin-film modules are used for indoor testing to quantify the relevant optical, thermal, and electrical parameters affecting their performance.

Until now, there has been considerable research on the thermal and electrical performance of STPV glazing systems. However, the individual study cannot provide optimal integration since their thermal, electrical, and daylighting performance influence each other. Furthermore, in this research, more attention is focused on the overall energy performance of STPV glazing through monitoring actual integrated prototypes. The concentration of the current work lies in establishing a clear comparison of different STPV technologies and conventional double-glazing systems under the exact boundaries and conditions. The energy performance of STPV glazing systems is related to many variables, and comparative studies indicate which STPV technology performs better and investigate their applicability in heat-dominating load climate locations like the United Kingdom.

Annual energy-saving potential deriving from the building integration of the STPV systems will be investigated through dynamic modeling. It is evident that non-validated models or assuming physical properties have been used in many studies in the field. In addition, this work also aims to develop and validate appropriate models (thermal, electrical) that will be used to investigate the effect of the STPV and critical design parameters (WWR, transparency, etc.) on the annual energy demand of a reference building. A variety of selection criteria are taken into consideration to propose the optimal integration of each STPV technology. In this way, this research will serve as a guide for the optimal integration of STPV technologies to provide maximum energy efficiency according to the characteristics and the use of the building itself. The methodology should be easily extended to other emerging PV technologies and building typologies to provide a new strategy for energy-efficient building design.

1.4. Research Questions

This research intends to address through experimental and simulation work the following issues:

- ❖ Preparation of several semi-transparent STPV glazing systems using a CdTe thin-film module and a suitable experimental test procedure to determine their thermal, optical, and electrical performance.
- ❖ The impact of various glazing parameters (optical, thermal) combined with STPV technology on the temperature profile and solar energy yield performance of the STPV windows.
- ❖ Development of a numerical simulation model to determine the impact of such technologies on the building energy performance and the grid as a whole.

1.5. Contribution to Knowledge

This research's contribution to knowledge could be summarised as follows:

- Further research and analysis of the possible impact that CdTe semi-transparent photovoltaics glazing systems would have if integrated within the building structure.
- Introducing a lab-based approach to assess the electrical, thermal, and optical characteristics of semi-transparent photovoltaic materials. Comparing results with single-glazing, clear double-glazing, and Argon-filled double-glazing samples.
- The overall energy assessment of the CdTe semi-transparent photovoltaics glazing systems at a location where the heating load is the biggest need to be addressed. This energy assessment was carried out on two different scale building settings, and different Window to Wall Ratios (WWRs) case studies.
- Investigating the impact of integrating semi-transparent photovoltaic glazing on the load flow and the stability of the whole electrical system.

1.6. Research Approach

The research approach can be divided into three main phases, as shown in Figure 1.1. These phases are the characterisation phase, simulation profiles building, and finally, the simulation phase. The characterisation phase was based on experiments utilising different measurement equipment to find the thermal, optical, and electrical properties of the existing CdTe STPV samples. Experimental tests and setups used by previous studies were reviewed to select the one that best fits the aim and objectives of the research, and as a result, a testbed has been constructed as an indoor test enclosure, and the results from different experimental tests were used to build the simulations profiles. As for the simulation's profiles phase, the required measurement equipment was identified and calibrated for precise data collection. The collected data from this set of equipment included solar irradiance, STPV glazing samples' generated power, and the Peltier units' power. The collected data were used to evaluate the thermal and energy performance of CdTe thin film-based semi-transparent photovoltaic glazing. STPV glazing performance was compared to conventional double and single glazing for a better physical interpretation of the results. The thermal performance was assessed by calculating the glazing under study's overall heat transfer coefficient (U-value) and solar heat gain coefficient (SHGC). The simulation phase aims to provide an overall energy assessment. This phase can be split into two parts. The first is an overall energy performance on a building level through a numerical model developed by the EnergyPlus software tool embedded within

Designbuilder software. In the second part of this phase, a load flow analysis on a grid level was carried out employing PowerFactory (DIgSILENT) software.

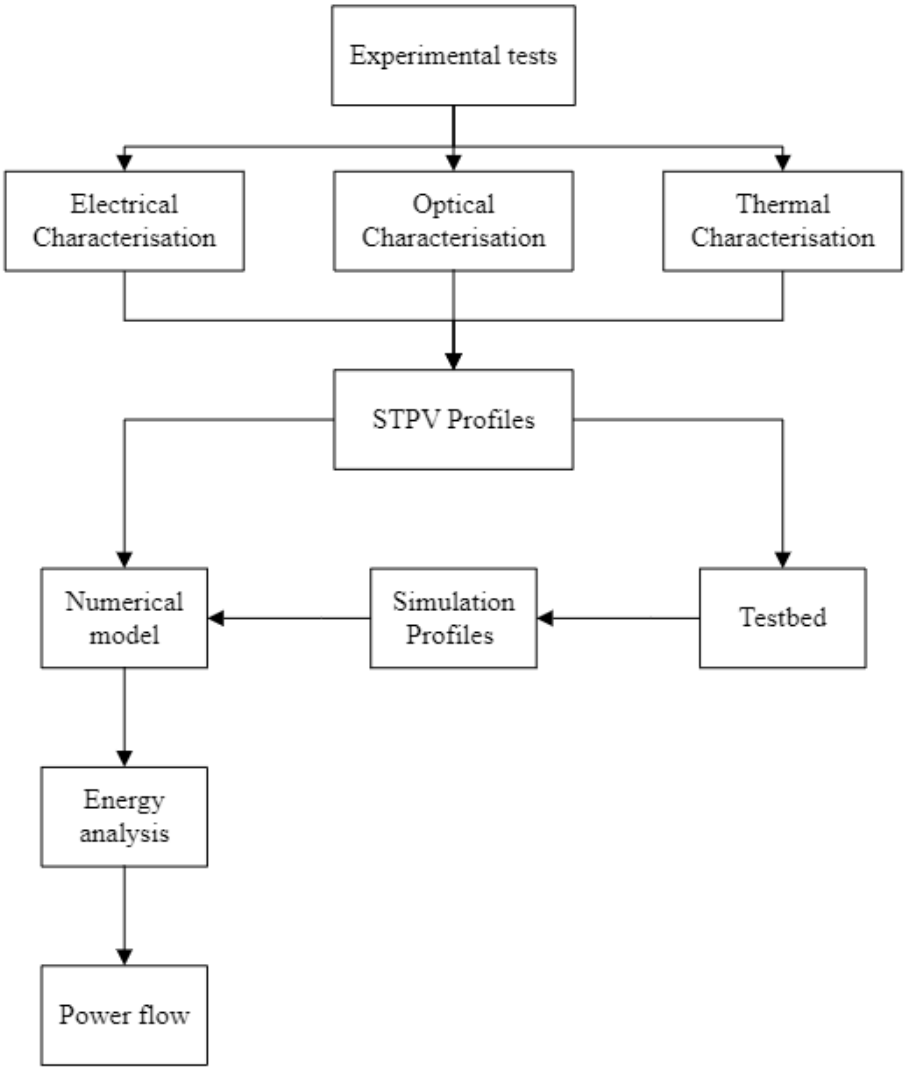

FIGURE 1.1 RESEARCH GENERAL APPROACH

1.7. Thesis Structure

The thesis follows the manuscript-based format consisting of six chapters, four main chapters, an introduction chapter, and a conclusion chapter. In the list below, a brief explanation for each chapter:

- Chapter 1: The motivation behind this research and its aim and objectives have been reviewed. Furthermore, the research approach and methodology have been briefly highlighted. Finally, the expected contribution to the field has been cited.
- Chapter 2: An in-depth literature review has been conducted in this chapter. The literature review started by looking into building energy consumption and investigating the different

renewable energy sources integrated and adapted into the building sector. Furthermore, a detailed study of the STPV technology has been carried out, and that review is constructed based on the solar cell materials used in this STPV. At the end of this chapter, a review regarding the integration of PV and STPV on the grid level has been shown.

- Chapter 3: The methodology of the research has been described, starting from the different equipment used in the practical set-up to collect the thermal, electrical, and optical data of the STPV glazing samples. A description of the numerical model follows this utilised to investigate the overall energy consumption by providing data from a Single glazing sample.
- Chapter 4: Analytical results from the thermal, electrical, and optical practical tests are discussed in detail. These results aim to characterise the CdTe STPV glazing samples, which would be employed in the numerical model developed by the Energyplus software to investigate the overall energy performance of these samples, which is discussed in detail in Chapter 5.
- Chapter 5: Numerical models have been developed to investigate the overall energy consumption of the practical set-up has been designed. This numerical model is then scaled up. In phase one, the experimental set-up is an office setting, and the results of STPV glazing systems are discussed and compared against reference glazing systems. Similarly, in the second phase, the office setting is scaled up into a whole building, and the overall energy consumption is investigated. The impact of integrating STPV glazing systems will be examined on a Grid level by tracking the load flow. An electrical system will be numerically simulated when a set of buildings utilising conventional Double-glazing systems and then when the same set using the optimal design reached in Chapter 5 is implemented.
- Chapter 6: A cumulative conclusion for the work described within the research and highlights potential further work in specific areas required for effective commercial implementation of the proposal.

CHAPTER 2
LITERATURE REVIEW

2. Literature Review

A profound literature review is essential to support the aim and objectives of the research. In this chapter, contributed studies and knowledge related to the research approach have been reviewed and classified into five sections:

- Building energy consumption 2.1.
- Glazing impact on the overall energy consumption 2.2.
- Renewable energy integration within buildings 2.3.
- Semi-transparent photovoltaic technology 2.4 and in this section, an in-depth analysis of the latest development of STPV glazing technologies and their effects, through experimental and simulation studies, are highlighted based on the solar cell's integrated material.

2.1. Building Energy Consumption

As mentioned above, the overall energy consumed by the building sector has increased immensely in the last decades. This consumption is estimated to be in the range of (30-40) % of the overall energy consumed globally [19]. Many attributes of the glazing systems can be identified as critical factors in the overall energy performance of the building sector, including but not limited to the glazing cover ratio of the wall (WWR) and the orientation of the glazing system, resulting in many researchers investigating these factors.

Many researchers have focused on the impact of the glazing system orientation, such as the research of Eljojo [20], which was based on developing a numerical model to investigate the effect of the glazing systems WWR and orientation on the overall energy performance. The outcomes indicated that the overall energy consumption could be reduced by 40%, and the emitted emission, especially CO_2, would be reduced by 30% when installing the glazing system in the optimal position. Similarly, Pai and Siddhartha's [21] research has found a correlation between the orientation of the glazing system and the potential to reduce the overall energy performance.

However, the glazing cover ratio of the wall or window-to-wall ratio (WWR) is the most impactful factor on the heating and cooling demand, which in part represents the bull of the overall energy consumption of the building sector. Youssef et al. [22] and Cannavale et al. [23] concluded that when the glazing systems cover smaller areas of the wall, the heating and cooling demands tend to decrease. Saridar and ElKadi's research [24] investigated the annual overall energy consumption when the glazing systems cover different areas of the wall, as well as when the glazing systems are installed in different orientations. The results have shown that the WWR is the most influential factor in the overall energy performance of the building.

In order to reduce the cooling and heating demands, shading devices were utilised, which led to decreasing the heat loss and the heat gain through the glazing system, which would reduce the heating and cooling demands. However, utilising such technology would reduce the amount of natural light entering the indoor environment. This reduction in the amount of natural light would lead to an increase in the artificial lighting demand [25]. It is worth mentioning that the geographical profile of the building location plays a major factor in the overall energy performance of the building.

The geographical profile is characterised by solar irradiance and ambient temperature impacting the glazing system analysis [26].

In conclusion, the overall energy performance of the building is dependent on the thermal and optical characteristics of the glazing systems. The thermal attributes tend to impact the heating and cooling demands, whereas the optical properties impact the artificial daylight demands. As a result, utilising a novel glazing system occurs after investigating the thermal, optical, and electrical attributes alongside the impact of this novel glazing system on the overall energy performance.

2.2. Glazing Impact on The Overall Energy Consumption

Glazing systems are crucial components of the building structure, as they represent the link between the inner environment of the building and the surroundings. The glazing systems' importance is amplified by enabling natural daylight into the indoor environment, which improves the building's indoor comfort levels. However, this ability of the glazing systems would lead to heat transfer through it, resulting in heat gain and losses. The heat gain and losses, in part, would impact the heating and cooling demand of the building and increase the overall energy consumption. The heating and cooling demands represent most of the overall energy consumption in buildings, which is mainly caused by the thermal insulation properties of the glazing systems, as stated in Jelle et al. research [27].

In summary, utilising glazing systems would result in heat gain and losses, which in part would lead to an increase in the cooling and heating demand. To overcome these obstacles and achieve an optimal glazing system that ensures a satisfactory level of indoor comfort while minimising the impact of heat transfer through it. Chow et al. [28] research has suggested that the optimal glazing system should be able to fully transmit the solar irradiance when it is operating in the visible light spectrum while fully reflecting the solar irradiance when it is operating in the infrared spectrum. In practice, this model only occurs in fully transparent glazing systems, which will be discussed below.

2.2.1. Single Glazing

A single glazing system encompasses one layer of glass embedded within a frame, Figure 2.1 below shows a Single Glazing sample. From an economic point of view, single-glazing systems tend to have lower initial and maintenance costs than other glazing systems [29]. The optical characteristics of the single-glazing systems lead to competent daylight performance due to their ability to transmit around 90% of the solar irradiance in the visible spectrum. Furthermore, single-glazing systems tend to decrease the heating demand due to their ability to transmit more than 80% of the solar irradiance in the infrared spectrum [30]. As for the insulation characteristics of the single-glazing systems, single-glazing systems tend to have a U-value around 6 W/(m^2.K), allowing high heat gain and losses, which results in increasing the heating and cooling demands. Thus, further research is needed to develop a glazing system that maintains an adequate daylight performance while improving the thermal attributes.

FIGURE 2.1: SINGLE GLAZING SAMPLE

2.2.2. Double Glazing

The double-glazing system encompasses two layers of glass separated by a gap filled with gas embedded within a frame, as shown in Figure 2.2. many researchers opted to investigate the impact that different gases tend to have on the insulation characteristics of the glazing. This interest was driven by the fact that gases tend to have a low thermal conductivity. For example, stagnant air has a thermal conductivity of 0.026 W/(m. K), Argon has a thermal conductivity of 0.016 W/(m. K), Krypton has a thermal conductivity of 0.0095 W/(m. K), and Xenon has a thermal conductivity of 0.005 W/(m. K) [30], [31]. Likewise, gases that absorb the solar irradiance in the infrared solar spectrum were utilised to improve the thermal characteristics of the glazing system by reducing the heat transfer through it [32]-[34].

Another aspect of the double-glazing systems was investigated, which is the width of the gap. This interest is driven by the fact that the distance between the two layers of glass affects the heat transfer through the glazing. As the width of the gap increases, the thermal conductivity decreases, leading to reducing the heat loss through the glazing. However, the gap width is dependent on the glazing system's geographical location of the building. However, an excessive increase in the gap would expand the convective heat transfer. Thus, an increment in the heat losses [26], [35].

FIGURE 2.2: DOUBLE GLAZING SAMPLE

2.3. Renewable Energy Integration within Buildings

Utilising single and double-glazing systems would not reduce the overall energy consumption of the building sector, while glazing systems enormously affect overall energy consumption. The development of solar cell materials technologies enabled the designing of more efficient PV systems as well as the integration of solar cells into the building fenestration. These improvement facilities utilise photovoltaic technologies either as a standalone system attached to the building (BAPV) or integrated into the structure of the building (BIPV) [7]-[10]. BIPV technologies would be utilised as a replacement for conventional building elements such as roof tiles and glazing systems with solar cells that generate electrical energy [27], [36], as shown in Figure 2.3. Many researchers have been intrigued by BIPV technologies due to the electrical energy generation aspect that could be added to the building structure [37].

FIGURE 2.3: BIPV EXAMPLES [38]

2.4. Semi-Transparent Photovoltaic Technology

As mentioned above, the glazing systems represent the weak link regarding the overall energy consumption of the buildings, and many researchers have proposed methods to develop and enhance the technologies that are utilised in the glazing systems. One of these methods was integrating solar cells into the glazing systems due to the duality of benefits that this technology possesses. Firstly, the ability to generate energy through the conversion of solar irradiance into electricity and the ability to improve the thermal performance of the building. This improvement occurs by reducing either the heating or cooling demand, depending on the embedded model.

Most researchers have opted toward investigating the effects that utilising STPV glazing systems has on buildings. These effects were studied by implementing experimental measures, which led to constructing testbeds and developing numerical models. Depending on the solar cells employed in the STPV glazing systems, the review of this research can be broken down accordingly. Most of the conducted research was based on integrating silicon solar cells, whether these cells were Crystalline Silicon (c-Si), or Amorphous Silicon (a-Si), or Cadmium Telluride (CdTe) solar cells. It is worth mentioning that there are huge efforts to make a breakthrough in utilising synthesis material [39] ls in solar cell technology, and the work of P. Selvaraj et al. [39] is a prime example. P. Selvaraj et al. were based on developing a dye-sensitised solar cells (DSSC) glazing system in the laboratory and then conducting several tests to identify the thermal, electrical, and optical characteristics of the DSSC glazing system.

The methodology used in the below literature can be classified into two distinctive methods. The first method would be based on constructing a testbed to collect data, then analysing this data, and drawing a conclusion based on the analysis. The other method would be developing a numerical model using a software tool and validating this model by comparing it with an experimental measurement of the STPV glazing system.

To simplify the process of the literature review, the review has been broken into two sections. The first section will review the work that has been based on utilising the different types of silicon solar cells. The second section will review the literature that has been based on utilising CdTe solar cells.

2.4.1. Silicon Solar Cells

2.4.1.1. Crystalline Silicon Solar cells (c-Si)

Peng et al. work in [2] was based on constructing a testbed to investigate the effects of employing a c-Si STPV glazing system. The investigated impacts were focused on the glazing systems' electrical, thermal, and daylight performance. The results indicated that the generated energy would peak when the glazing system faces the south and southwest orientations with a daily average electrical production of (1.9-1.94) kWh. Furthermore, the daylight performance of the sample delivered sufficient daylight for around 80% during the experiments. The results on the thermal performance have indicated that utilising a conventional Low-E double-glazing system would be more efficient. The effect of the surrounding shading has been recorded and would decrease the overall generated energy. This decrement depends on the shape of the shading, whether horizontal or vertical. In addition, the solar cells' temperature is another factor that affects the generated energy.

Bambara and Athienitis's [40] work was based on simulating the effects of integrating a c-Si STPV glazing system in an agricultural building. The study established a link between the economic return of implementing such a system and the life cycle, thermal, electrical, and daylight parameters. The results indicated that implementing the STPV glazing system would increase the lighting load by at least 80%, saving around 40% of this load energy. Furthermore, the system would lead to a decrease in the heating load by more than 10%. However, considering the life cycle, a 30% deterioration in the performance would make it less feasible to implement.

Lu and Law [41] showcased the effects of implementing a c-Si STPV glazing system over the energy overall consumption for the whole building. The experiments were conducted in Hong Kong, where the cooling load is the dominating load. The cooling load, whether it was for cooling the water or as a part of the HVAC system, has decreased by more than 60% as it mitigated the solar heat gain. The optimal orientation was investigated, and the southeast has provided the most efficient overall energy consumption.

Xu et al. [18] research was based on developing a numerical model to be validated using experimental measures for the c-Si STPV glazing system. The aim was to find the optimal coverage ratio levels (transparency levels, low coverage levels, high transparency, but it depends on the way the solar cells are installed, not the structure of the material) for the STPV taken into consideration (WWR), STPV samples orientation and simulated zone area (room depth). The results indicated that as the coverage ratio of c-Si solar cells in the glazing system increases, the electrical conversion ability of the glazing system decreases because of the increment of c-Si solar cells' temperature (although the increase in the coverage ratio means more active solar cells and as a result more electricity). Furthermore, the lighting load increases with the decrement of the glazing transparency capabilities; what is more, the daylight performance was affected more by the area depth than the WWR the glazing system occupies. The heating and cooling load have an opposite trend when compared with the lighting load driven by the geometrical profile of central China.

Yun et al. [42] have focused on investigating the effects of installing a passively ventilated double-glazing c-Si STPV glazing system on various aspects of the building in the quest to find the optimal glazing system that contains solar cells. The work was based on the Environmental System

Performance for Research (ESP-r) software to compare the results in three different locations in the continent: Madrid (Mediterranean climate), London (moderate climate), and Stockholm (cold climate). The results indicated that the WWR in London is the biggest to achieve maximum efficiency, whereas, in Madrid, the WWR tends to be lower to reduce the passive heating element and reduce the cooling demand. However, in Stockholm, the integration of such a system does not provide a sufficient improvement in overall energy consumption. Integrating the system in small rooms tends to have a better energy consumption due to the lighting demands. To reach an optimal design regarding this system, the addition of insulation materials is crucial, as indicated in the results.

Refat and Sajjad's [43] research has investigated the impact silicon-based STPV glazing systems would have on building energy consumption by developing a numerical model. The results have indicated that utilising STPV glazing systems with clear glazing being the inner surface material at WWR%= 60% or more would increase overall energy consumption regardless of location. Furthermore, using such a system at WWR% = 10% would reduce the overall energy performance between (20-50) %, depending on the location. However, replacing the clear glazing with Low-e material for the inner surface of the STPV glazing systems would reduce the overall energy performance by (45-70) %, depending on the location.

Wu et al. [44] have developed a numerical model to investigate the effects shading sources have on the electrical and thermal performance of the c-Si STPV glazing system. The results have shown that as the shadow width increases, the generated energy and the heat gain decrease. April has the most significant drop in the generated power by 15%. Furthermore, in August, the heat gain dropped by 1.2%, decreasing the cooling demand.

Xiong et al. [45] studied the effects on the electrical performance of the c-Si STPV glazing system impacted by the inter-building while under shading conditions by developing a numerical model. The results highlighted that the solar irradiance in December decreased by 36% and the generated energy by 40%. Furthermore, the solar conversion ability of the c-Si STPV glazing system decreased by 39%.

2.4.1.2. Poly-Crystallin Silicon Solar Cells (p-Si)

Ploy-crystallin silicon solar cell materials are similar to c-Si solar cells, but the structure process of the solar cells is different [46]. The developed works that used p-Si STPV include the following.

Wong et al. [15] have introduced a novel way to integrate STPV solar cell materials into residential building roofs and develop a numerical model. A correlation between the effectiveness of the glazing system and the location's geometrical profile has prevailed. The proposed system achieved an overall annual heating saving but will result from increasing the cooling one. Efforts are spent to develop an optimised model. With various weather conditions, their proposal revealed the energy-saving potential for moderate and temperate climates. Fung and Yang [47] investigated the thermal performance and, specifically, the heat gain aspect of the building model deploying a p-Si STPV glazing system. The considered factors are the orientation of the glazing, the transparency (solar cells coverage area), the electrical efficiency of the glazing system, and the structure of the system. The p-Si STPV glazing system has the highest heat gain when the glazing is southwest, orienting the

heat gain to about 230 kWh/m^2. The heat gain reduces when the transparency reduces with a difference of 70% drop between the highest and lowest transparency, and the drop is caused by the absorbance of the solar radiation by the solar cells. At the same time, the solar cells' efficiency tends to have a minor effect on the heat gain due to the structure of the glazing system. Also, the results indicated that the difference between the thinnest and thickest glazing gives around a 15% drop in heat gain. With that being said, the effect of the structure is marginal since increasing the thickness of the glazing system will lead to an increase in thermal resistance.

Park et al. [48] investigated the electrical performance of an STPV glazing system, taking into consideration the following aspects: solar radiation, the climate profile of the location, and the glazing structure. The results revealed minor differences between transparent and coloured glazing. A transparent outdoor surface and a bronze one are tested. It was expected that the indoor temperature during the summer would be higher than in winter. However, the STPV glazing tends to have the opposite results, reasoned by the models tend to have a variable amount of solar radiation depending on the climate profile of the location, and the location tends to have seasonal rains during the summer, which will reduce the solar radiation gain at its peak, furthermore, the generated electricity in the cold seasons tend to be greater than the generated amount in the hot seasons which is driven by the temperature of the solar cells and as the temperature of the solar cells increases the generated energy decreases by (0.4-0.6)% for each 1℃ surge.

Zhang et al. [49] research examined the electrical and thermal results of implementing p-Si PV-Thermoelectric (PV-TEC) technology into the STPV glazing systems model by developing a mathematical model. the results indicated that if the PV-TEC or the STPV-TEC glazing systems tends to consume the same amount of energy, which is around 71.8 kWh.

Karthich et al. [50], [51] studied the buildings' overall energy performance when p-Si STPV glazing systems were utilised within the roof structure by developing a numerical model. The results have shown that the light demand of the building has decreased by (87-131) kWh annually, depending on the transparency of the model [50]. Furthermore, integrating phase-changing materials (PCM) would reduce the p-Si STPV glazing system surface temperature by 9°C. Furthermore, the electrical conversion ability of the glazing would increase by 9.4% [51].

2.4.1.3. Amorphous Silicon Solar Cells (a-Si)

Cheng et al. [52] investigated the effects of installing an a-Si STPV glazing system on daylight performance and overall energy consumption. The results have been interpreted considering the WWR, the transparency levels of the glazing system, and the orientation of the glazing. The results indicated that the daylight performance tends to improve as the transparency levels increase to a certain level and peaked when the transparency was 60%, which is driven by the fact that the useful daylight illuminances that meet the threshold have increased across the whole simulation setting. Also, the increase in transparency levels increased the heat gain, which would have a positive impact on the heating demand. However, the cooling load would increase, which is not an issue for cold-climate locations. The outcomes indicated that the increase in the transparency levels tends to increase the overall energy consumption by 23%. Achieving optimal design required transparency in the range of (40-50) %, south-oriented, and the WWR would be in the range of (40-50) %.

Peng et al. [5], [16], [53] used an a-Si STPV double-glazing system aiming to optimise air gap width to maximise energy savings. The results have stated that utilising an optimised model would generate around 65 kWh/m^2 annually and reduce the overall energy consumption by 50%. It has been identified that a 400 mm air gap would lead to an overall energy consumption of 290 kWh annually, which is a reduction of 58% compared with a conventional clear double-glazing system [5]. The other part of the research has focused on the effects that a suitable ventilation system installation would have on the overall energy performance [16], [53]. The results indicated that utilising a ventilation system would lead to enhancement of the temperature distribution across the whole a-Si STPV glazing system, achieving a reduction of the solar heat gain by 20% while the energy generation changed marginally by 3%. The reason behind this enhancement is the fact that utilising a ventilation system would reduce the solar heat gain and, as a result, the cooling demand; however, the surface temperature of a-Si solar cells is not affected significantly. Miyazaki et al. [6] found that the daylight control mechanism has a catalyst effect on the overall performance. Without daylight control, compensation in the transparency levels is needed. To increase the generation aspect of the glazing system, the transparency levels would decline, and as a result, the heating and lighting demand would increase due to the lack of the passive heating element against the natural light that the indoor environment receives. However, if a daylight control algorithm were implemented, the optimal design would deliver an overall energy saving of 55%. The delivered optimal model covered 50% of the wall area, and the transparency was 40%.

Weng et al. [8] work was also based on developing a validated numerical model that utilises an a-Si STPV glazing system. The purpose was to identify the optimal structure that contains the a-Si STPV as part of the insulation materials of the glazing system. The results have indicated that the air gap depth tends to have a marginal effect due to the climate profile of the location where the experiments took place. is found that a Low-E glass layer is required to achieve the optimal structure that would achieve an overall energy saving of 25% compared to a single glazing system and 11% in comparison with Low-E glazing.

Weng et al. [9] work was to determine the difference between the double skin façade (DSF) STPV (with a large air gap of 400 mm) and Insulation Glazing Unit (IGU) STPV (no big air gap). The results of the thermal analysis of the models have shown that DSF-STPV will reduce the heat, gain which leads to a reduction in the cooling load, while the STPV-IGU will increase the heating gain element which consequently will reduce the heat load. Whereas, comparing both models with a conventional glazing system would result in a reduction of around 30% for STPV-DSF and STPV-IGU. The research has examined the effect of the ventilation system with STPV-DSF and compared it with STPV-IGU. The results indicated that STPV-IGU is especially better when the louvers are open. Olivieri et al. [13] work has been based on developing multiple numerical models utilising different a-Si STPV glazing systems. This work aimed at exploring the outcomes of applying different STPV glazing systems at different WWRs, to present the optimal energy-saving potential point of view. The results have indicated that a-Si STPV glazing systems tend to have identical performance to the conventional clear double-glazing system, or at best a decrement of around 6% in the energy consumption levels when the glazing systems cover a small area of the wall (WWR ≤ 30%). However, when the STPV glazing system covers an intermediate area of the wall or covers most of the wall (WWR > 30%), the energy-saving potential increases and ranges between (15-60) % compared with a conventional clear double-glazing system. Regarding the indoor comfort levels, the glare

phenomena only occurred when the weather profile was examining the indoor comfort levels at midday, in winter conditions, and under clear skies situation.

Song et al. [10] investigated the effects of utilising an a-Si PV glazing system that is installed on the roof of the building and compared it with a conventional double-glazing system while monitoring the different incident angles. The results have indicated that installing the a-Si PV glazing system with a 30˚ tilt angle south oriented south-oriented is the optimal state for the location of experiments. Furthermore, the azimuth angle played a focal point regarding the output energy generated which could be, around 22% improvement when it is 0˚ if compared with 90˚.

Yoon et al. [54] research has investigated the effects of the surface thermal profile using a practical testbed, including the evaluation of a conventional double-glazing system and a-Si STPV glazing system at different tilt angles. The results indicated that the a-Si STPV glazing systems that are installed flat (0˚ tilt angle) tend to have higher external surface temperatures when compared with similar glazing systems but installed at different tilt angles (30˚ and 90˚) during the cold weather conditions (winter), whereas this trend is reversed in the hot weather conditions (summer). As for the internal comfort levels, the results indicated that utilising an a-Si STPV glazing system would lead to a lower ambient temperature during the day and a higher one during the night. These results are driven by the fact that a-Si STPV glazing systems tend to have a lower heat gain coefficient, and higher ability to execute thermal insulation when compared with the conventional double-glazing systems.

He et al. [55] Research has analysed the electrical and thermal performances of a-Si STPV double-glazing system and single-glazing system. This research was achieved through a heat balance analysis that has been validated through a practical testbed. The results indicated that an a-Si STPV double-glazing system reduces the solar heat gain and subsequently reduces the heat demand driven by the fact that the air gap decreases the solar cell's surface temperature when compared with a single-glazing system.

The results in [56] indicated that implementing an STPV double-glazing system would at least reduce the overall consumption by 23% without any ventilation element and an extra 5% with it. The ventilation element tends to reduce the solar heat gain of the indoor environment leading to reduce the cooling load, but minimal impact on the efficiency of the solar cells.

Peng et al. [57] developed a numerical model that utilises a-Si STPV double-glazing ventilated system and validated this model through a comparison with a practical testbed setup. The results indicated that the numerical model predicted that the model m would generate electrical energy of 11.19 kWh in October 2012 and 13.96 kWh in January 2013, whereas the actual results were 11.46 kWh and 13.56 kWh. These results indicate that the numerical model is accurate and can be used as a stepping stone in the optimisation stage for future works.

Didoné and Wagner [58] used a-Si and organic STPV glazing system in South America (Brazil). The research has compared the STPV glazing systems and traditional systems (single-glazing, double-glazing, and Low-E). The results indicated a reduction in the overall energy consumption ranging between (39-43)% depending on the geographical location. Also, the authors, concluded that utilising Low-E glazing systems for the glazing that are orientated towards least the solar radiation

while implementing STPV glazing systems on the other glazing would present the optimal model regarding the energy performance.

Zhang et al. [59] research has focused on establishing the difference between utilising the STPV glazing systems and the evolved glazing systems. These glazing systems (Double-glazing and Low-E) tend to be more efficient from the point of view of overall energy performance. The comparison was established with a numerical model that has shown the effects of utilising a-Si STPV glazing system, double-glazing, and Low-E glazing systems. The results indicated that the STPV glazing system achieved a decrease of 48% and 38% in the solar heat gain respectively. But on the downside, the heating load and the daylight demand tend to increase because STPV glazing restricts the amount the natural light and solar radiation that passively reduces the lighting load as well as the heating load.

Chen et al. [60] research investigated the Solar Heat Gain Coefficient (SHGC) with different tilt angles while a-Si STPV glazing system is connected to an electrical load. The results indicated that the SHGC of the STPV double-glazing is lower than the STPV glazing system due to the existence of Low-E materials in the STPV double-glazing system. It is found that if the tilt angle is less than 45˚, then the decrease in the SHGC is marginal, which is around 5%. However, if the angle is between 45˚, and 70˚ the decrement in the SHGC is around 20%. Furthermore, the electrical loads tend to have minimal effect on the SHGC of (3-6) %.

Cuce et al. [61] work aimed toward identifying the thermal characteristics of the heat insulation solar glass (HISG), which is a type of a-Si STPV glazing system. The results indicated that the U-value of HISG is 1.1 W/(m^2.K). Comparing the HISG with a conventional clear double-glazing system, the HISG tends to represent a much better insulation tool.

Peng et al. [62] aimed to develop an accurate numerical model using SAPM software through experimental tests based on a testbed utilising an a-Si STPV glazing system. The model results have proven to be precise under clear sky conditions only with a margin of error of 3% compared with a 14% margin of error under overcast sky conditions.

Chae et al. [63] work based on developing three numerical models that use the different structures of hydrogenated amorphous silicon (a-Si H) STPV glazing systems in six other locations. The results indicated that the climate profile of the location represents a critical factor in the overall energy performance of the model.

Wang et al. [64]studied the impact that a-SiGe DSF-STPV glazing system would have on the overall energy consumption of the building by developing two test rigs to collect the data. The experimental results have underlined that the electrical efficiency of the a-SiGe DSF-STPV glazing system is around 6%. Furthermore, the results indicated that the generated energy is inadequate to cover the testing rig's electrical load. In addition, the UDI is reduced by 50%. On the other hand, the thermal characteristics of a-SiGe DSF-STPV glazing system represent a better insulation tool when compared with the conventional transparent double-glazing system.

Tian et al. [65]-[67] research has investigated the thermal and indoor environment comfort levels utilising a-Si (DSF/IGU) STPV glazing system through a series of experimental tests [65], as well as the saving potential in the overall energy consumption when utilising a-SiGe STPV glazing system

[66]. The results have indicated that the electrical efficiency of the a-Si (DSF/IGU) STPV glazing systems is around 5.5%. Furthermore, the ambient temperature of the indoor environment is lower by 5°C compared with conventional transparent double-glazing [65]. As for the a-SiGe STPV glazing system, the overall energy consumption would be reduced by 30% under clear sky conditions compared to conventional transparent glazing [66]. Moreover, the a-SiGe STPV glazing systems led to a decrease in the cooling demand during the summer period, which led to a reduction in overall energy consumption by 29% [67].

Cheng et al. [68] studied an office setup's overall energy consumption and daylight performance while utilising an a-Si STPV-DSF glazing system. The results highlighted that the annual energy consumption of an optimised a-Si STPV-DSF glazing system is 33.9 kWh/m^2, representing a reduction of 9.4 kWh/m2 compared with a conventional transparent double-glazing system. Furthermore, the N-daylit ratio of this system is around 57%.

2.4.1.4. Comparing the c-Si and a-Si solar cells

Few researchers have opted toward establishing a comparison between integrating c-Si and a-Si solar cells into the glazing system. This section will go through a limited number of works in this field.

In the research of Skandalos et al. [4], [69] an in-depth analysis in relation to the thermal characteristics, alongside the optical performance, has been conducted. As for the electrical performance, the analysis was dependent on tracking the cooling and heating demands. The results were generated from multiple validated numerical models; these models were developed using multiple software packages that identified the thermal, optical, and electrical characteristics and then imported to the TRNsys software tool to do the heat balance analysis. The results have indicated that utilising STPV glazing systems would lead to a reduction in the solar heat gain by around 30%, which would lead to a decline in the cooling load. However, the lighting load, as well as the heating, demand would increase. As for the optical, aspect applying STPV reduces the glare by around 22% for the c-Si solar cells and, 27% for the a-Si solar cells. Finally, a-Si solar cells operate efficiently in low solar radiant situations, while c-S is more effective in converting solar radiation into electrical energy. Saber et al. [17] reviewed the different types of PV technologies, and an in-depth analysis was conducted to evaluate their effects when these technologies are implemented. The results have shown that p-Si solar cells tend to have a better electrical performance compared with c-Si and a-Si solar cells. (This research has investigated PV units on the roof).

The research of Kapsis and Athienitis [70] has studied the outcomes of utilising different solar cells (p-Si & a-Si) integrated into the glazing system and their effect on the overall energy performance. The results have revealed that the orientation of the glazing system alongside the WWR and the artificial light controlling mechanism are significant factors in the overall energy performance. The optimal design has been able to present a low consumption ratio. The annual consumption ratio is as low as 5 kWh/m^2. It should be noted that the research geographical location tends to have a dominant cooling load hence, the transparency levels were as low as 10%.

Hwang et al. [71] investigated the optimal tilt angle and orientation where the integrated c-Si and a-Si solar cells into the buildings would generate the most energy through a validated numerical model. The research outcomes showed that the optimal tilt angle is in the range of (40°- 60°), as the solar cells are oriented to the south. Moreover, the c-Si solar cells generated 6% of the needed energy when installed. Furthermore, the most optimal design has reduced the overall energy consumption by 5%.

Mesloub et al. [72] investigated the impact of a-Si and c-Si STPV glazing systems on the overall energy consumption of a building through a numerical model. The results highlighted that the STPV glazing systems would reduce the cooling load consumption by 75% compared with conventional transparent double-glazing. Furthermore, the overall energy consumption would be reduced by 58%. On the other hand, the light demand consumption would increase by 20%.

2.4.2. CdTe Solar Cells

Cadmium telluride is a crystalline compound resulting from the combination of cadmium and tellurium. It is composed of a cadmium atom with 48 protons in its nucleus and 2 valence electrons, covalently linked to a telluride atom with 6 valence electrons. The direct bandgap of 1.4 – 1.5 eV and a significant absorption coefficient make CdTe highly efficient. Based on the data presented in the chart, this bandgap corresponds to photons with a wavelength of 825 nm, leading to a power density of 1.25 kW/m^2/nm [73].

Many researchers have focused on using CdTe solar cells because of their higher electrical efficiency and unique thermal characteristics. Barman et al. [11] work was based on developing multiple validated numerical models to employ different CdTe STPV glazing systems. The outcomes were tested against transparency, orientation, and WWR. The results have indicated that the south orientation leads to the highest energy generation, particularly with low transparencies. The cooling and heating demands tend to be affected in a contrary manner when comparing the effect of the WWR and the transparency levels. A reduction of 60% in the overall energy consumption levels when compared with a conventional glazing system is achieved.

The results in [12] indicated that the STPV glazing system should cover more than 30% of the wall area to influence the overall energy performance. Furthermore, when the STPV glazing system covers 45% of the wall area or more, the amount of energy that is generated tends to increase, especially when most of the glazing system is covered by solar cells. Their optimal design would cover 75% of the wall area by glazing, with solar cells covering 80%. Regarding the indoor environment comfort levels, employing STPV glazing systems tends to eradicate the glare phenomena that usually occur when utilising conventional clear double-glazing systems.

Sabry [14] has developed a numerical model on MATLAB using Custom Neural Network (CNN). The results have provided the electrical profile of the CdTe STPV units alongside the I-V curves. The results have highlighted that the CdTe STPV glazing model would generate 22 W at an irradiance of 1000 W/m^2 while the temperature is at 45°C.

Alrashidi et al. [74] research has investigated the thermal characteristics of a CdTe STPV glazing system through a practical setup. The results have indicated that the U-value of the CdTe STPV glazing system is 2.7 W/(m^2.K), which is lower than the conventional clear single glazing system by

3 W/(m^2.K). Moreover, utilising the CdTe STPV glazing system would reduce solar heat loss by 40% when compared with a conventional clear glazing system.

Sun et al. [75] analysed the daylight performance of different STPV glazing systems (CdTe and c-Si) under different levels of transparency and different WWRs. The outcomes of the research have established that applying STPV glazing systems would reduce the probability of the over-illuminate phenomena occurring, as well as limiting the possibility of the glare phenomenon happening, compared with the conventional clear double-glazing systems as the transparency levels decline. In [76], they explored the overall energy performance alongside the daylight performance, which was conducted under different levels of transparency and different WWRs. The results indicated that STPV glazing systems for WWR of 30% or less would not lead to any sensible lessening of the overall energy consumption even if the whole glazing system has been replaced with a CdTe PV glazing. As for the energy consumption, the optimal model would be a CdTe STPV glazing system that is 20% transparent and covers 75% of the wall area. This model decreases the overall energy performance by 73% or 1017 kWh annually compared to a clear double-glazing system.

Liu et al. [77] research has examined the effects of installing a CdTe glazing system into the fabric of the building and specifically the daylight performance. Using CdTe STPV glazing systems is going to increase the ratio of the useful and desirable illuminance, especially when the glazing is covering a large area of the wall (WWR ≥ 70%). Furthermore, the CdTe STPV glazing system would limit the glare potential [77]. Additionally, the colour comfort analysis has been evaluated based on the Correlated Colour Temperature (CCT) and Colour Rendering Index (CRI). The results indicated that CdTe STPV glazing systems present an efficient method to control the amount of the CCT within the transmitted light to the indoor environment. As for the CRI aspect, all of the CdTe STPV samples obtained a CRI of > 97; however, the minimum comfort colour levels of the transmitted daylight through glazing should be 90 or more (CRI > 90) [78].

By developing a numerical model, Preet et al. [79] investigated the overall energy performance of CdTe STPV-DSF glazing systems under different ventilation models. The results indicated that utilising the mechanical ventilation mechanism in the STPV-DSF glazing systems would reduce the overall energy by 4% in June, 10% in October, and 14% in December. In addition to that, the mechanical ventilation method reduced the gap temperature by 1.83°C on average.

Ghosh et al. [80] examined daylight performance and the indoor environment comfort levels while integrating STPV glazing systems by developing a numerical model. The results indicate that the visible light transmittance (VLT) needed to be between (50-70) % for the model to provide acceptable indoor comfort levels. While in summer, the model with 70% VLT provided adequate indoor comfort levels. However, the glare phenomena occurred midday.

2.5. Literature Review Summary

After analysing the literature, the following gaps can be identified:

- Further research and analysis are needed to determine the potential impact of integrating CdTe semi-transparent photovoltaic glazing systems into building structures.
- A lab-based approach to assess the electrical, thermal, and optical characteristics of semi-transparent photovoltaic materials.

- Investigating the overall energy assessment of the CdTe semi-transparent photovoltaics glazing systems at a location where the heating load is the biggest need to be addressed.
- Investigating the overall energy assessment of the CdTe semi-transparent photovoltaics glazing systems on two different scale building settings while covering different Window-to-Wall Ratios (WWRs).
- Investigating the impact of integrating semi-transparent photovoltaic glazing on the load flow and the stability of the whole electrical system.

CHAPTER 3
EXPERIMENTAL APPROACH

3. Experimental Approach

This chapter aims to establish the experimental methodology used to characterise the different glazing samples examined in this research. The characterisation process can be categorised into three distinctive classes which are thermal properties, optical properties, and electrical properties.

This chapter is going to discuss the physical properties of the samples that are used in this research as well as details the experimental set-up that is used to get the different properties for these samples.

3.1. Glazing Samples

In this research, six different CdTe STPV glazing samples, as well as two clear double-glazing samples and a clear single-glazing sample, were utilised. Table 3.1 shows the glazing samples that are being tested in this research, whereas Table 3.2 enlists the physical attributes of each sample.

TABLE 3.1: GLAZING SAMPLE'S PHYSICAL PROPERTIES

Sample	Sample type	Solar cells materials
S1	STPV	CdTe
S2	STPV	CdTe
S3	STPV	CdTe
S4	STPV	CdTe
S5	STPV	CdTe
S20	STPV	CdTe
S21	STPV	CdTe
DG1	Double Glazing	N/A
DG2	Double Glazing	N/A
SG1	Single Glazing	N/A

TABLE 3.2: THE PHYSICAL ATTRIBUTES OF THE GLAZING SAMPLES

Sample	Dimensions (cm)	Thickness (mm)	Structure	Gap (mm)	Gap filled material
S1	15*15	7	Glass-CdTe-Glass	N/A	N/A
S2	15*15	7	Glass-CdTe-Glass	N/A	N/A
S3	15*15	28	Glass-CdTe-Glass-Gap-Glass	17	Air
S4	15*15	7	Glass-CdTe-Glass	N/A	N/A
S5	15*15	7	Glass-CdTe-Glass	N/A	N/A
S20	15*15	7	Glass-CdTe-Glass	N/A	N/A

S21	15*15	7	Glass-CdTe-Glass	N/A	N/A
DG1	20*20	14	Glass- Gap - Glass	6	Air
DG2	20*20	14	Glass-Gap - Glass	6	Argon
SG1	30*30	6	Glass	N/A	N/A

The samples S1, S2, S3, S4, S5, S20, and S21 are the CdTe STPV glazing samples. Whereas the DG1, which is a Clear air-filled double-glazing system, is going to represent the reference point similar to what has been discussed in the literature review chapter. The SG1 is a clear single-glazing sample, which is going to represent an example of the collected data from the practical setup, which is going to be explained in this chapter.

3.2. Characterisation Approach

To comprehend the impact that CdTe STPV glazing systems tend to have on the overall energy performance of the building sector, an approach to identify the thermal, optical, and electrical attributes is needed. It needs to be noted that the integration of such technology tends to be influenced by the geographical and climate profile in which the building resides. As such, an optimised module delivers a glazing system with an output that is balanced from the point of view of transparency as well as efficiency. This module needs to extend both the electricity generation and energy savings potential while keeping an adequate level of indoor comfort depending on the building and how it is going to be utilised. To achieve this purpose, many researchers have developed numerical models using different simulation tools that enable them to investigate the impact of different parameters, including the glazing systems characteristics (Thermal, optical, and electrical), the climate profile of the building location, as well as the building usage purposes and even the possible impact that shading could have. These studies have been reviewed in-depth in the 2nd chapter of this thesis (Literature Review). To attain the objectives discussed above, which aim to facilitate the transition of the building sector towards a more sustainable approach, appropriate models should be developed and validated through experimental tests. After that, a comparison between the existing CdTe STPV samples should be in detail.

The generated energy, as well as the thermal performance, contribute to the overall energy performance of CdTe STPV glazing systems, which would be examined experimentally as well as through developing numerical modules utilising software tools. Through the experimental tests, the CdTe STPV sample's thermal, optical, and electrical characteristics would be quantified, which is essential to construct each sample's unique profile. This profile is going to be computed into the numerical model to calculate the overall energy performance and saving potential of each CdTe STPV sample profile in comparison with the conventional transparent double-glazing systems. Furthermore, essential parameters and data are collected to be used in the validation process of the different numerical models.

3.2.1. CdTe STPV Electrical Characteristics

CdTe STPV samples consist of CdTe solar cells. These cells convert the absorbed solar radiation into direct current (DC) energy, depending on their conversion efficiency [81]. The conversion efficiency

(η) of the CdTe STPV samples solar cell is defined as the ratio of the maximum generated output power ($Pout$) to the input power (Pin), which is shown Equation 3.1:

$$\boldsymbol{\eta = \frac{Pout}{Pin}}$$ **EQUATION 3.1**

As for the value of input power (Pin), it is the result of the solar irradiance at the standard testing conditions (STC), which is 1000 W/m^2 multiplied by the area of the CdTe sample. As for the generated output power ($Pout$), which is the result of the multiplication of the output voltage (V) and current (I) between the terminals of the CdTe STPV glazing samples. Whereas the maximum generated output power ($Pout$) is needed to achieve maximum efficiency, which occurs at the maximum power point (MPP) as shown in Equation 3.2. However, the temperature of solar cells and the insolation levels need to be considered as they impact the output generated power.

$$\boldsymbol{P_{max} = V_{max} * I_{max}}$$ **EQUATION 3.2**

The maximum power point rests between short-circuit and open-circuit conditions, as shown in part (A) in Figure 3.1, which displays the generalised current and voltage characteristics for photovoltaic solar cells. In short-circuit conditions, the PV unit is connected to a load that is too small and is almost equal to zero. At that condition, all converted solar irradiance flows through the diode, and the current reaches the peak value, which is short-circuit current (I_{sc}). In open-circuit conditions, the PV unit is not connected to a load, which means that no current flows through the diode, which means that the output voltage reaches a peak value, called open-circuit voltage (V_{oc}). The maximum output power is reached when the current and voltage are below these levels, at the MPP where the current and voltage are noted as I_{MP} and V_{MP} respectively. To compute the difference between the output power at MPP and the maximum theoretical power that could be generated, the Fill-Factor (FF) is calculated. The Fill Factor is the ratio between the maximum output generated power at MPP to the product of the open-circuit voltage times the short-circuit current, as shown in Equation 3.3. This ratio provides an indication of the quality of the solar cells, and the closer the Fill-Factor is to unity, the output generated power increases, as shown in part (B) of Figure 3.1 below.

$$\boldsymbol{FF = \frac{P_{max}}{V_{OC} * I_{SC}} < 1}$$ **EQUATION 3.3**

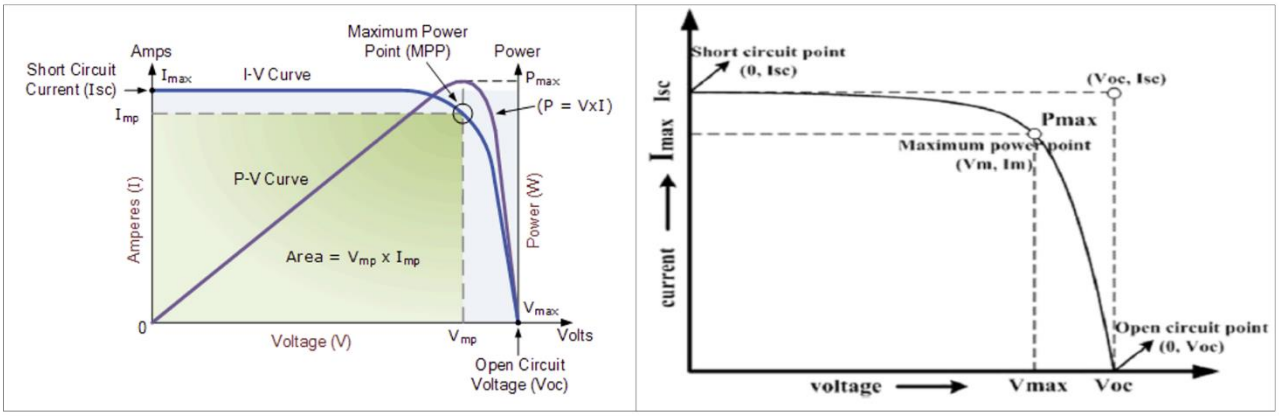

FIGURE 3.1: (A) GENERALISED ELECTRICAL CHARACTERISTICS FOR PV UNITE [82], (B) GENERALISED I-V CURVE AND THE FF [83]

It is worth mentioning that the PV module's Photons operate under specific parts of the solar radiation spectrum. If the solar irradiance photons' energy is below the bandgap, the photons are going through the PV unit, while when the photon's energy is beyond the bandgap, the PV unit temperature is going to increase [84].

With that in mind, the solar cells act as a simple p–n junction diode when the solar irradiance is lacking and as a result, the solar cells' attributes adhere to the Shockley diode equation [85] shown in Equation 3.4.

$$\boldsymbol{I_D = I_o\left[exp\left(\frac{qV}{akT}\right) - 1\right]}$$

EQUATION 3.4

Where:

$\boldsymbol{I_D}$: The Diode current (Ampere).

$\boldsymbol{I_o}$: The diode current at saturation (Ampere).

$\boldsymbol{q}$ **:** The absolute value of the electron's charge ($1.602 * 10^{-19}$ Coulombs).

$\boldsymbol{V}$**:** The voltage of the solar cell (Voltage).

$\boldsymbol{a}$**:** The ideality factor of the diode (unitless).

$\boldsymbol{k}$**:** The Boltzmann's constant (Joule /Kelvin).

And the ratio (kT/q) is known as the Thermal Voltage (V_t) and measured in voltage. Under these circumstances, the ideal solar cell can be presented as a Single-Diode model, as shown in Figure 3.2 below. Where I_s represent a current source, I_D the diode current and I is the total current all measured in Ampere.

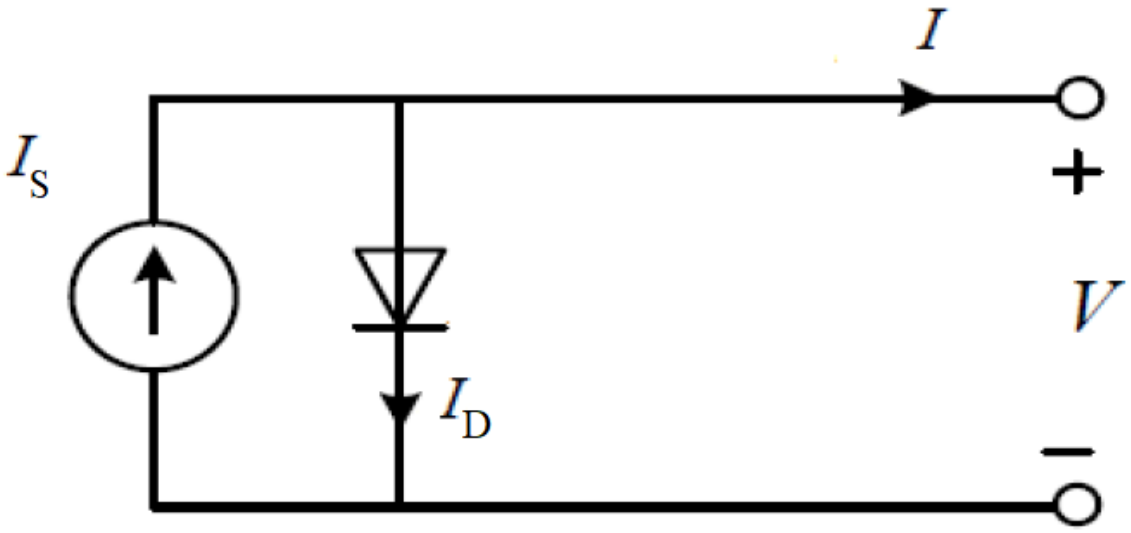

FIGURE 3.2: SINGLE DIODE MODEL [86]

When the solar cells absorb part of the solar irradiance, Losses caused by the current flow and electrode resistance occur, which can be translated to the equivalent circuit by incorporating resistance in series (R_s). Furthermore, the increase in the solar cell's temperature due to the conversion process can be presented in the equivalent circuit by introducing a parallel resistance (R_{sh}) to the model [87] as shown in Figure 3.3.

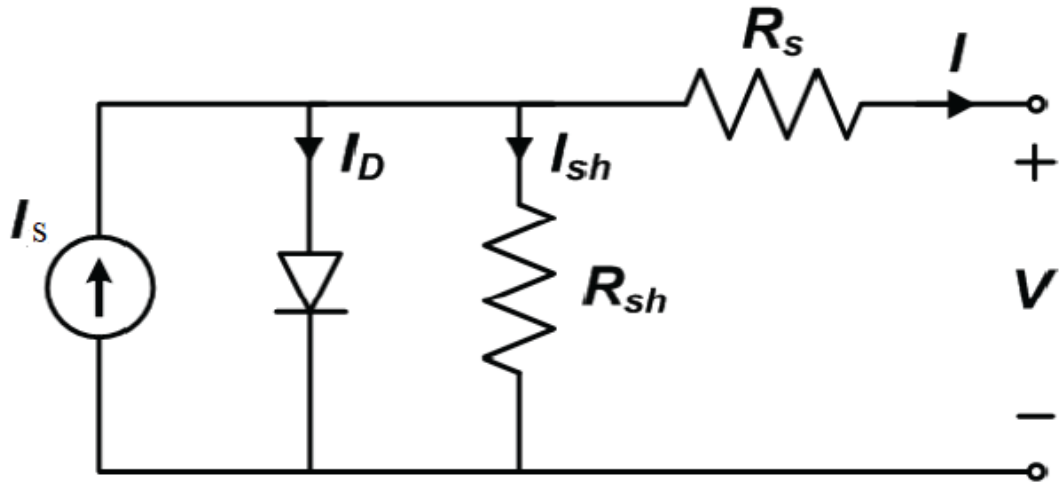

FIGURE 3.3: PRACTICAL EQUIVALENT CIRCUIT DIAGRAM [82]

Five parameters needed to be identified to solve the equivalent model. These are the current source (I_s), the diode saturation current (I_o), the series resistance (R_s), the parallel resistance (R_{sh}) and the ideality factor (a). These parameters can be obtained from the datasheet and the provided information from the solar cell manufacturer, as indicated by De Soto et al. [88]

3.2.2. CdTe STPV Optical Characteristics

After identifying the electrical characteristics of the integrated CdTe solar cells within the STPV samples, the different CdTe STPV glazing system's optical and thermal characteristics ought to be examined. The optical characteristics observe the glazing interaction with the solar irradiance. Under a conventional transparent glazing system, the glazing interaction with solar irradiance can be classified into three outcomes; primarily transmitted through the glazing into the indoor environment, a small fraction is absorbed within the fenestration of glazing layers as well and a small fraction is reflected [89]. However, the utilised samples have integrated CdTe solar cells would reduce the amount of the transmitted solar irradiance and increase the other two components [47]. In summary, the optical characteristics can be categorised into three distinctive values; these are transmittance, absorbance, and reflectance. These values are dependent on the incident angle, and the wavelength of solar irradiance [90]. These characteristics are obtained through experimental tests utilising a spectrometer, and the summation of them should equal unity [81], as shown in Equation 3.5 below.

$$\boldsymbol{\rho(\lambda,\theta)+\tau(\lambda,\theta)+\alpha(\lambda,\theta)=1} \qquad \textbf{EQUATION 3.5}$$

Where:

ρ: The reflected solar irradiance (unitless).

τ: The Transmitted solar irradiance (unitless).

α: The absorbed solar irradiance (unitless).

λ: The spectrum of the solar irradiance (nm).

θ: The incident angle of the solar irradiance (degree).

The fenestration of the STPV glazing systems is a crucial point that needs to be taken into consideration. Integrating opaque solar cells into the glazing, which is common in the c-Si STPV glazing systems, leads to inter-reflections within the glazing different layers. As a result, the effective transmitted and absorbed solar irradiance needs to be calculated. Contrary to implementing thin film solar cells as in a-Si and CdTe STPV glazing systems where the fenestration has transparent parts [47].

The optical characteristics and especially the transmitted and absorbed solar irradiance metrics are essential in quantifying part of the thermal characteristics, specifically the solar heat gain coefficient for the CdTe STPV glazing samples, which is going to be discussed below.

3.2.3. CdTe STPV Thermal Characteristics

The thermal attributes of CdTe STPV glazing samples are represented with two fundamental metrics: the Solar Heat Gain Coefficient (SHGC) and the Heat transfer coefficient (U-value).

3.2.3.1. Solar Heat Gain Coefficient (SHGC)

SHGC is a metric that depends on the optical characteristics of the CdTe STPV glazing systems, especially the values of the transmitted and absorbed solar irradiance [91]. Furthermore, SHGC is a unitless metric that quantifies the part of solar irradiance reaching the indoor environment through the glazing system, as well as a measurement for solar heat gain through the glazing structure [92]. SHGC can be calculated according to Equation 3.6 below [93].

$$\boldsymbol{SHGC(\lambda,\theta) = \tau(\lambda,\theta) + N * \alpha(\lambda,\theta)} \qquad \textbf{EQUATION 3.6}$$

Where:

τ: The Transmitted solar irradiance (unitless).

α: The absorbed solar irradiance (unitless).

λ: The spectrum of the solar irradiance (nm).

θ: The incident angle of the solar irradiance (degree).

$SHGC$: The Solar Heat Gain Coefficient (unitless).

N: The inward-flowing fraction of the absorbed radiation (unitless).

The inward-flowing fraction of the absorbed radiation (N) is a unitless ratio between the U-value and the external heat transfer in which both are measured in (W/m^2), $N = \frac{U}{h_e}$ [94].

3.2.3.2. Heat transfer coefficient (U-value)

The heat transfer coefficient (U-value) is a coefficient that calculates the transferred energy through the glazing system. The transferred energy occurred through the interchanging of irradiation and convective heat between the different sides of the glazing (the inner and outer surfaces) [95]. The heat transfer coefficient is dependent on the heat flux (W/m^2) and the temperature difference between the inner and outer surfaces of the glazing system (Kelvin) and it could be assessed by Equation 3.7 below [96]-[98].

$$\boldsymbol{U = \frac{Q}{\Delta T}} \qquad \textbf{EQUATION 3.7}$$

Where:

U: the heat transfer coefficient (W/m^2.K)

Q: The heat flux (W/m2)

ΔT: The temperature difference between the inner and the outer surface of the glazing system (Kelvin).

3.3. Indoor Experimental Set-Up

In this section, the indoor testing setup is going to be discussed in detail. First, the enclosed testbed details and literature background. Following that, the configuration of the solar simulator that had been designed to evaluate the overall energy performance of the testbed would be highlighted. Furthermore, the equipment that has been utilised to characterise the various CdTe SPTV glazing samples are listed with sample data for the transparent single glazing sample (SG1).

3.3.1. Enclosed Testbed Setup

To investigate the impact that CdTe STPV glazing systems could have on the overall energy performance, a series of experimental tests identify the key attributes of these systems. A key component for these tests is an enclosed testbed, and the employed enclosed testbed is based on the Guarded Hot Box developed by Fung et al. [99] and the Mobile Window Thermal Test (MoWiTT) developed by Robinson and Littler [100].

3.3.1.1. Guarded Hot Box and Mobile Window Thermal Test

Guarded hot box is an experimental setup that has been developed to measure the U-value for a certain sample. The Guarded hot box contains three divisions: the guard box and the metering box, and the sample that is going to be tested is placed between the cold box and the metering box. The cold aims to manage low temperatures representing the operated cooling system. As for the guard box, it isolates the metering box and aims to control the temperature and maintain it at passable levels to minimise heat losses. Finally, the metering box holds a heater, which facilitates the transfer of heat from the metering box to the cold one through the tested sample [99] as shown in Figure 3.4 below.

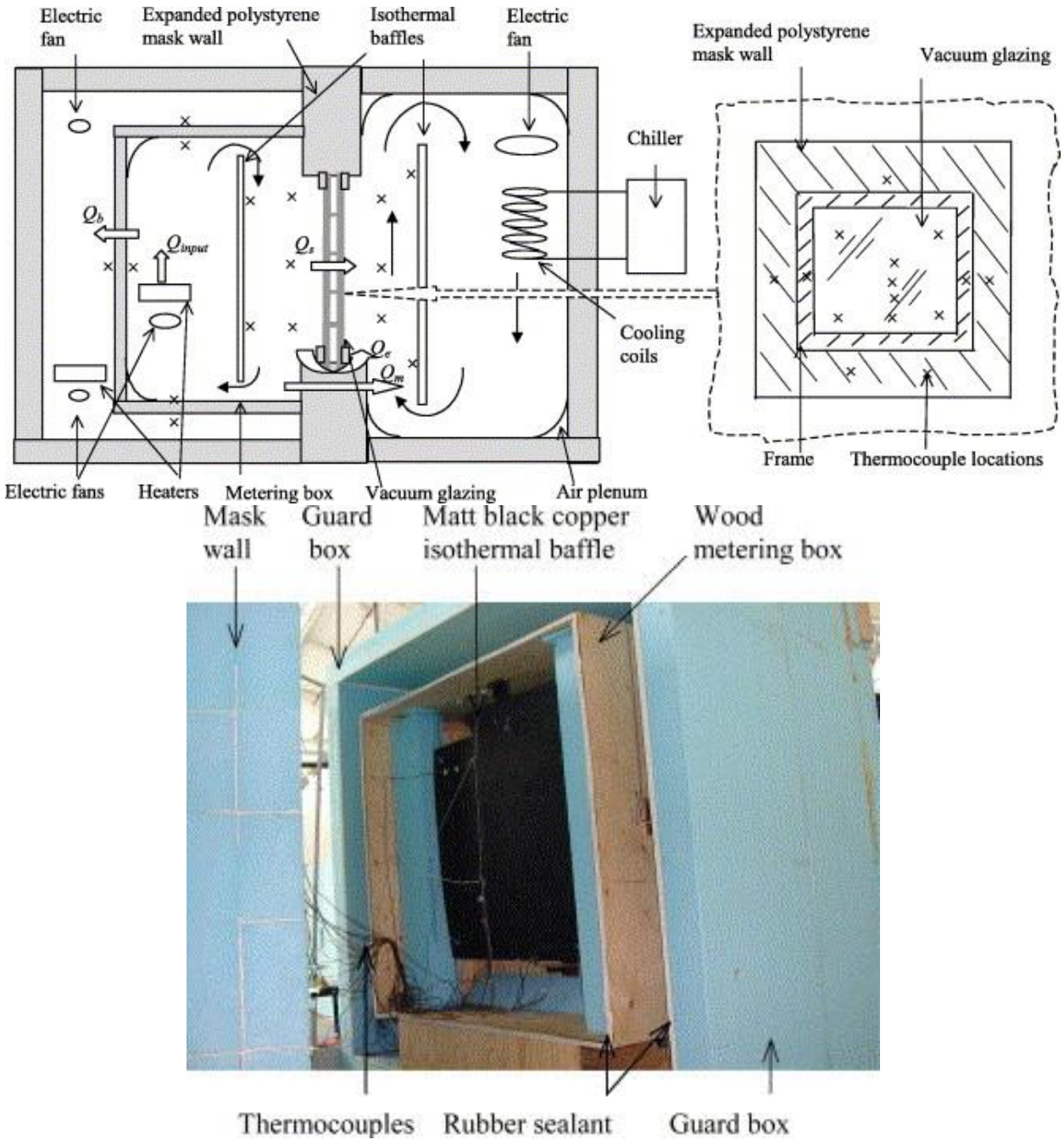

FIGURE 3.4: GUARDED HOT BOX [99].

The Mobile Window Thermal Test (MoWiTT) is an experimental setup that aims to measure the U-value similar to the Guarded hot box. In contrast, the MoWiTT provides the ability to investigate the impact the surrounding environment could have on the thermal performance of the tested sample in practice, and Figure 3.5 below shows the concept design of the Mobile Window Thermal Test (MoWiTT) [100].

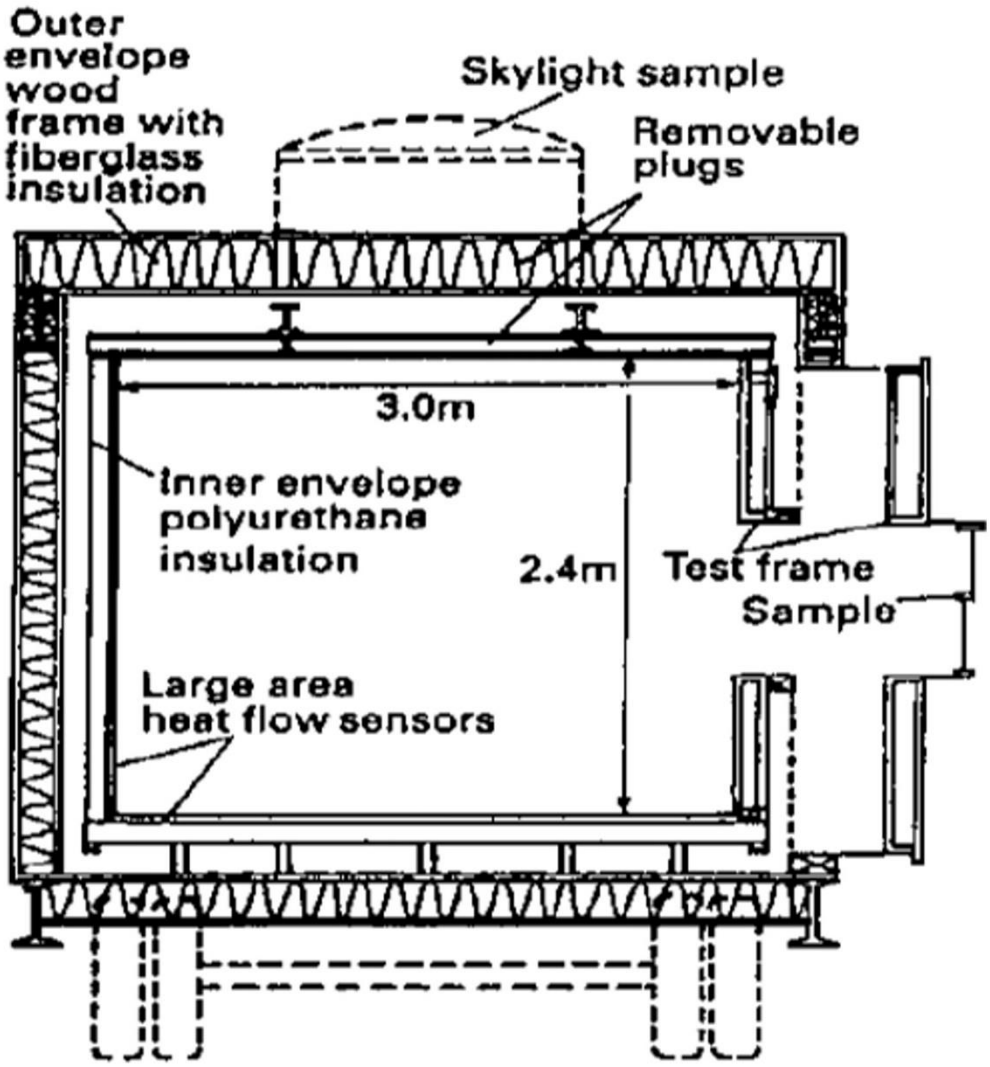

FIGURE 3.5: MOBILE WINDOW THERMAL TEST (MOWITT) [100].

3.3.1.2. Research Enclosure Testbed Setup

Enclosure testbed setups are utilised to conduct a series of experimental tests while controlling the indoor environment temperature by managing the heating and/or cooling systems within the testbed. The literature has shown the outcome data of these tests are reliable regardless of the size of the enclosure, whether the enclosure is a real-size testbed or a scale-down testbed such as the one utilised in this research [101]-[103].

3.3.1.2.1. Enclosure Testbed Attributes

The enclosure testbed was developed to conduct a series of tests which entailed collecting the required data to build the electrical, thermal, and optimal profiles of the different CdTe STPV samples. These tests were performed in the power and transmission lab located in the Sheaf Building, Sheffield Hallam University, Sheffield, United Kingdom. Furthermore, the experimental tests were performed under a controlled setting and specifically under standard testing conditions

(STC); where the ambient is 25°C, the air mass is 1.5, the wind speed is 1 m/s, and the solar irradiance is 1000 W/m^2. The temperature is controlled by a central heating system that is implemented in the building, whereas the air mass and the wind speed are controlled through a mechanical ventilation system. Finally, a solar simulator has been developed to provide consistent solar irradiance.

As for the testbed itself, the enclosure was equipped with thermo-electric coolers (Peltier unit) to maintain the ambient temperature inside it, which is shown in Figure 3.6 below, and Table 3.3 shows the Peltier electrical and physical characteristics below as well.

FIGURE 3.6: THERMO-ELECTRICAL COOLER (PELTIER UNITE)

TABLE 3.3: PELTIER'S PHYSICAL AND ELECTRICAL CHARACTERISTICS

Specification	Data
Dimensions	0.2 m * 0.15 m * 0.15 m
Weight	0.44 kg
Structure	Aluminium
Voltage	12 V DC
Current	2 A DC

The enclosure testbed dimensions are 0.3 m * 0.3 m * 0.225 m, constructed utilising Polyisocyanurate laminated with aluminum foil which is considered a well-insulated cooler/warmer

material. The utilised materials were selected to ensure that the thermal disturbances could be neglected. The physical attributes of the enclosure testbed are listed in Table 3.4, whereas the schematic diagram and the developed enclosure testbed are shown in Figure 3.7, and Figure 3.8 shows the developed testbed with three installed pelters units and two thermo-coupler, one to measure the indoor environment and the other is to control the when the Peltier's are operating.

TABLE 3.4: ENCLOSURE TESTBED PHYSICAL PROPERTIES

PHYSICAL PROPERTIES	Data
Dimensions	0.3 m * 0.3 m * 0.255 m
Glazing Area	0.0324 m^2
Structure Materials	Polyisocyanurate laminated with aluminum foil
Wall thickness	0.6 m

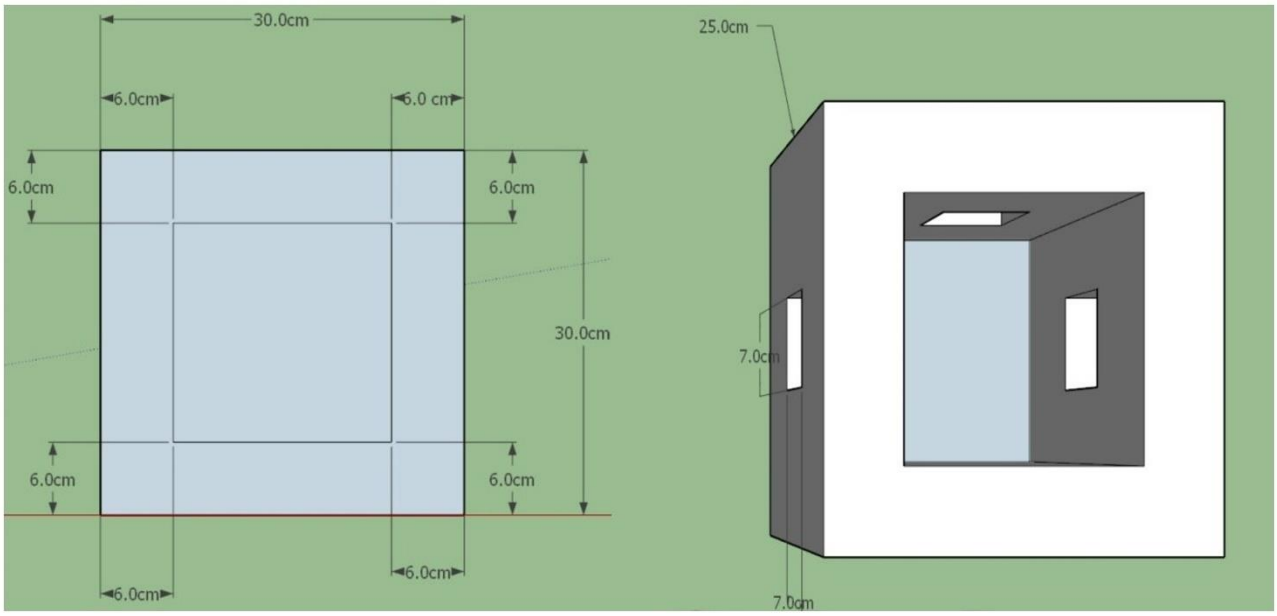

FIGURE 3.7: THE SCHEMATIC DIAGRAM OF THE ENCLOSURE TESTBED

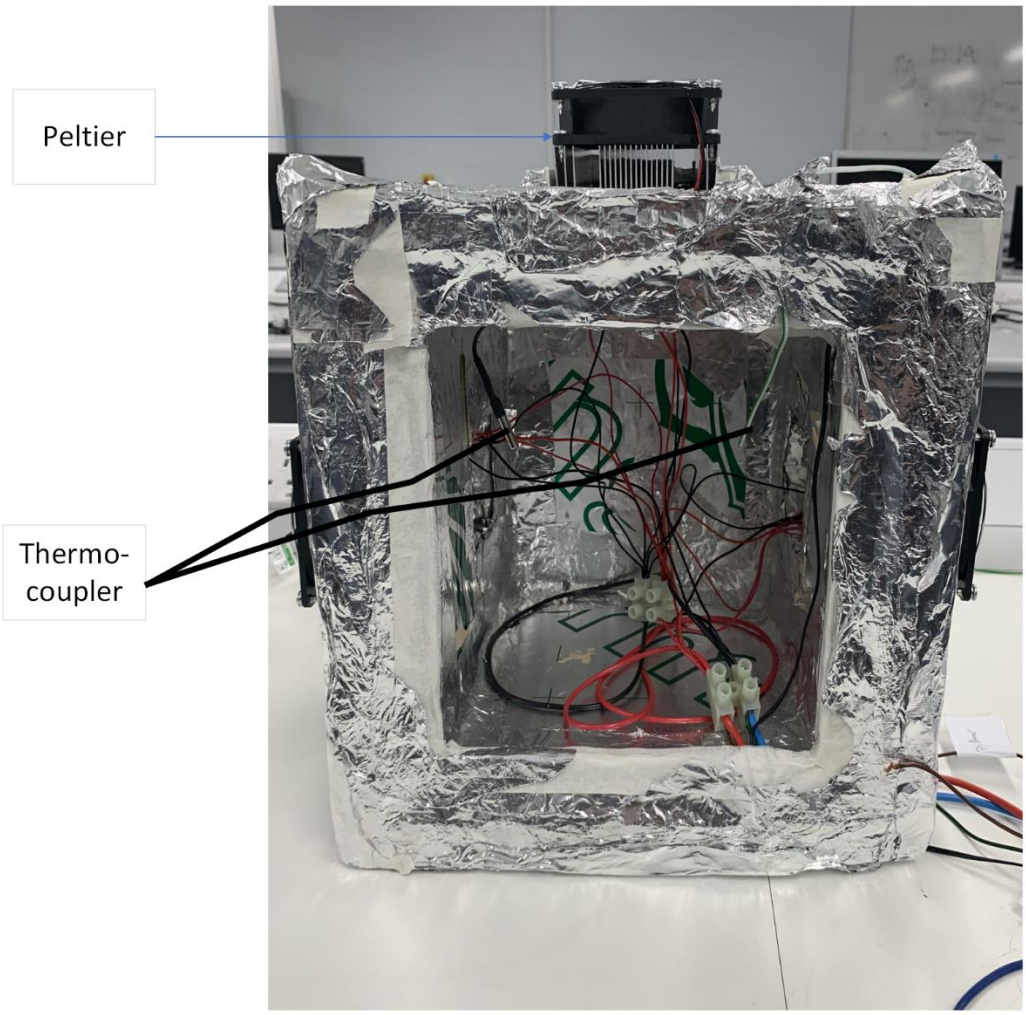

FIGURE 3.8: THE DEVELOPED ENCLOSURE TESTBED

3.3.2. Solar Simulator

As stated above, the experimental tests have been conducted in a lab setting and under controlled conditions. One of these requirements is providing a constant volume of solar irradiance which was 1000 W/m^2 and as a result, a solar simulator was developed.

Due to the limited area of the research space of the lab, a modified solar simulator needed to be introduced to follow the full movement of the sun during the day, which is shown in Figure 3.9 below. To achieve constant solar irradiance while maintaining a similar movement, the developed solar simulator was split into two components. First, the sun simulator, which is the stationary part, consists of nine halogen lamps bolted into a frame and the illuminations of these lamps are controlled by a transformer, which is shown in Figure 3.10.

The second part is the movement simulator, which is a flat plate that moves in two axes. The movement is powered by two DC motors, an Electrical linear actuator (RS PRO Miniature 1774499) which moves vertically, helped by a spherical ball joint installed below the flat plate, and a Geared DC motor (111.3763.20.00E) which operates in an angular manner. A control unit operated by the data logger (NI cDAQ-9178) has been installed. This unit contains two DC-Motor Drivers (EM-174A) with an internal DC power supply (RSP-75-3.3) and multiple potentiometers to control the speed of

both motors in case the unit is operated manually. The movement simulator components are listed in Table 3.5 below.

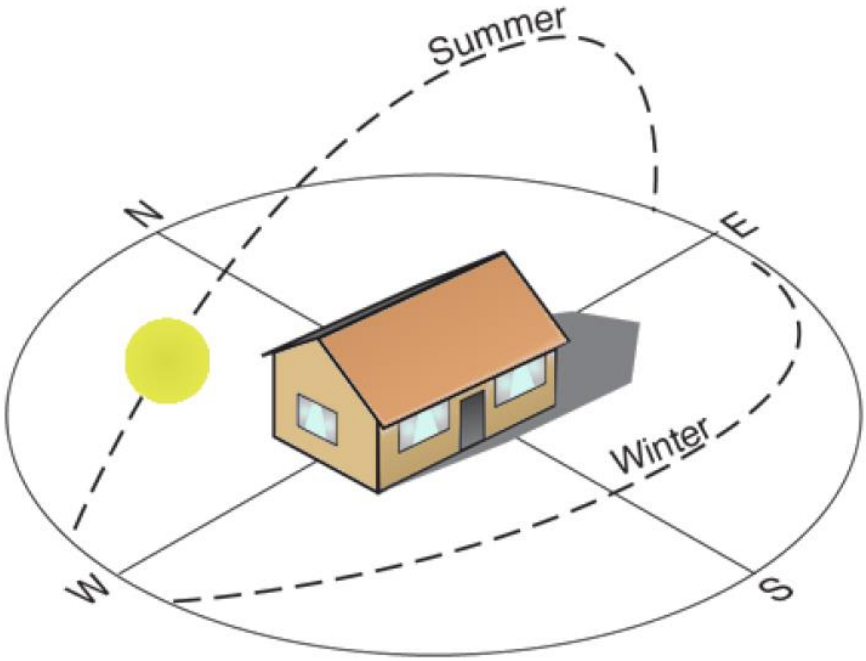

FIGURE 3.9: THE SUN'S PATH THROUGH THE DAY

FIGURE 3.10: THE SUN SIMULATOR

TABLE 3.5: MAIN COMPONENTS OF THE MOVEMENT SIMULATOR

Component	Manufacturer information	Specification
Geared DC Motor	DOGA 111.3763.20.00E	12 Vdc, 25 RPM, 6 Nm
Electrical Linear Actuator	RS PRO Miniature 1774499	24 Vdc, 4500 N, 305 mm
DC Power Supply	RSP-75-3.3	220 Vac/ 3.3 Vdc
Motor Driver	EM-174A	12/24 Vdc, 8 A

The figures below show the different parts of the movement simulator. Figure 3.11 shows the internal components of the control unit frame, which contain two DC Motor Drivers with a DC power supply. Whereas Figure 3.12 shows the linear actuator, rotating motor, and the special ball joint. Figure 3.13 shows the utilised data logger in the experiments. Finally, Figure 3.14 shows the fully developed solar simulator that will be utilised in this research.

FIGURE 3.11: CONTROL UNIT COMPONENTS

FIGURE 3.12: THE ELECTRICAL LINEAR ACTUATOR, GEARED DC MOTOR, AND SPHERICAL BALL JOINT

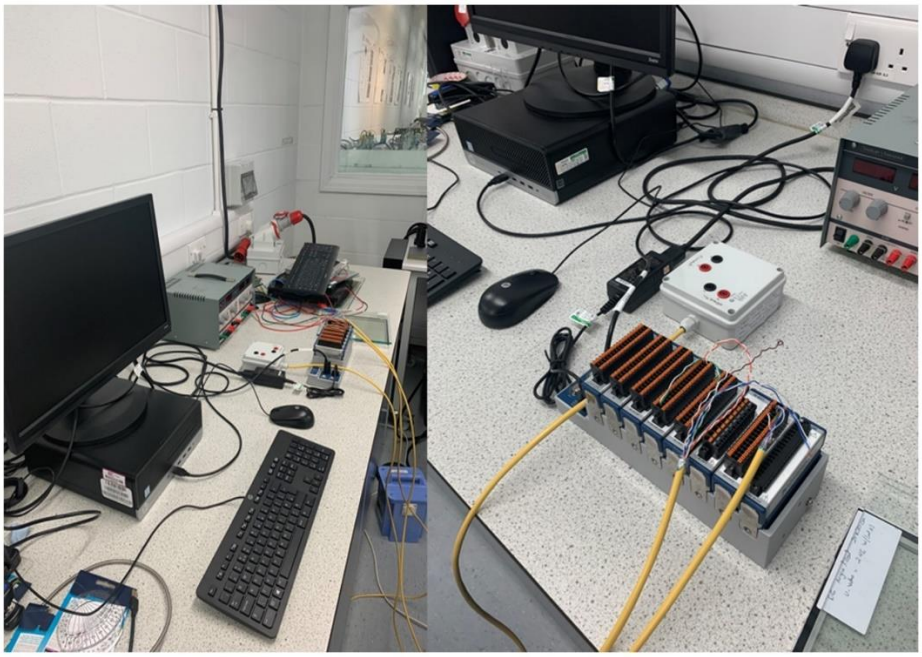

FIGURE 3.13: NI CDAQ-9178 DATA LOGGER CONNECTED TO PC AND THE MOVEMENT SIMULATOR

FIGURE 3.14: SOLAR SIMULATOR

3.3.3. Testing Setup and Sample Data

In this section, the implemented testing setups will be discussed, and sample data will be presented here. The testing setups are divided into three main sets:

- Electrical testing setup, which generates the I-V and P-V curves for the integrated CdTe solar cells within the CdTe STPV glazing samples.
- Optical testing setup, which provides the three optical characteristics of STPV glazing samples transmittance, reflectance, and absorbance of solar irradiance.
- Thermal testing setup, which aims toward calculating the U-value metric for the various glazing samples.

Furthermore, a transparent single-glazing sample (SG1) was used as an initial test subject to ensure that all the testing setups worked correctly. These results are going to be presented below.

3.3.3.1. Electrical Characterisation Testing Setup

The Electrical Characterisation Testing Setup aims to identify the electrical characteristics of the CdTe STPV glazing samples. These characteristics are presented by the I-V and P-V curves. These curves help identify the maximum power generated, the efficiency of each sample, and the fill-factor as well, which all of these have been discussed in-depth in section 3.2.1.

The solar simulator, along with two digital multi-meters and a potentiometer (0-1kΩ), were employed to generate the I-V and P-V curves. The solar simulator aims to deliver a constant solar irradiance equal to 1000 W/m^2, whereas the digital multi-meters record the output current and voltage. The potentiometer facilitates transiting the test from the short circuit condition to the open circuit condition.

Figure 3.15 shows the Electrical Characterisation Testing Setup for sample S1. The SG1 sample was not used due to the lack of solar cell materials in its fenestration.

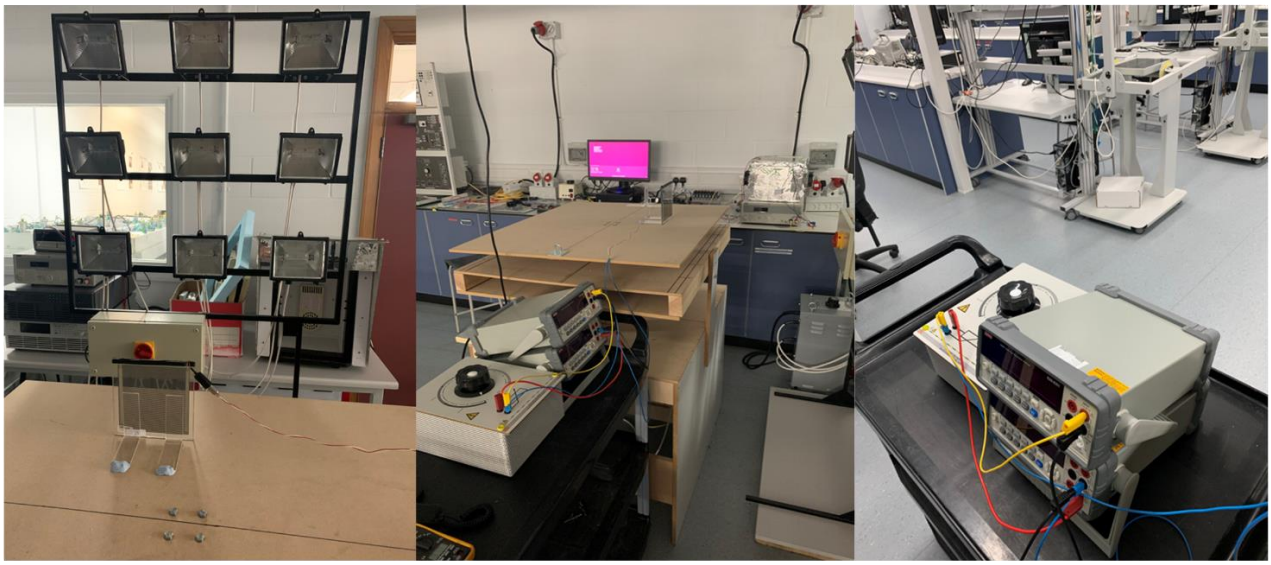

FIGURE 3.15: ELECTRICAL CHARACTERISATION TESTING SETUP

The output results of the Electrical Characterisation Testing Setup for sample S1 is listed in Table 3.6, where the MPP is reached when the potentiometer is equal to 200Ω. The current and the voltage at the MPP are 83.34 mA, and 6.05 V, respectively. Thus, the maximum output power is 504.21 mW according to Equation 3.2, and the electrical efficiency (η) is 0.02 according to Equation 3.1. Whereas Figure 3.16 shows the I-V and P-V curves for sample S1.

TABLE 3.6: ELECTRICAL CHARACTERISTICS OF S1

R	I (mA)	V (Volt)	P (mW)
Short Circuit	122.10	0.07	8.67
1	121.26	0.12	14.55
2	120.90	0.15	18.14
3	120.60	0.22	26.53
5	120.60	0.30	36.18

10	120.00	0.57	68.40
20	118.50	1.12	132.72
30	117.57	1.42	166.95
50	114.00	2.28	259.92
100	104.85	3.84	402.62
200	83.34	6.05	504.21
300	66.57	7.47	497.28
500	47.34	8.77	415.17
1000	27.96	9.53	266.46
Open Circuit	0.00	10.17	0.00

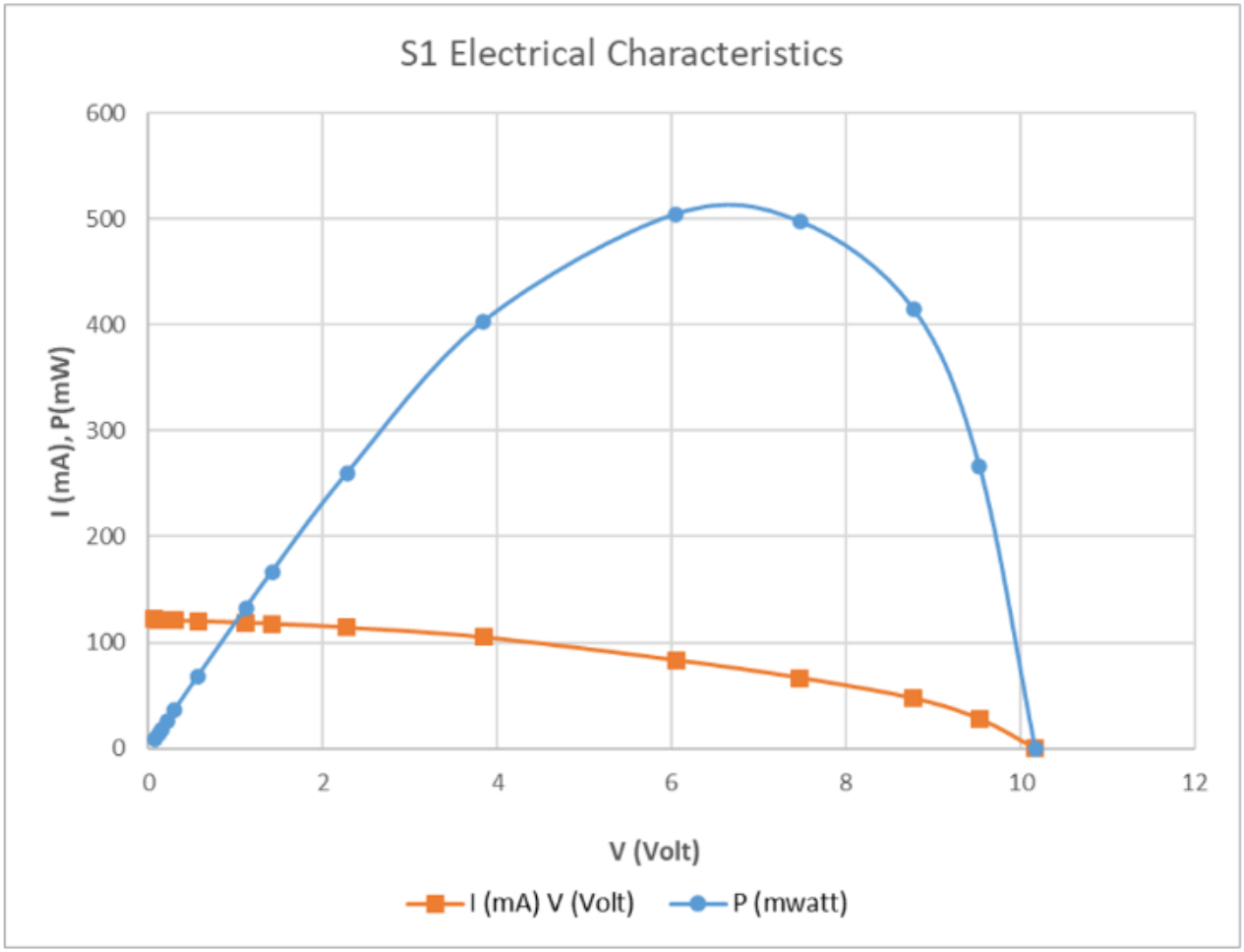

FIGURE 3.16: THE I-V AND P-V CURVES FOR S1

3.3.3.2. Optical Characterisation Testing Setup

The optical characteristics of a glazing sample are identified by how this sample interacts with the solar irradiance. As stated in the section 3.2.2, with a conventional transparent glazing sample, most of the solar irradiance is transmitted through the sample into the indoor environment, while a fraction of the solar irradiance is absorbed by the fenestration of the sample. Similarly, a fraction of solar irradiance is reflected by the sample fenestration.

In summary, there are three optical characteristics:

- The transmittance of the glazing sample.
- The absorbance of the glazing sample.
- The reflectance of the glazing sample.

And the summation of these three attributes is unity, according to Equation 3.5. In order to acquire this data, a spectrometer from Avantes (Avaspec-ULS-EVO-RS) that covers 200-1100 nm wavelength along with a Lightsource (Avalight-DHc), which provides deuterium light and halogen light sources that deliver 200-2500 nm wavelength were used, and the Avasoft software recorded the results. Figure 3.17 shows the optical characterisation testing setup, and Figure 3.18 shows the SG1 sample being tested at 0° angel.

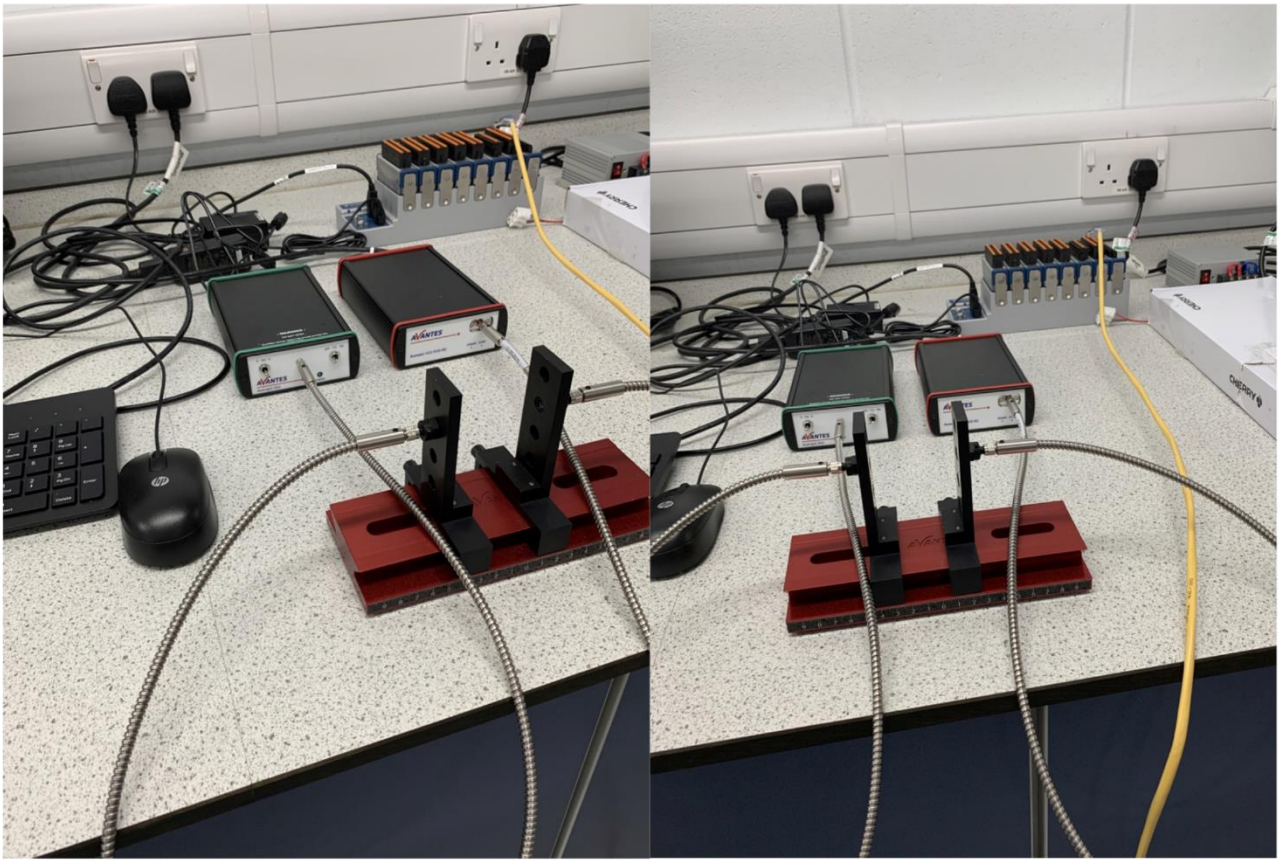

FIGURE 3.17: SPECTROMETER (AVASPEC-ULS-EVO-RS) ALONG WITH A LIGHTSOURCE (AVALIGHT-DHC)

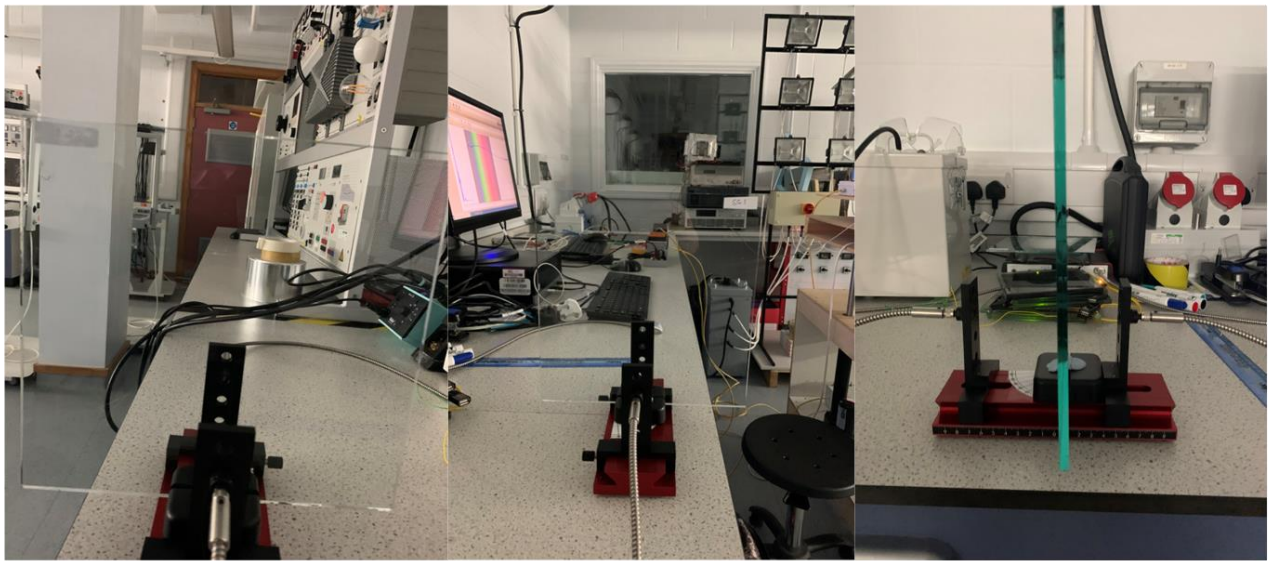

FIGURE 3.18: THE OPTICAL CHARACTERISATION TESTING FOR SG1 AT 0°

Each sample has been subjected to multiple iterations of the optical testing under different incident angles, specifically from 0° to 40° due to the testing setup limitation.

The results of the optical characterisation testing for SG1 are shown in Figure 3.19 and Figure 3.20. The absorbance ability is measured in the Absorbance Unit. Absorbance Unit is an industrial metric scaled from 0-5, where 0 indicates that the glazing sample does not absorb any fraction of the solar irradiance, whereas 5 indicates the glazing sample is opaque and absorbers the whole solar irradiance.

The results indicate that the average transmittance ability for the SG1 sample under the visible light spectrum (380-780) nm is 81.09%, whereas the average absorbance ability for the SG1 sample under the visible light spectrum is 17.26%. The reflectance ability for the SG1 sample under the visible light spectrum is 1.65%, according to Equation 3.5.

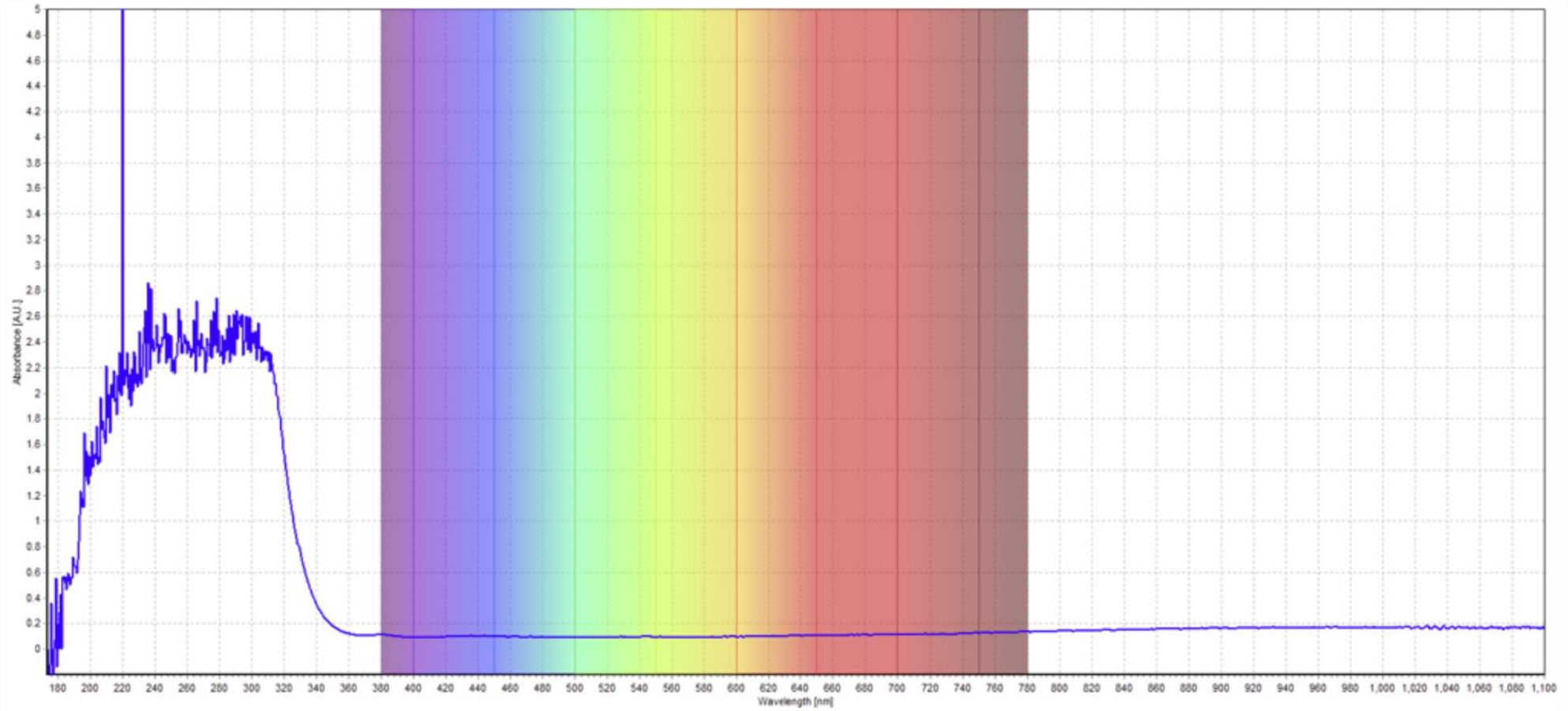

FIGURE 3.19: SG1 ABSORBANCE ABILITY RESULT (A.U)

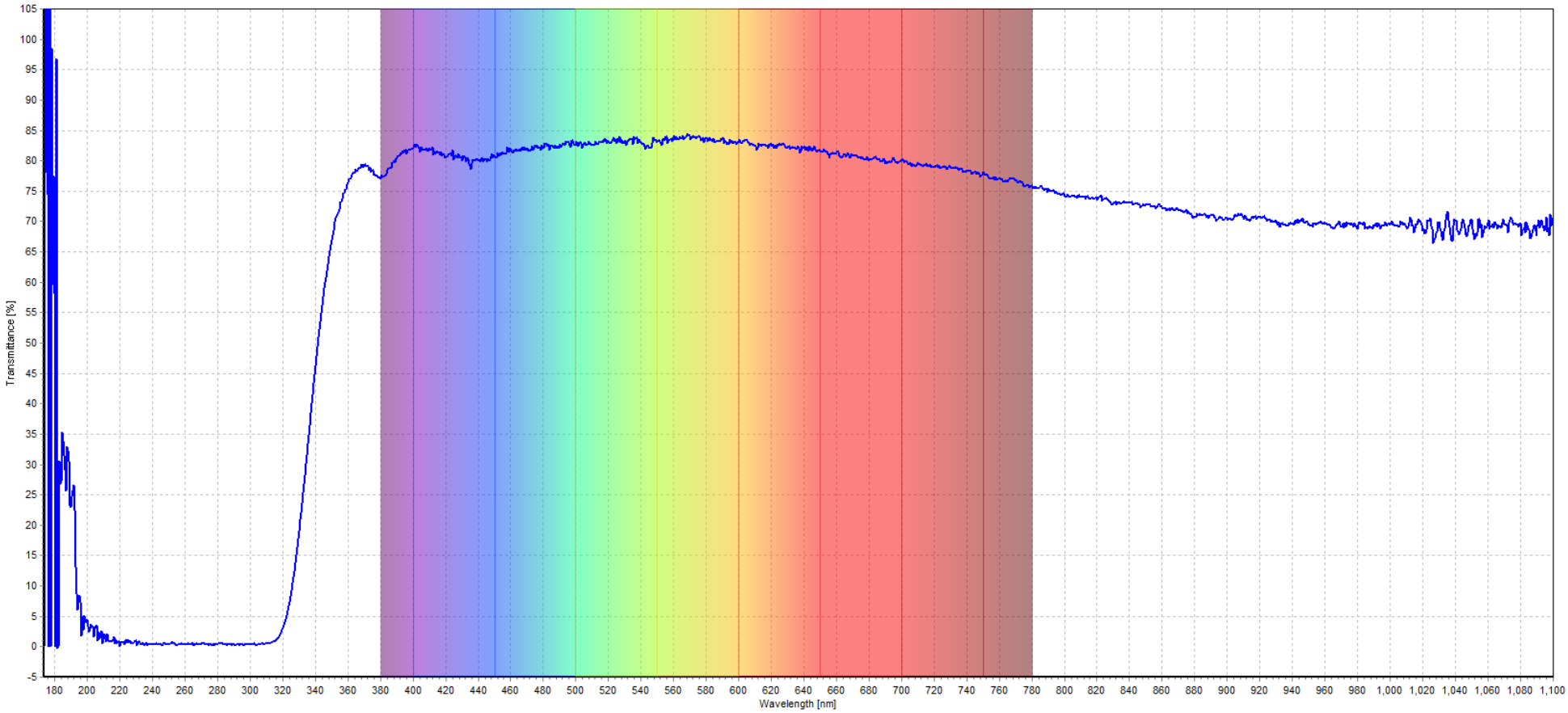

FIGURE 3.20: SG1 TRANSMITTANCE ABILITY RESULT (%)

3.3.3.3. Thermal Characterisation Testing Setup

The Thermal Characterisation Testing Setup aims to identify the thermal characteristics of the CdTe STPV glazing samples. These characteristics are presented in the U-value and SHGC metrics.

3.3.3.3.1. SHGC Characterisation Testing Setup

The SHGC is dependent on the transmittance and absorbance abilities of the glazing samples, which has been discussed in-depth in section (3.2.3). The tests were going to be conducted under the visible light spectrum using the light source (Avalight-DHc) of the spectrometer (Avaspec-ULS-EVO-RS) that is used in the optical characterisation testing setup. However, each sample has been subjected to multiple iterations of the optical testing under different incident angles, from 0° to 40°.

Figure 3.21 and Figure 3.22 show the transmittance and absorbance results for the SG1 sample under the condition of being subjected to visible light spectrum under different incident angles. The average value of the outcome results of the transmittance tests for the SG1 sample is 74%, whereas the average value of the absorbance tests for the SG1 sample is 15.81%.

These results are utilised in calculating the SHGC metric according to Equation 3.6, as for the inward-flowing fraction of the absorbed radiation (N) it was dependent on the work of Collins and Harrison [104]. The average SHGC for the SG1 sample is 0.77, and Figure 3.23 shows the output value of the SHGC metric for the SG1 sample at each incident angle that has been tested.

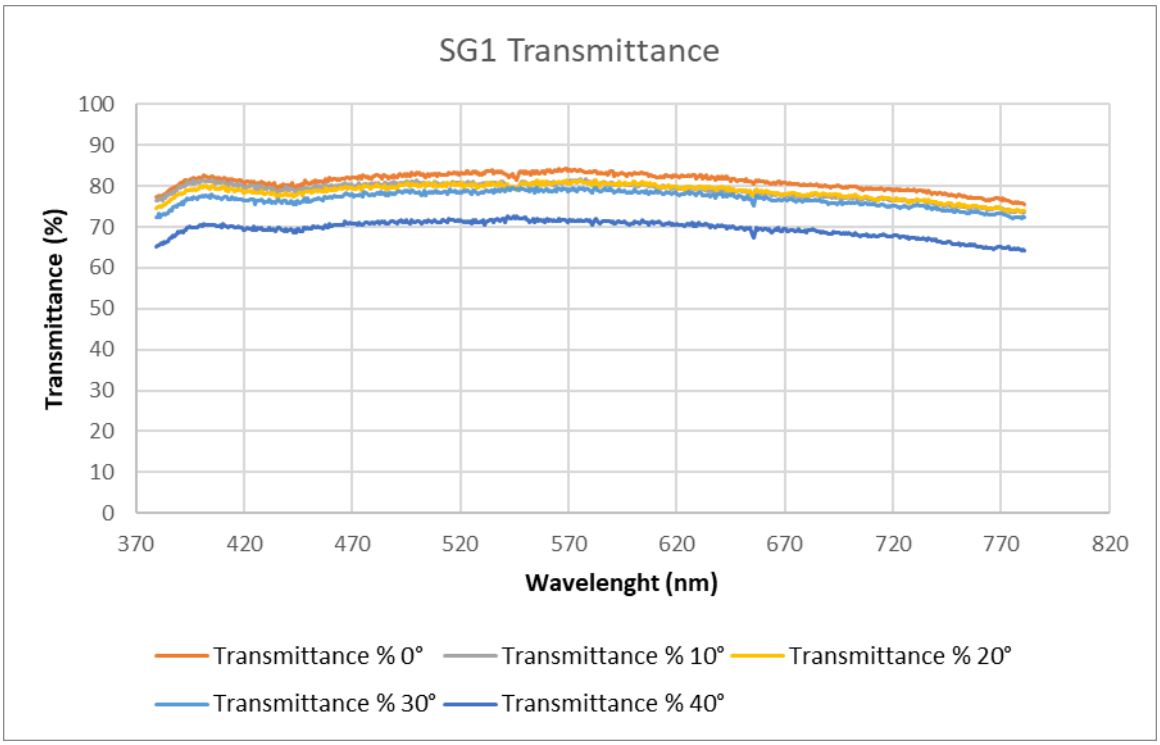

FIGURE 3.21: THE TRANSMITTANCE RESULTS FOR SG1 UNDER DIFFERENT INCIDENT ANGLES

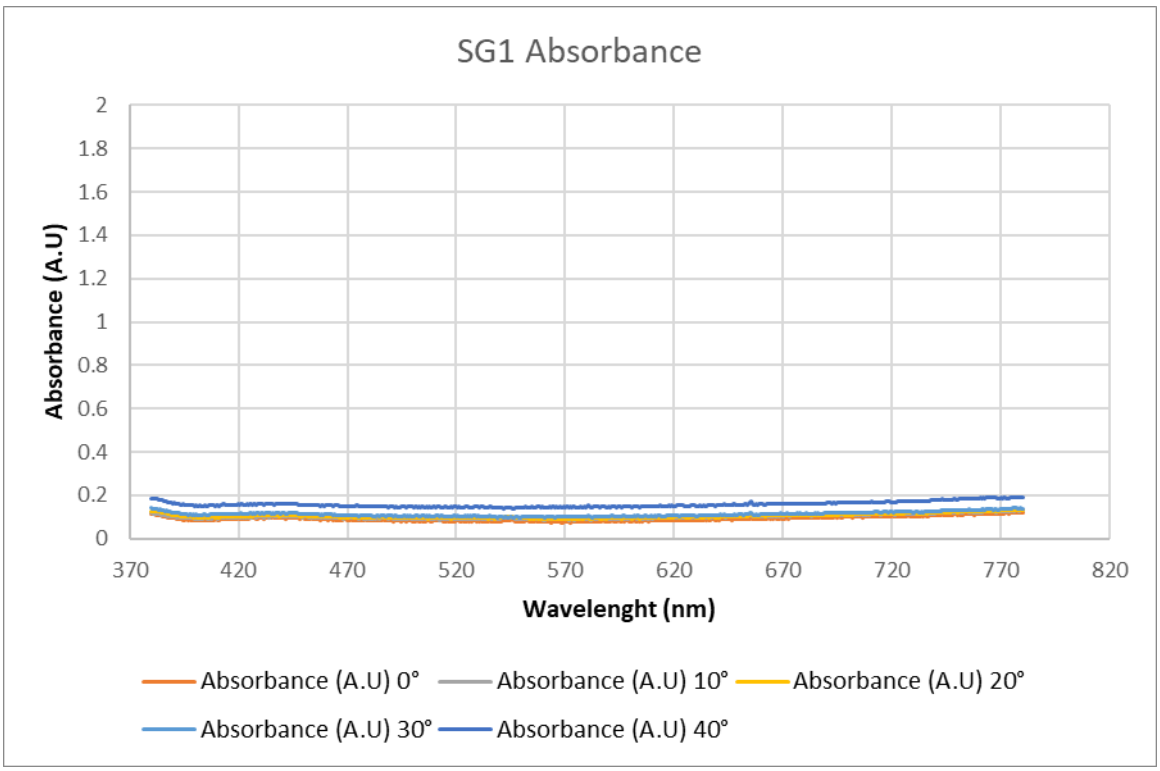

FIGURE 3.22: THE ABSORBANCE RESULTS FOR SG1 UNDER DIFFERENT INCIDENT ANGELS

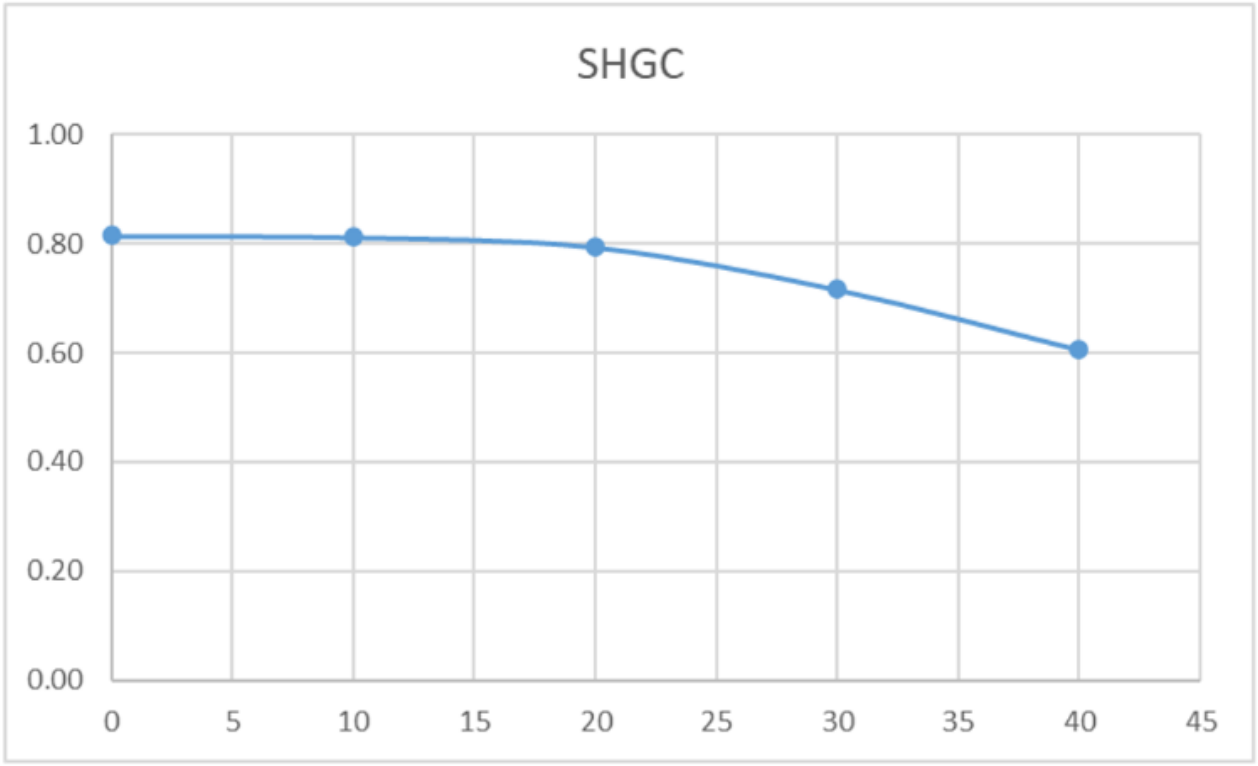

FIGURE 3.23: SHGC FOR SG1 UNDER DIFFERENT INCIDENT ANGELS

3.3.3.3.2. U-value Characterisation Testing Setup

In order to measure the U-value of the different glazing samples, the value of the heat flux, the inner surface temperature as well as the outer surface temperature need to be quantified. In order to acquire these values a specialised kit from greenTEG (g-SKIN U-VALUE KIT 2615C) which consists of a heat flux sensor, two thermocouple sensors, and a data logger that are shown in Figure 3.24. The collected data from the experiments are transferred by the data logger to a specialised software called greenTEG Logger 1.02.10 to analyse it.

FIGURE 3.24: G-SKIN U-VALUE KIT 2615C

Figure 3.25 shows the practical setup utilised in the experiment to measure the U-Value metric for the different glazing samples. It is worth mentioning that the Peltier units were used to ensure that the enclosure testbed ambient temperature was higher than the lab ambient temperature to facilitate the heat flux from the indoor environment to the outdoor one through the glazing sample similar to Fang et al [99] work.

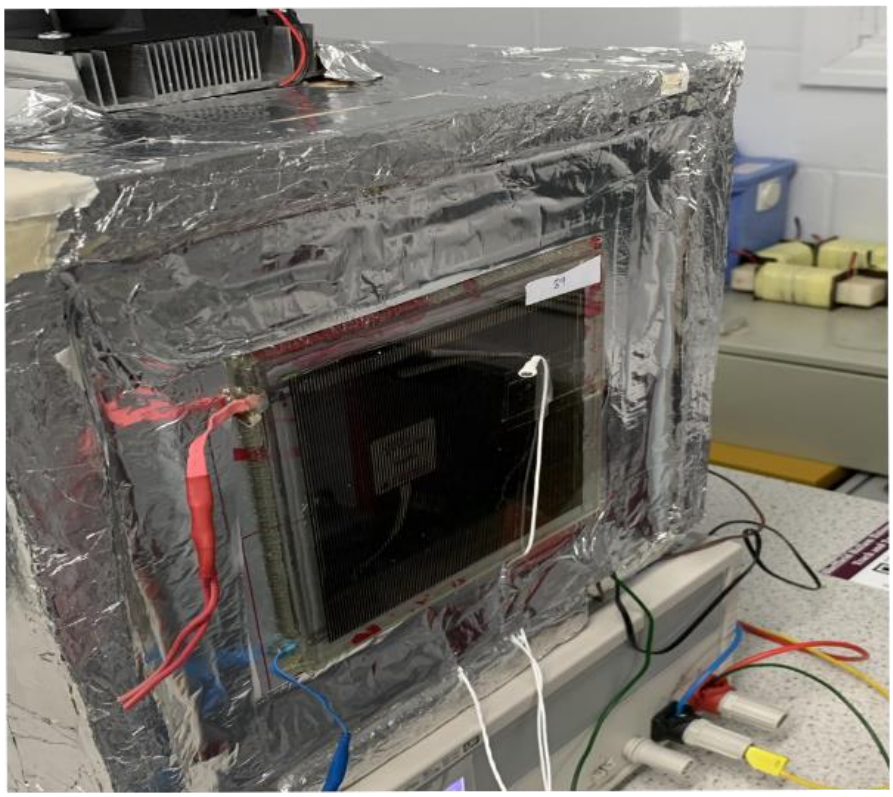

FIGURE 3.25: THE PRACTICAL SETUP OF U-VALUE MEASUREMENT FOR STPV SAMPLE

Figure 3.26 shows the results of the U-value experiment for the SG1 sample. The average value for the heat flux is -23.58 W/m^2 whereas the negative value is an indication of the heat transfer direction (indoor to outdoor). The average values of inner and outer surface temperatures are 27.59°C, and 23.81°C respectively. Applying the average values in Equation 3.7 would provide the U-Value of the SG1 sample, which is 6.24 W/(m^2.K).

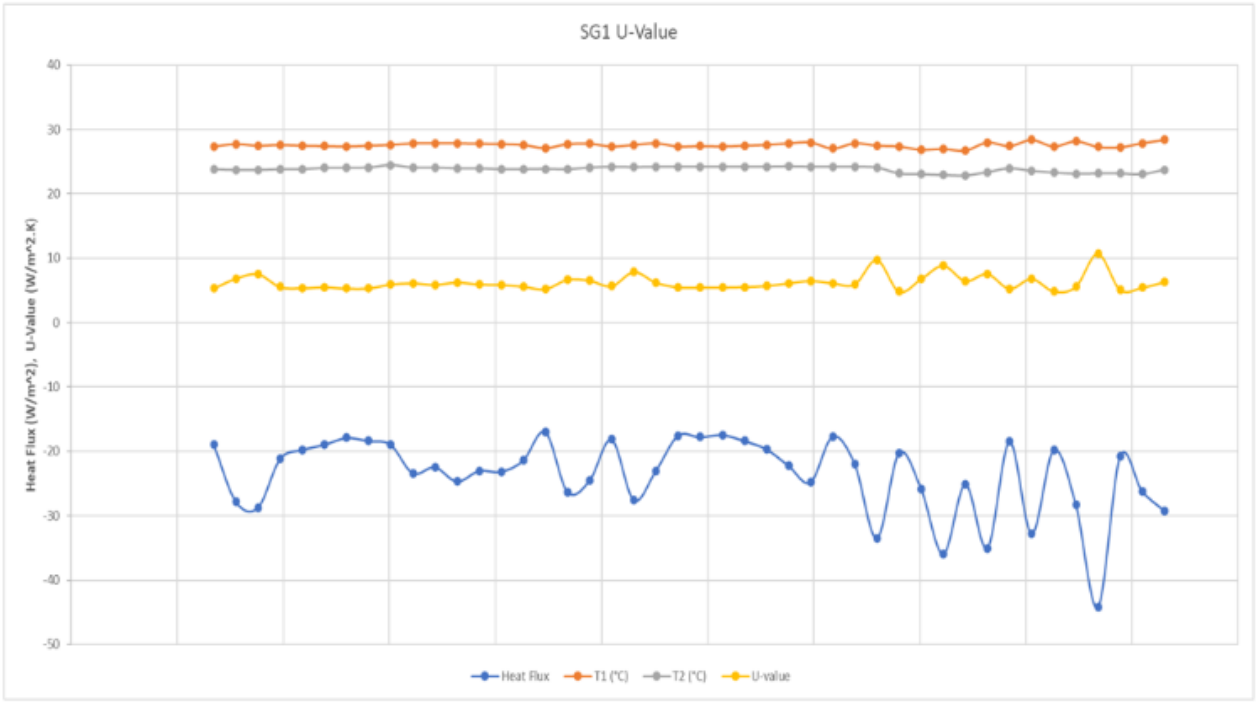

FIGURE 3.26: THE U-VALUE RESULT OF THE SG1 SAMPLE

CHAPTER 4
CHARACTERISATION RESULTS

4. Characterisation Results

In this chapter the electrical, thermal, and optical attributes of the glazing systems samples that have been highlighted in Table 3.1 and Table 3.2 are quantified, through the experimental approach outlined in chapter 3 to be utilised in the overall energy performance analysis.

The characterisation process for the reference points is going to include profiling the optical and thermal attributes of the glazing samples, unlike the STPV glazing systems there are no electrical characterises due to the lack of solar cell materials in these glazing systems.

4.1. Optical Characterisation

As has been illustrated in Chapter 3, section3.2.2; there are three optical traits. These traits are transmittance, absorbance, and reflectance where the summation of these three equals unity.

The optical tests were conducted at different angles (0°- 40°) to determine the optical characteristics of the glazing samples. These tests measured the transmitted and absorbed solar irradiance metrics, which are essential in quantifying the solar heat gain coefficient. As for the reflectance attributes for the glazing samples, Equation 3.6 were used to calculate it.

The analysis of the optical results will focus on the wavelength from (370-780) nm which covers the visible light wavelength, which is essential for the thermal and optical analysis of the STPV glazing system [95]-[98].

4.1.1. Referencing Glazing

In this research, three reference points are going to be utilised (DG1, DG2, DG3), which are shown in the Figure 4.1 below.

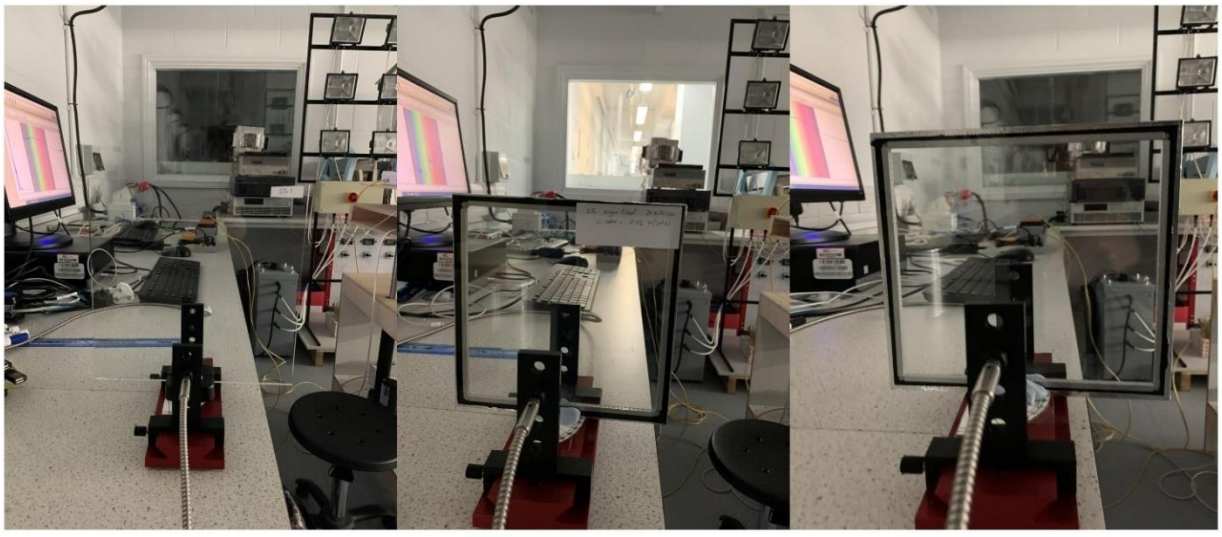

FIGURE 4.1: REFERENCING POINTS, FROM LEFT TO RIGHT, SG1, DG2, DG1

The optical test results for the referencing points SG1, DG1, and DG2 are shown in the Figure 4.2 , Figure 4.3 and Figure 4.4 respectively.

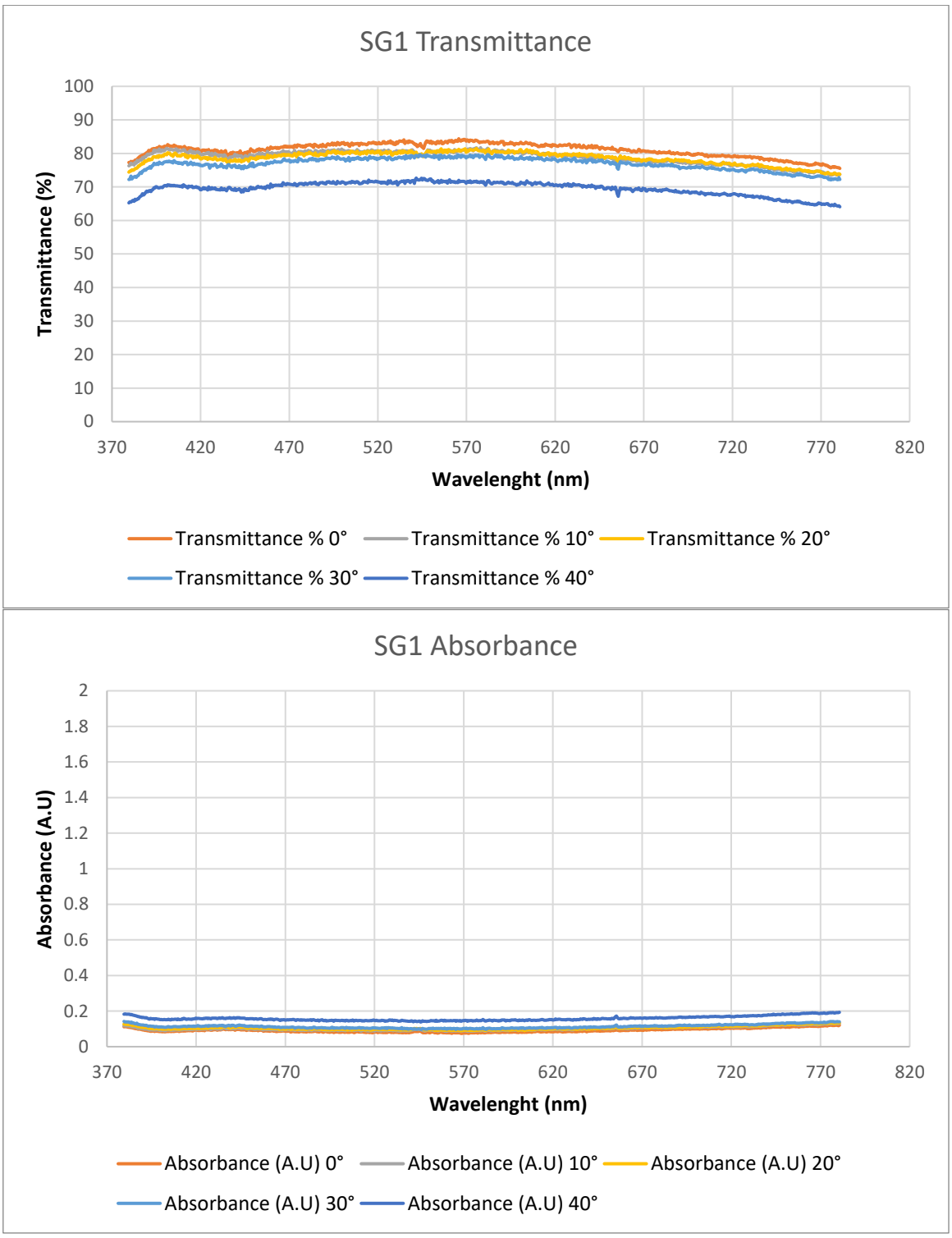

FIGURE 4.2: SG1 TRANSMITTANCE AND ABSORBANCE

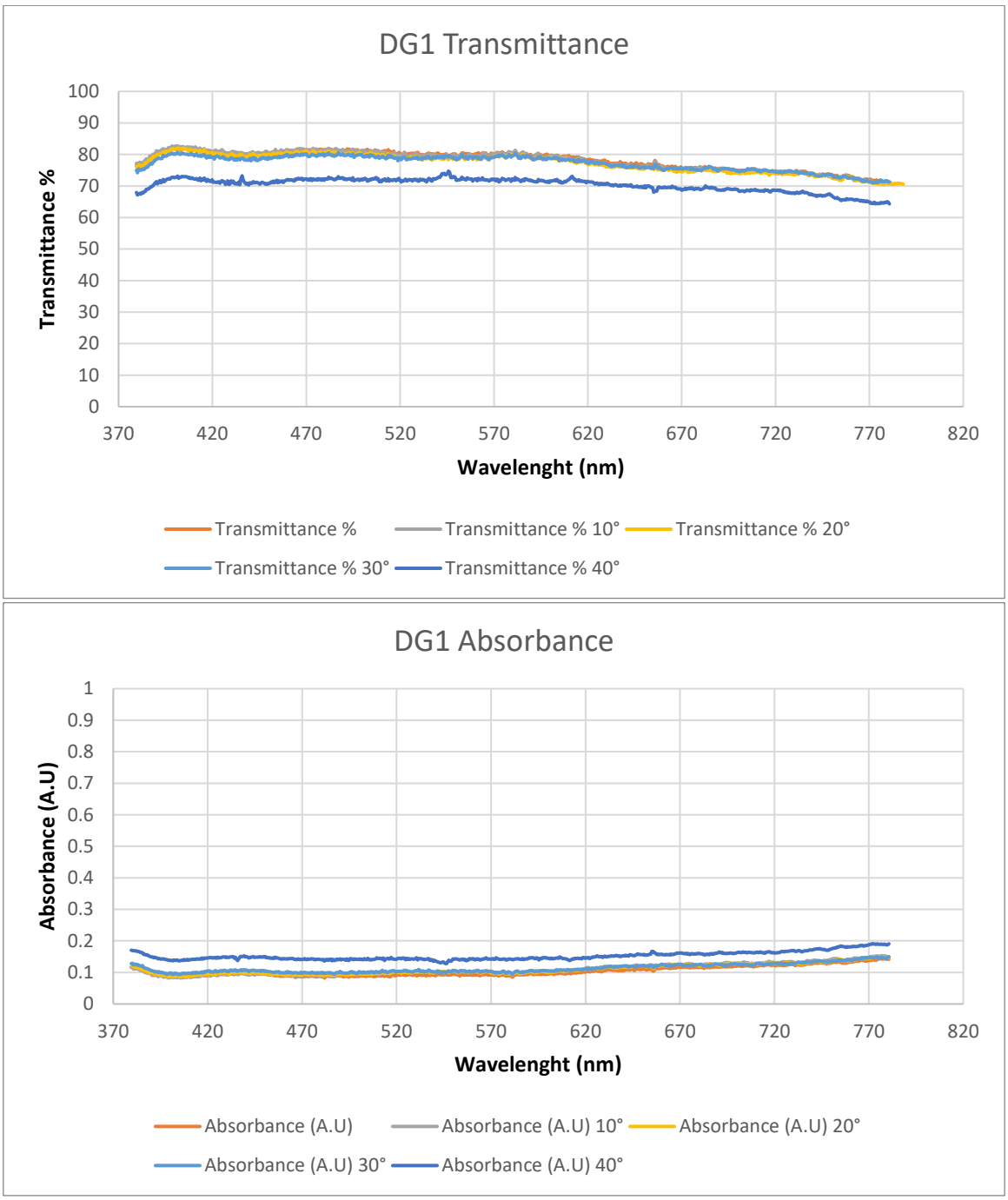

FIGURE 4.3: DG1 TRANSMITTANCE AND ABSORBANCE

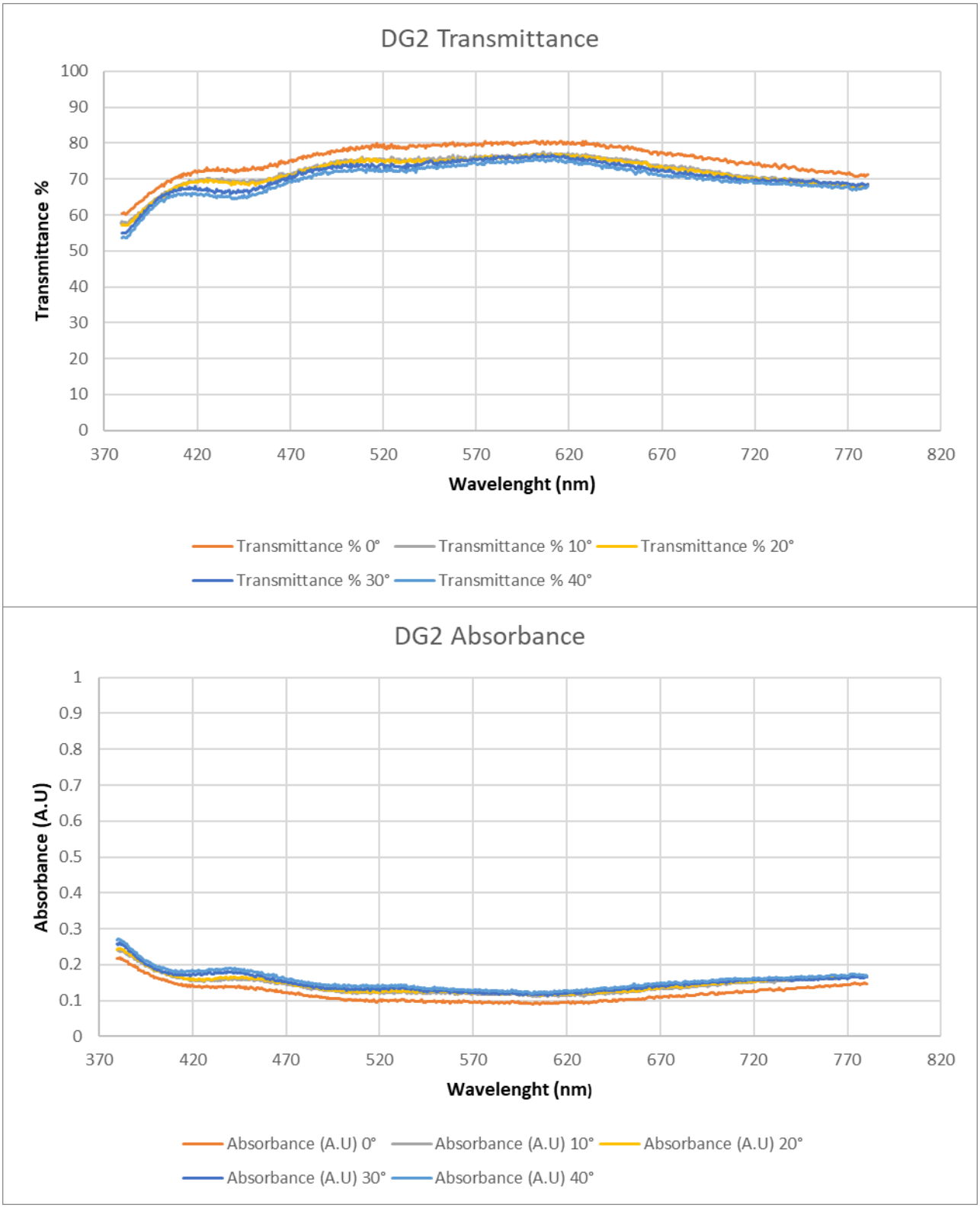

FIGURE 4.4: DG2 TRANSMITTANCE AND ABSORBANCE

To simplify the analysis process of the outcomes, the mean values for the optical test results were listed in Table 4.1

TABLE 4.1: THE OPTICAL TEST RESULTS FOR REFERENCE POINTS

Sample	Transmittance%	Absorbance%	Reflectance%
SG1	74	15.81	10.19
DG1	69.83	14.97	15.20
DG2	65.26	14.02	20.72

The findings indicate that as the angle of solar irradiance increases, the reference glazing's capacity to transmit light decreases, while its capacity to absorb light increases. These outcomes can be attributed to the fact that as the angle of solar irradiance increases, the reflectance of the glazing sample also increases, resulting in a decrease in transmittance. Moreover, the frame of the glazing may contribute to this effect, given the limitations of the testing equipment. As the angle increases, it is more likely for the frame of the sample to absorb a portion of the solar irradiance, especially in the DG1 and DG2 at 40°. Furthermore, the reflectance and transmittance of a glazing sample are directly influenced by its physical structure. In particular, an increase in sample thickness leads to a corresponding increase in reflectance, while transmittance decreases accordingly.

4.1.2. STPV Glazing

The STPV samples that are going to be investigated are shown in Figure 4.5.

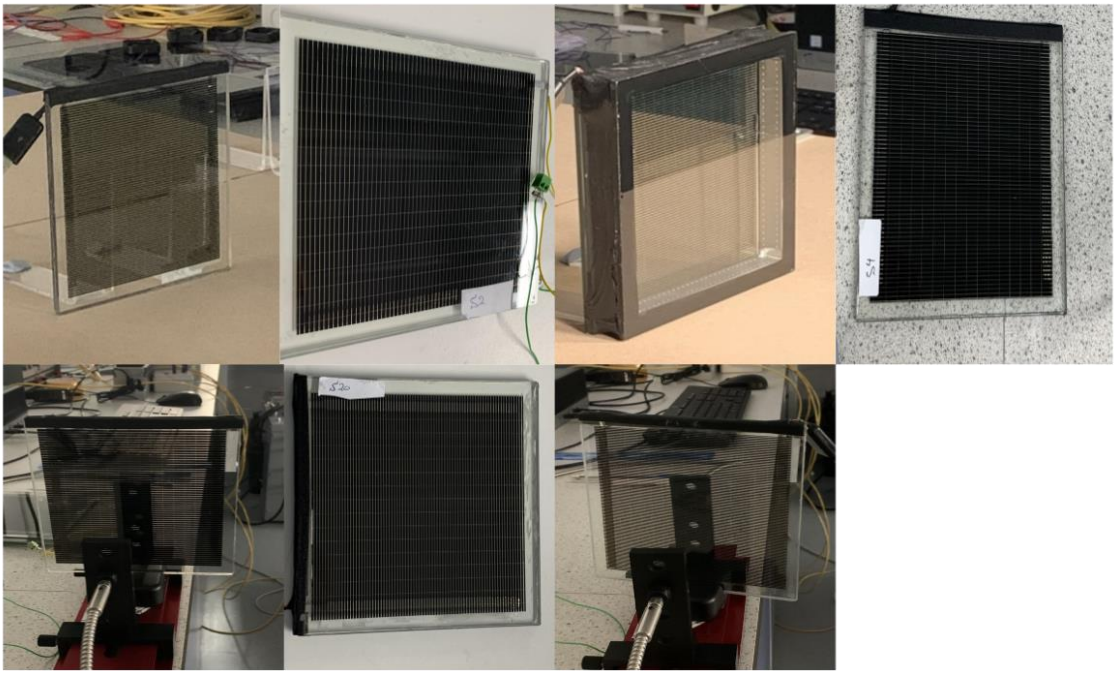

FIGURE 4.5: STPV SAMPLES, FROM LEFT TO RIGHT S1, S2, S3, S4, S5, S20 AND S21

The Optical characteristics of STPV glazing samples are shown in the Figure 4.6, Figure 4.7, Figure 4.8, Figure 4.9, Figure 4.10, Figure 4.11, and Figure 4.12 below.

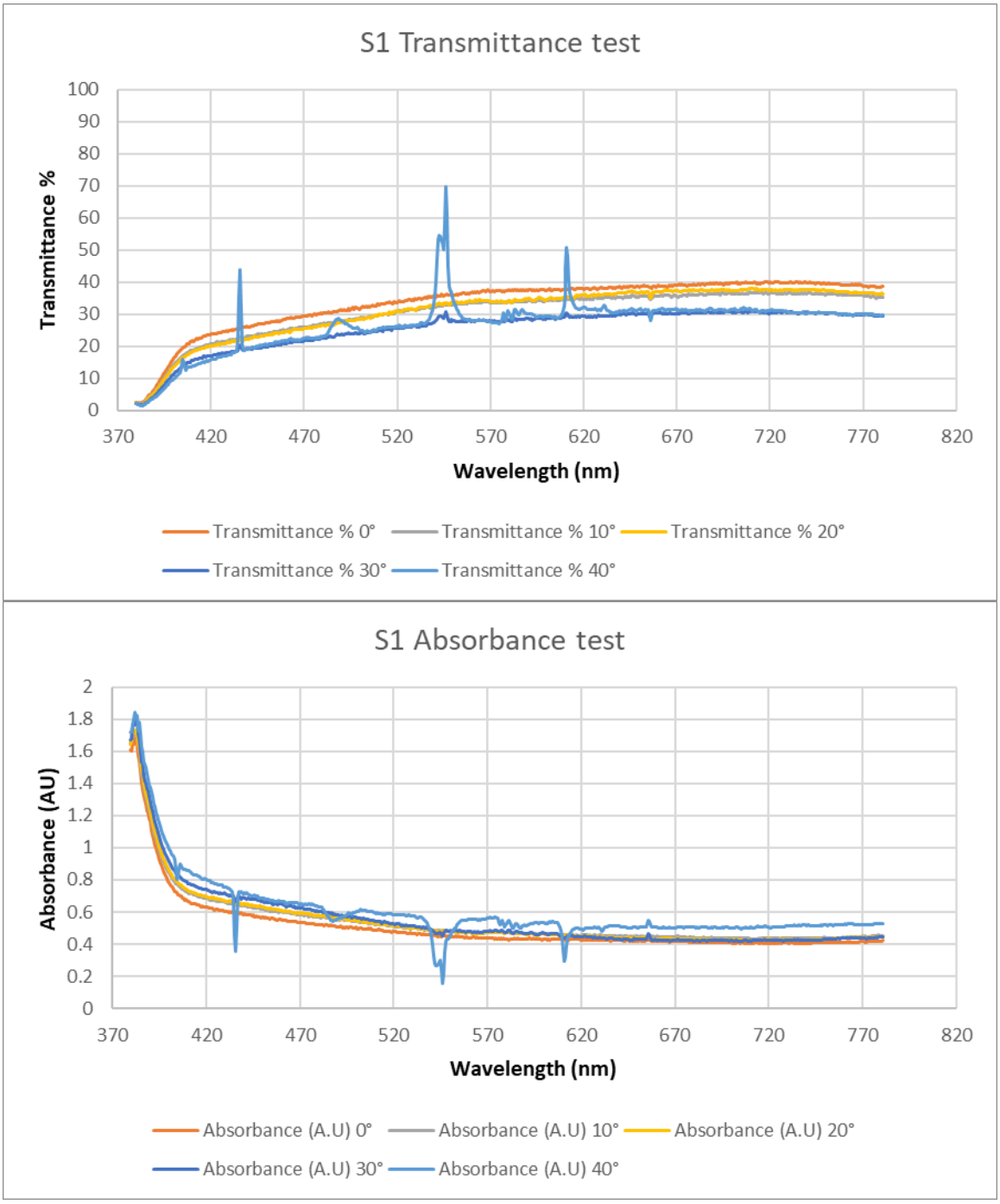

FIGURE 4.6: S1 TRANSMITTANCE AND ABSORBANCE

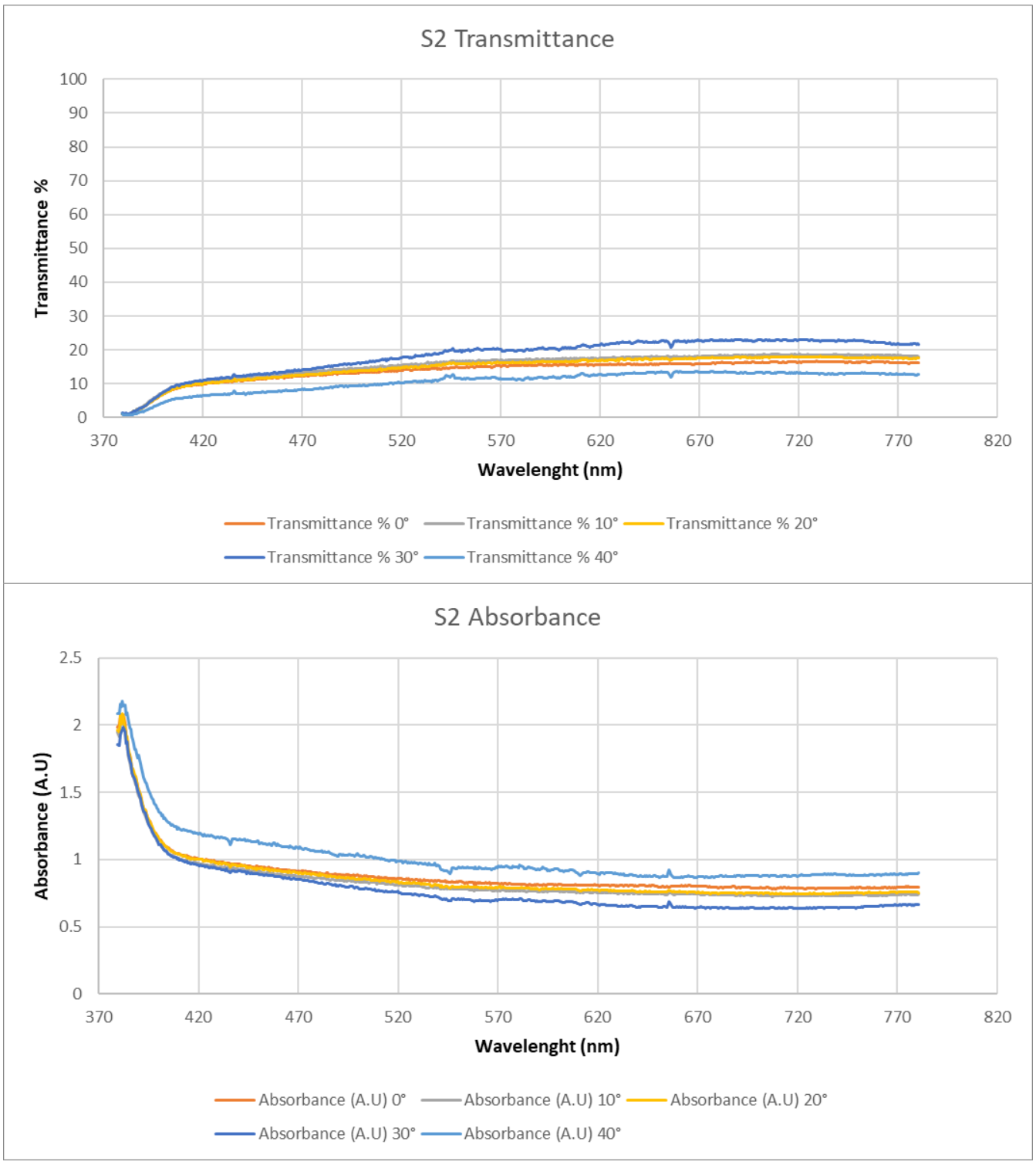

FIGURE 4.7: S2 TRANSMITTANCE AND ABSORBANCE

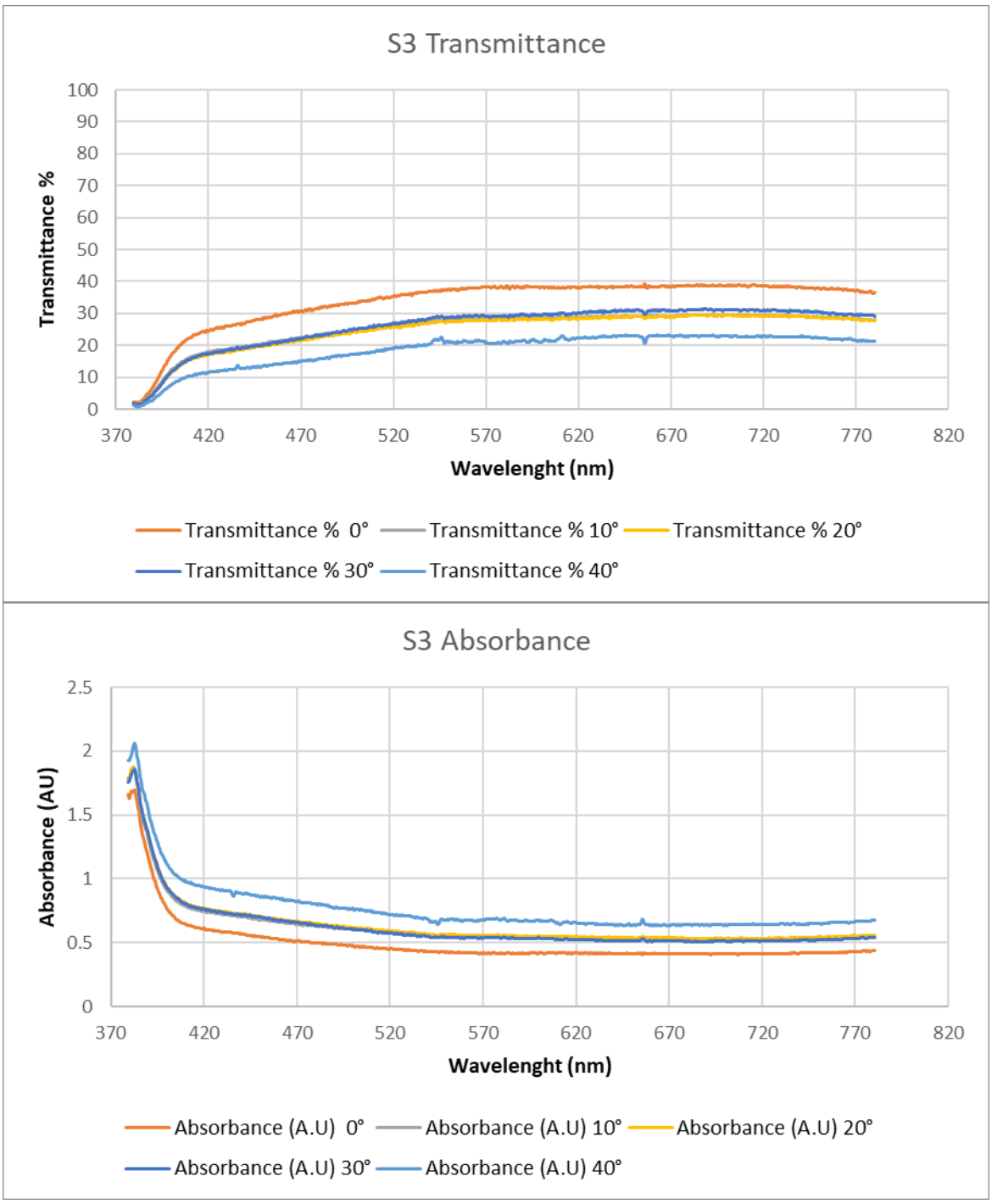

FIGURE 4.8: S3 TRANSMITTANCE AND ABSORBANCE

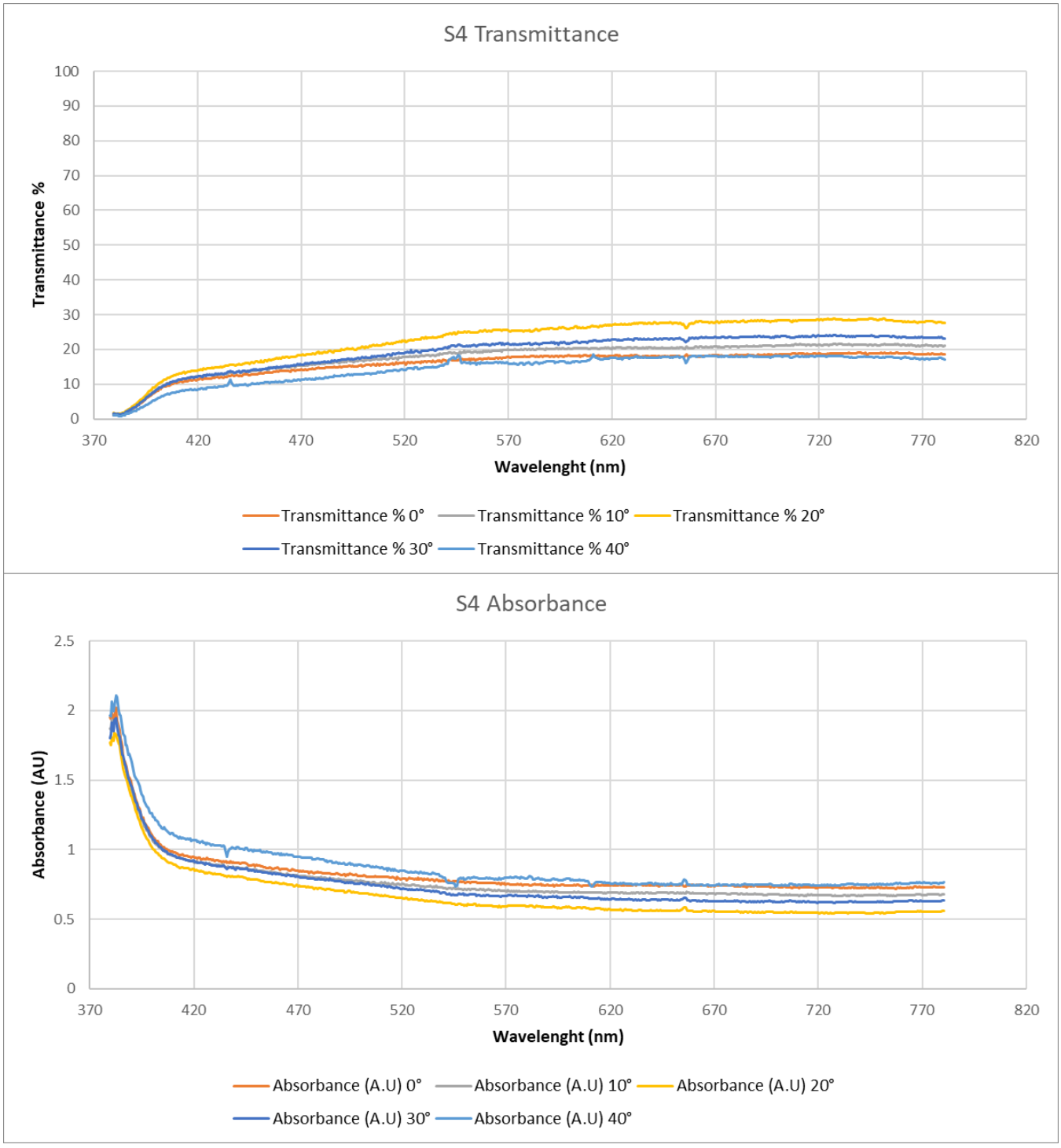

FIGURE 4.9: S4 TRANSMITTANCE AND ABSORBANCE

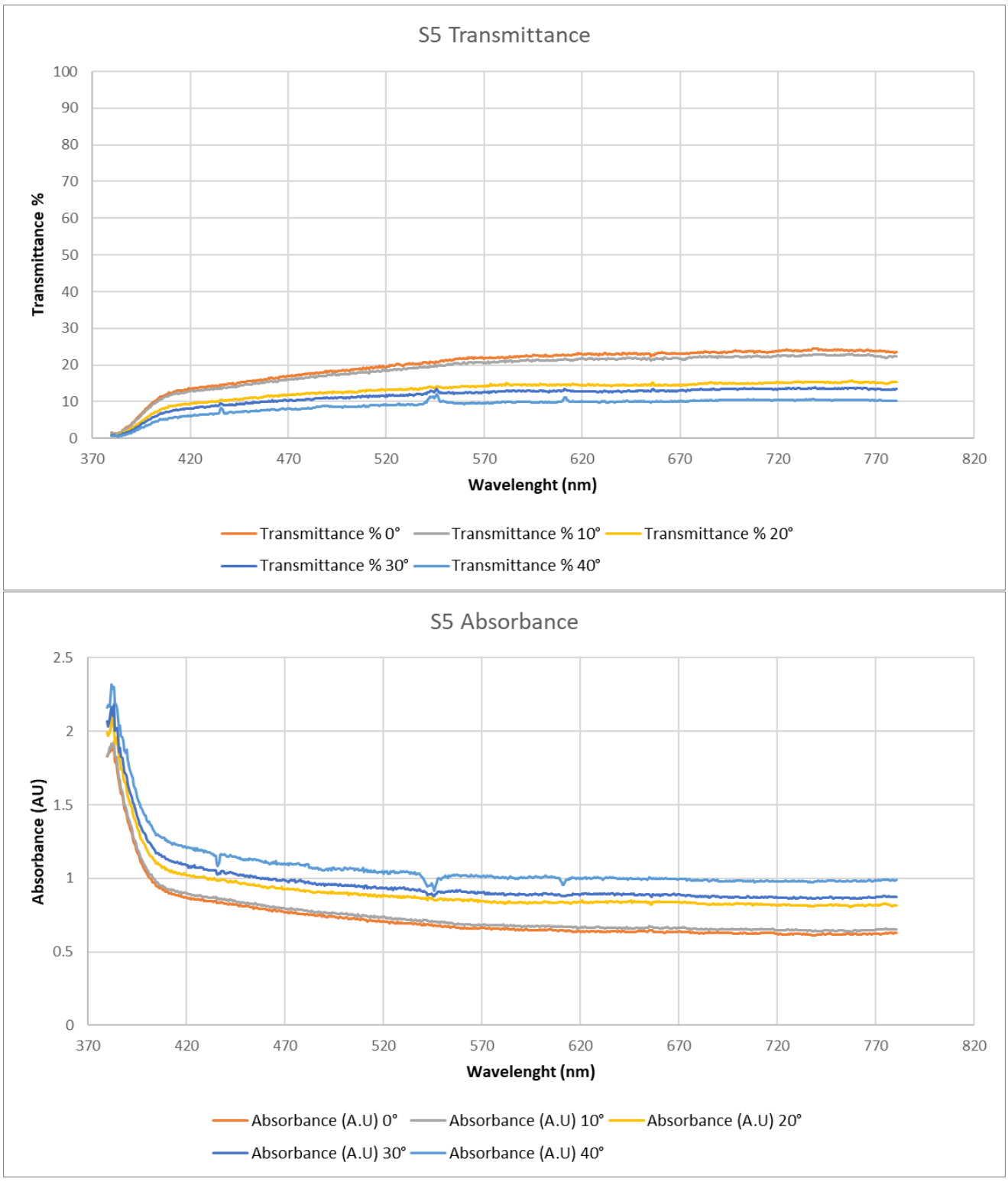

FIGURE 4.10: S5 TRANSMITTANCE AND ABSORBANCE

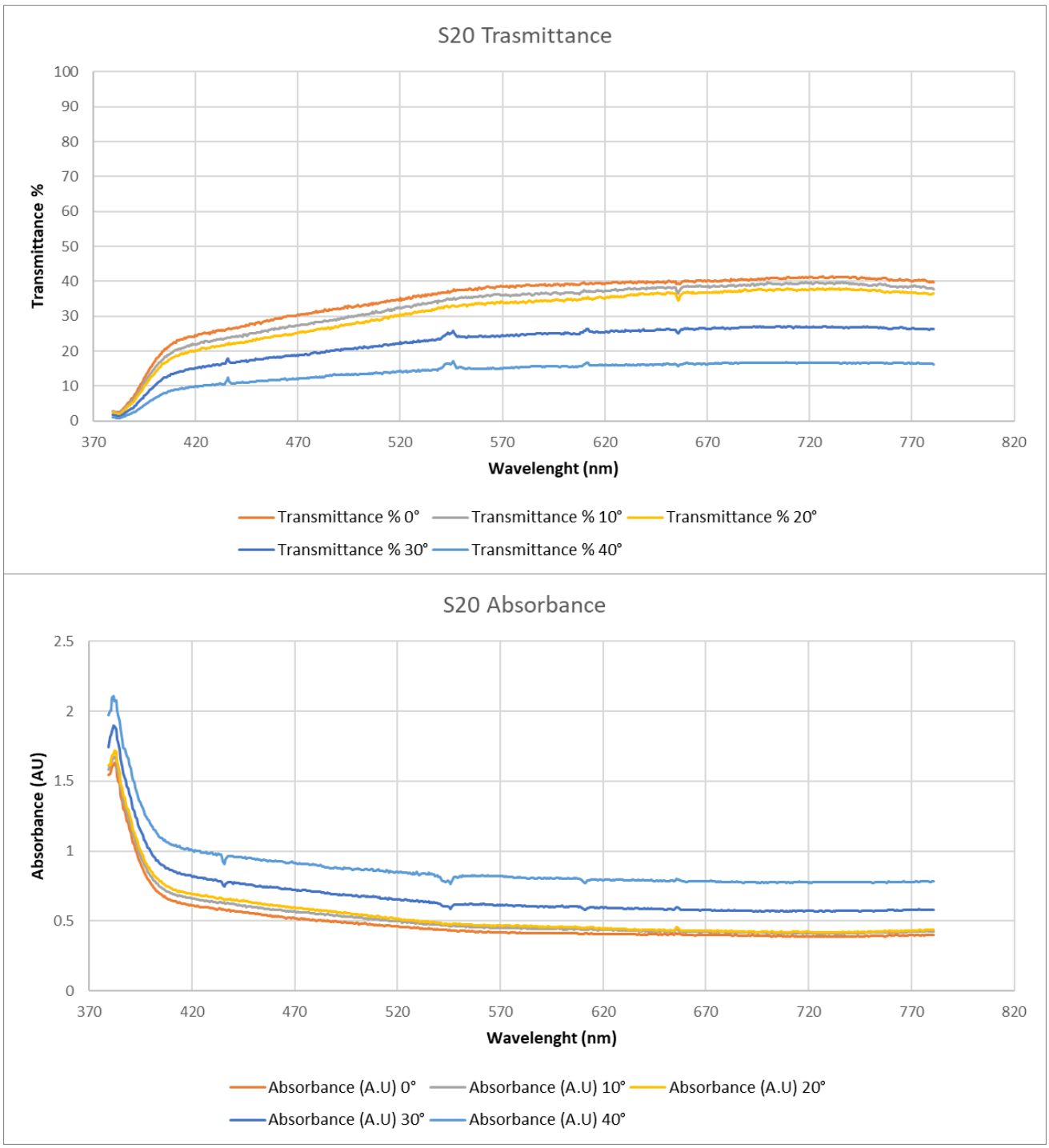

FIGURE 4.11: S20 TRANSMITTANCE AND ABSORBANCE

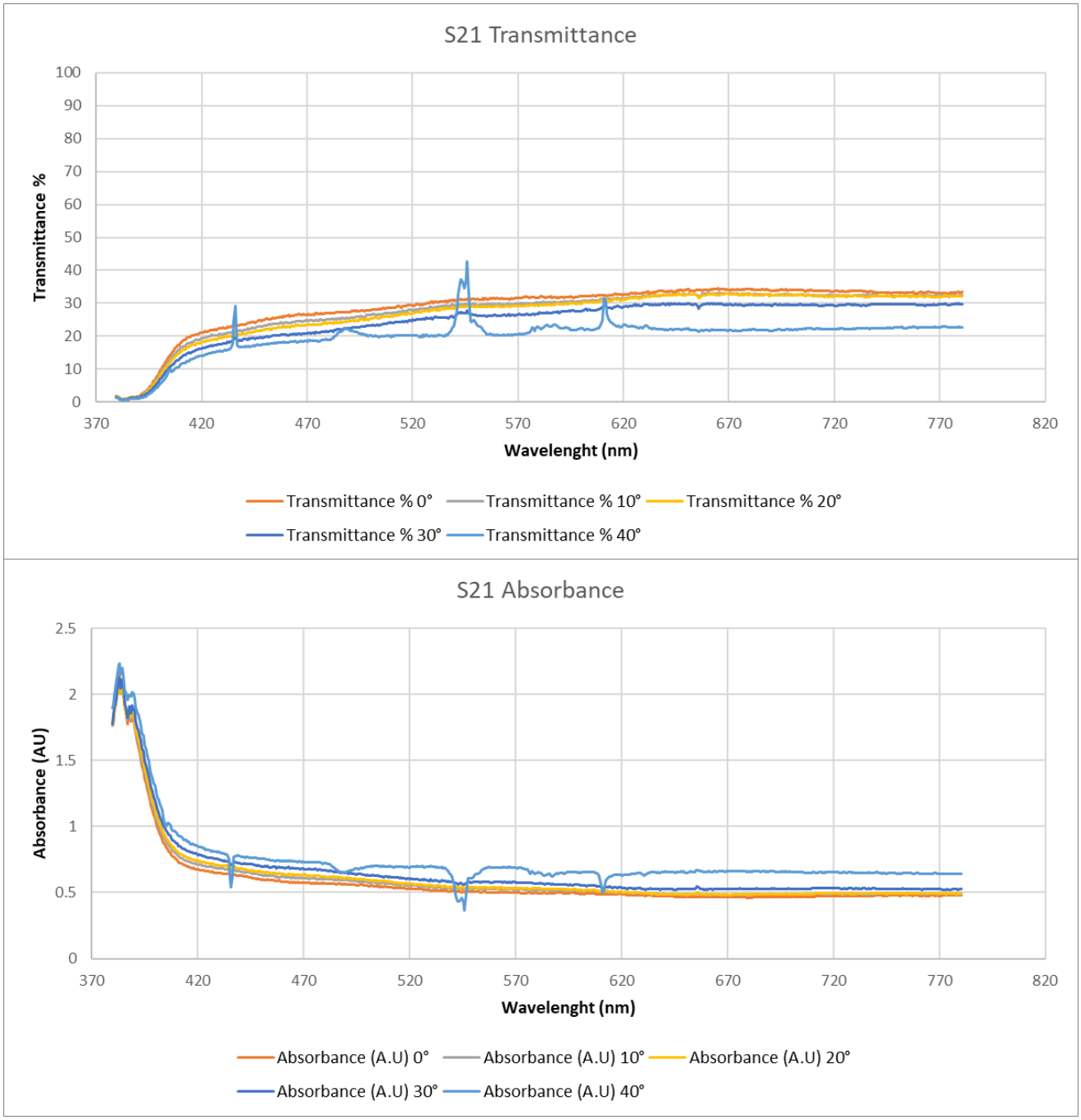

FIGURE 4.12: S21 TRANSMITTANCE AND ABSORBANCE

The outcomes of the tests follow a similar trend to the reference points, the transmittance of the visible light decreases as the solar irradiance increases while the absorbance increases. In addition to the aforementioned reasons for the increase in reflectance, the limitation of the testing equipment that leads to the frame of the sample impacts the outcome and the physical structure of the sample itself. The existence of CdTe solar cell and how its fenestration increases the amount of absorbed and reflected visible light leading to a decrease in the transmittance ability of the STPV glazing samples.

The results indicate that S1 tends to have the most transmittance ability with in-average transmittance capability of 26.24% followed by S20 with 23.25% followed by S3 with 23.2%. It is worth mentioning that the S3 sample is a double-glazing sample where that sample's physical structure reduces the transmittance capability. Whereas S2 tends to allow the least amount of visible light to go through it with a transmittance ability of around 13.14% and the full mean values for the optical attributes for STPV samples are summarised in Table 4.2.

TABLE 4.2: THE OPTICAL TEST RESULTS FOR STPV SAMPLES

Sample	Transmittance %	Absorbance%	Reflectance%
S1	26.24	6.23	67.53
S2	13.14	3.62	83.23
S3	23.20	5.64	71.16
S4	17.11	4.42	78.47
S5	13.55	3.71	82.74
S20	23.25	5.62	71.13
S21	22.45	5.49	72.05

The CdTe STPV glazing samples exhibit a noteworthy decline in their visible light transmission capacity when compared to the reference point. For example, the leading performing STPV sample, S1, displays a reduction of 47.76% in transmittance ability compared to SG1, 43.06% compared to DG1, and 39.02% compared to DG2. This trend is consistent across all STPV glazing samples and is mainly attributed to the incorporation of CdTe solar cells in their structures.

4.2. Thermal Characteristics

As highlighted in 3 section 3.2.3, the thermal characterisation process involves two key metrics: the heat transfer coefficient (U-value) and the solar heat gain coefficient (SHGC). This section will delve into the results of the thermal characterisation process for the glazing samples outlined in Table 3.1, as discussed in Chapter 3 section Thermal Characterisation Testing Setup3.3.3.3.

4.2.1. Solar Heat Gain Coefficient (SHGC)

As discussed above, the SHGC is a unitless metric that quantifies the part of solar irradiance reaching the indoor environment through the glazing system, as well as a measurement for solar heat gain through the glazing structure that depends on the optical characteristics of the CdTe STPV glazing systems, especially the values of the transmitted and absorbed solar irradiance.

Furthermore, SHGC is dependent on the transmittance and absorbance abilities of the glazing samples. These results are utilised in calculating the SHGC metric according to Equation 3.6.

4.2.1.1. Reference Points

SHGC results for the reference points are shown in Figure 4.13 below.

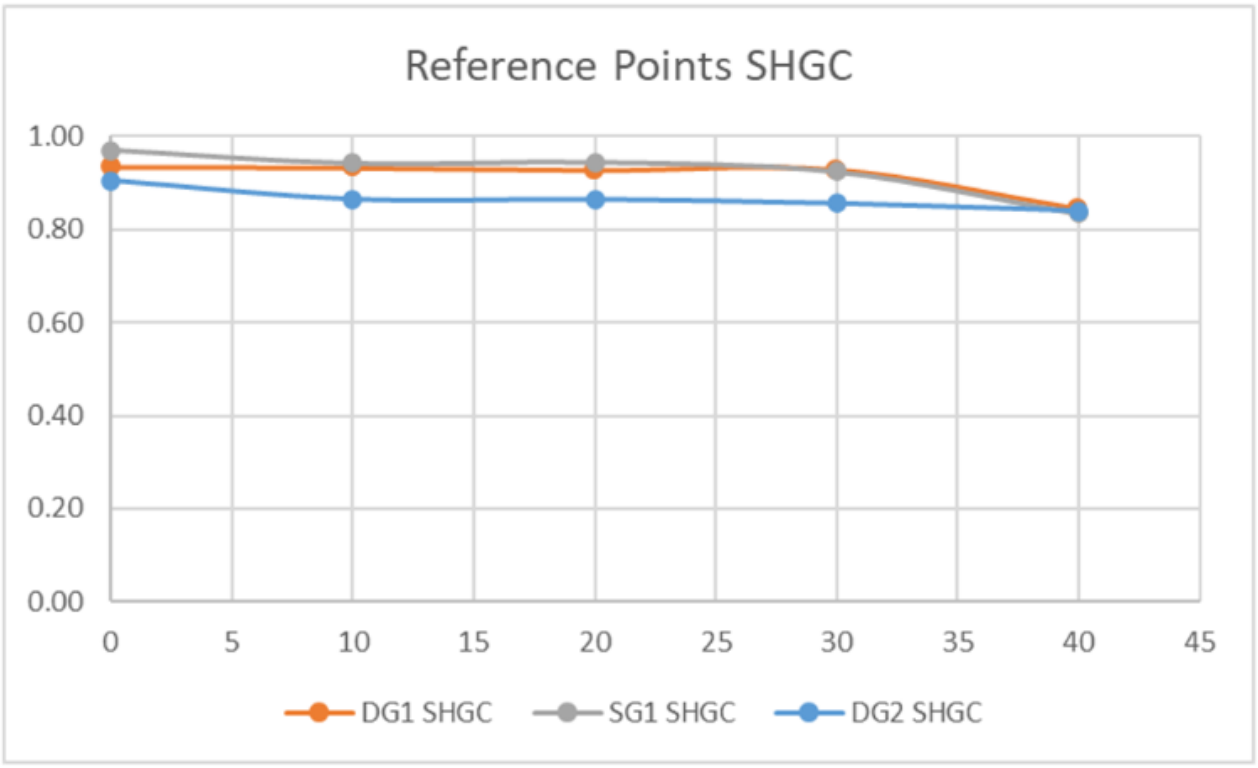

FIGURE 4.13: SHGC FOR REFERENCE POINTS UNDER DIFFERENT INCIDENT ANGLES

The SHGC results for the reference points indicate that SG1 has the highest SHGC with 89%, followed by DG1 with 84% and then DG2 with 78%. As the SHGC metric is dependent on the Optical characteristics, the physical structure, and the thickness of the sample in particular contribute to these results. SG1 has the lowest thickness which translates to lower reflectance capability and higher transmittance hence higher SHGC when compared with DG1 and DG2. The full mean values for the SHGC of the reference points samples are summarised in Table 4.3.

TABLE 4.3: SHGC FOR REFERENCE POINTS

Sample	SHGC
SG1	89%
DG1	84%
DG2	78%

4.2.1.2. STPV Glazing

The SHGC metric results for STPV glazing samples are shown in Figure 4.14 below.

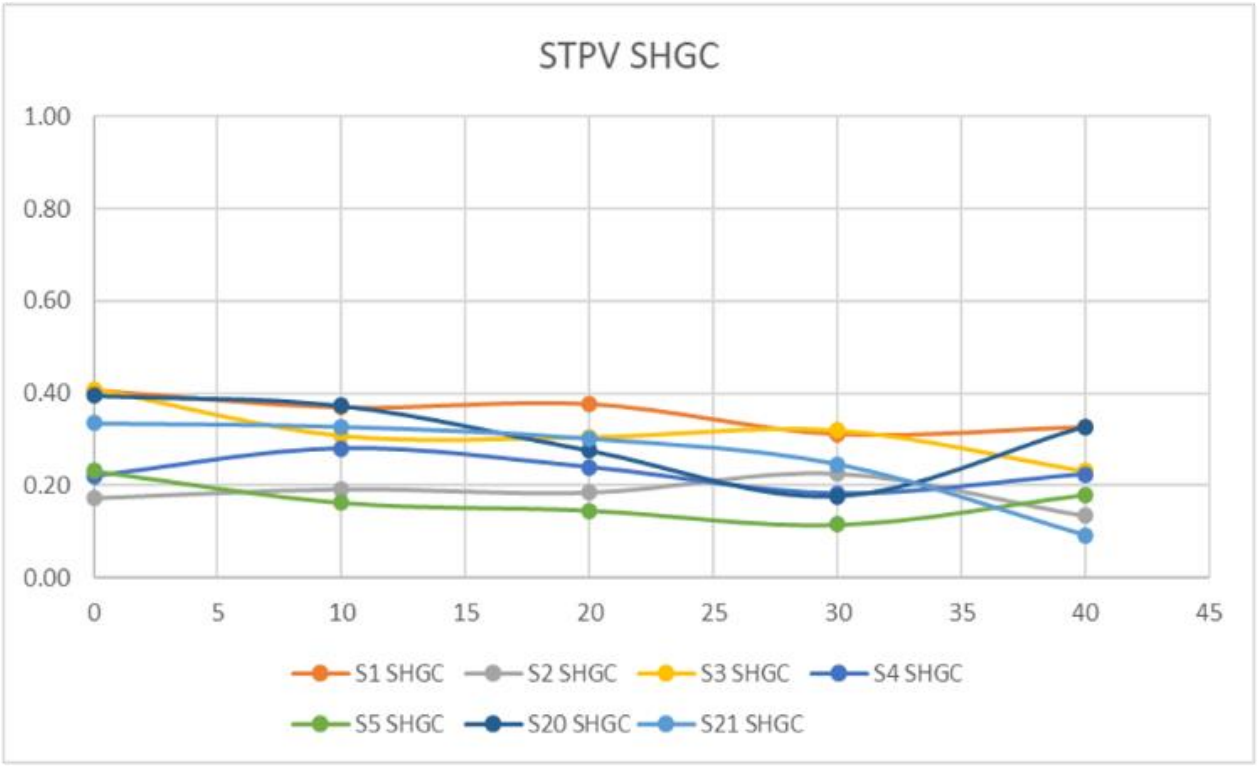

FIGURE 4.14: SHGC FOR STPV SAMPLES UNDER DIFFERENT INCIDENT ANGLES

The SHGC results for the STPV glazing samples indicate that S1 has the highest SHGC with 32%, followed by S3, S20, and S21 with 28%. Whereas S2 and S5 have recorded the lowest SHGC metric result with 17%. Alonge the fact that the SHGC metric is dependent on the Optical characteristics, and the physical structure. The existence of the CdTe solar cells reduces the visible light that penetrates the glazing sample and as a result, will reduce the SHGC metric considerably when compared with the reference points as seen in Figure 4.15. The full mean values for the SHGC metric for the STPV glazing samples are summarised in Table 4.4.

TABLE 4.4: SHGC FOR STPV GLAZING SAMPLES

Sample	SHGC
S1	32%
S2	17%
S3	28%
S4	21%
S5	17%
S20	28%
S21	28%

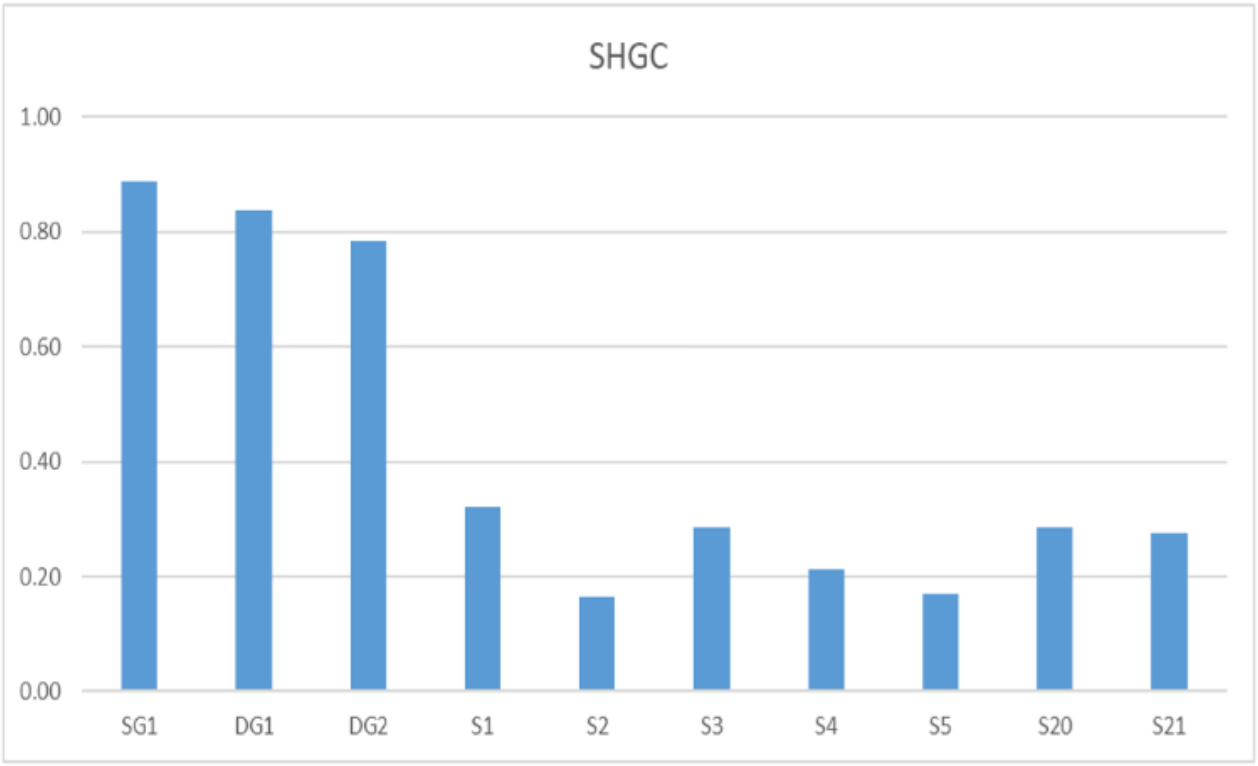

FIGURE 4.15: SHGC FOR THE GLAZING SAMPLES

4.2.2. Heat transfer coefficient (U-Value)

As discussed in Chapter 243, the U-value is a coefficient that calculates the amount of energy transferred through the glazing system. This transfer occurs through the exchange of irradiation and convective heat between the inner and outer surfaces of the glazing. The U-value is determined by the heat flux (W/m2) and the temperature difference between the surfaces of the glazing system (Kelvin). Equation 3.7 can be used to assess the U-value, and the results have been collected according to the testing process outlined in Section 3.3.3.3.2. The lower the U-value outcome is, the better the insulation capability of the glazing sample is.

4.2.2.1. Reference Points

The U-Value results for the reference points DG1 and DG2 are shown in the Figure 4.16 and Figure 4.17 below. Whereas the U-value Results for SG1 are shown in Chapter 3, Figure 3.26.

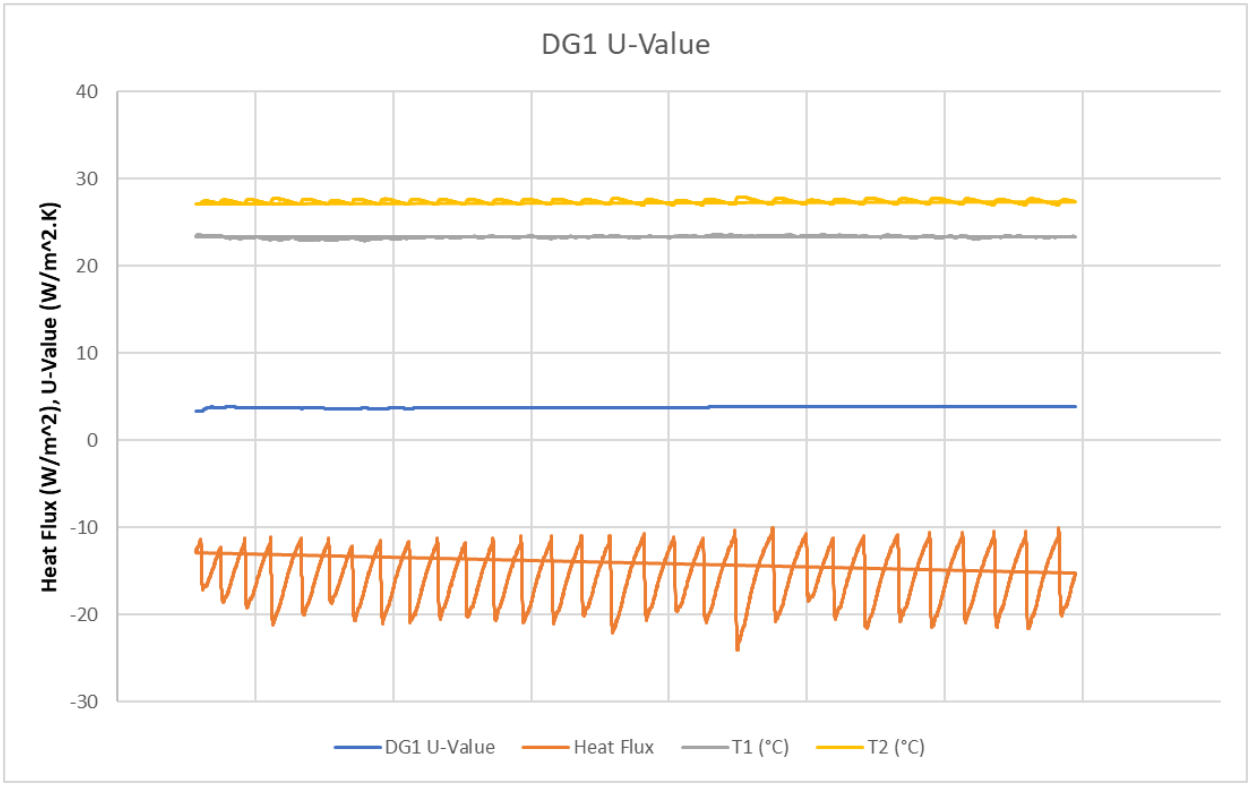

FIGURE 4.16 THE U-VALUE RESULT OF DG1 SAMPLE

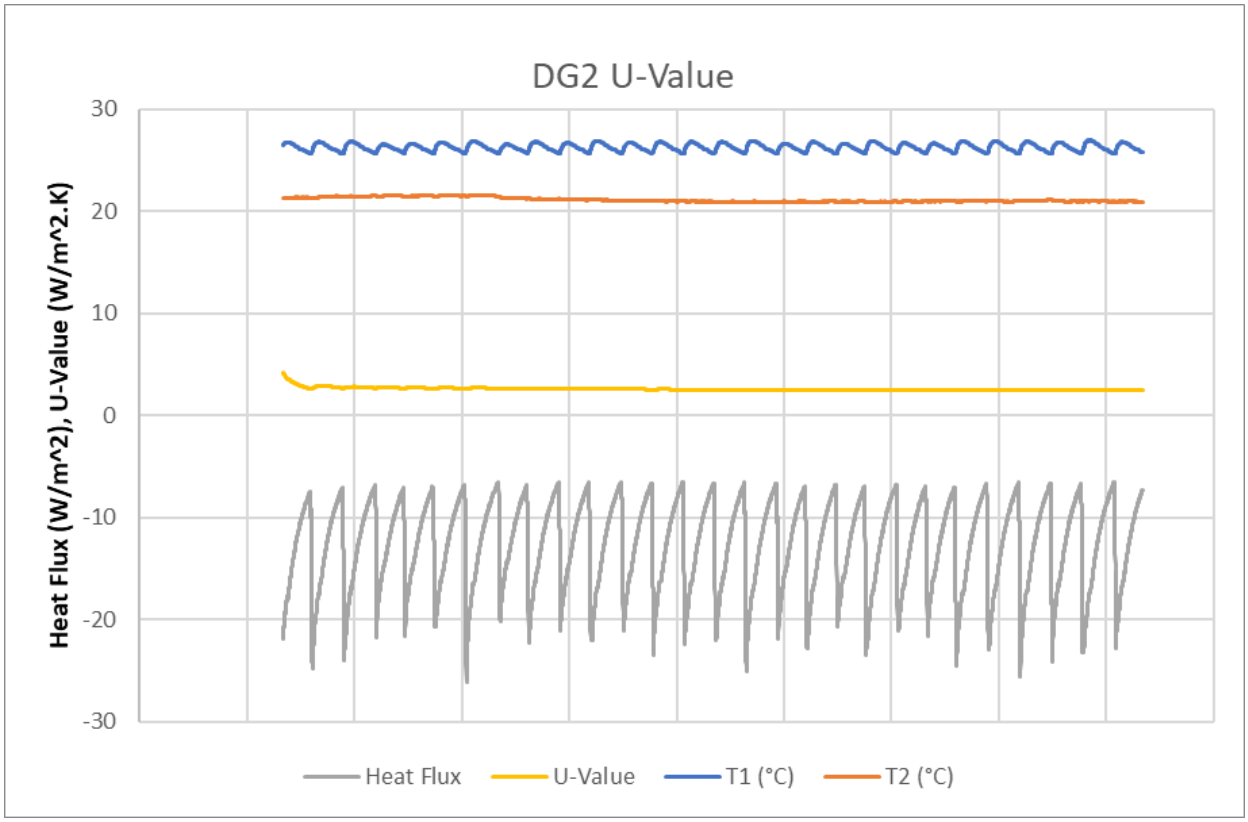

FIGURE 4.17: THE U-VALUE RESULT OF THE DG2 SAMPLE

According to the U-value tests conducted on the reference points, it is evident that the SG1 sample has the highest U-value of 6.24 W/(m^2.K). This indicates that the SG1 sample tends to absorb a significant amount of solar heat irradiance while simultaneously losing a substantial amount, resulting in greater heating, and cooling requirements.

DG2 has the lowest U-value by 2.46 W/(m^2.K), which means that the DG2 sample represents a much better insulation tool. This can be attributed to the use of Argon gas in the gap of the DG2, as the gas displays low thermal conductivity.

As for DG1, Double glazing with an air-filled gap is the most common type of glazing utilised in practice, the U-value test outcome indicates that DG1 U-value is around 3.78 W/(m^2.K), which is an intermediate insulation tool.

4.2.2.2. STPV Glazing

The U-value results for STPV glazing samples are shown in Figure 4.18, Figure 4.19, Figure 4.20, Figure 4.21, Figure 4.22, Figure 4.23 and Figure 4.24 below.

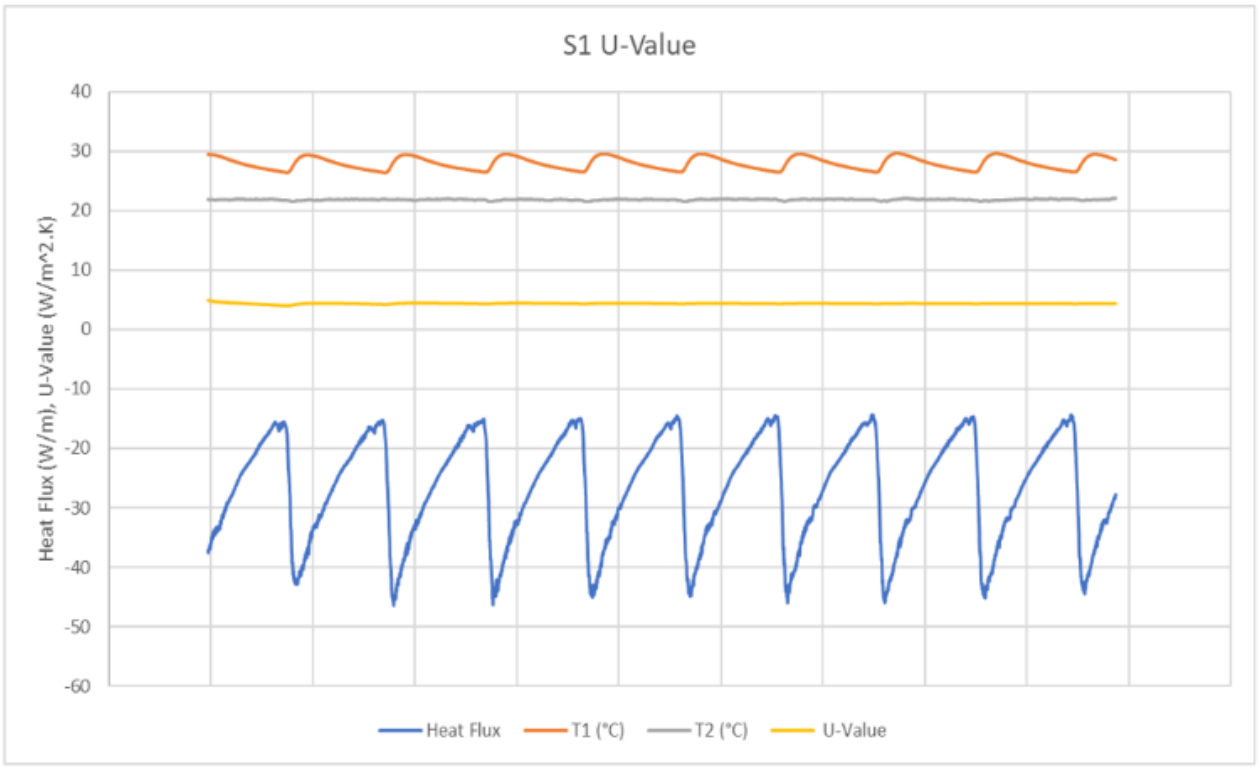

FIGURE 4.18: THE U-VALUE RESULT OF THE S1 SAMPLE

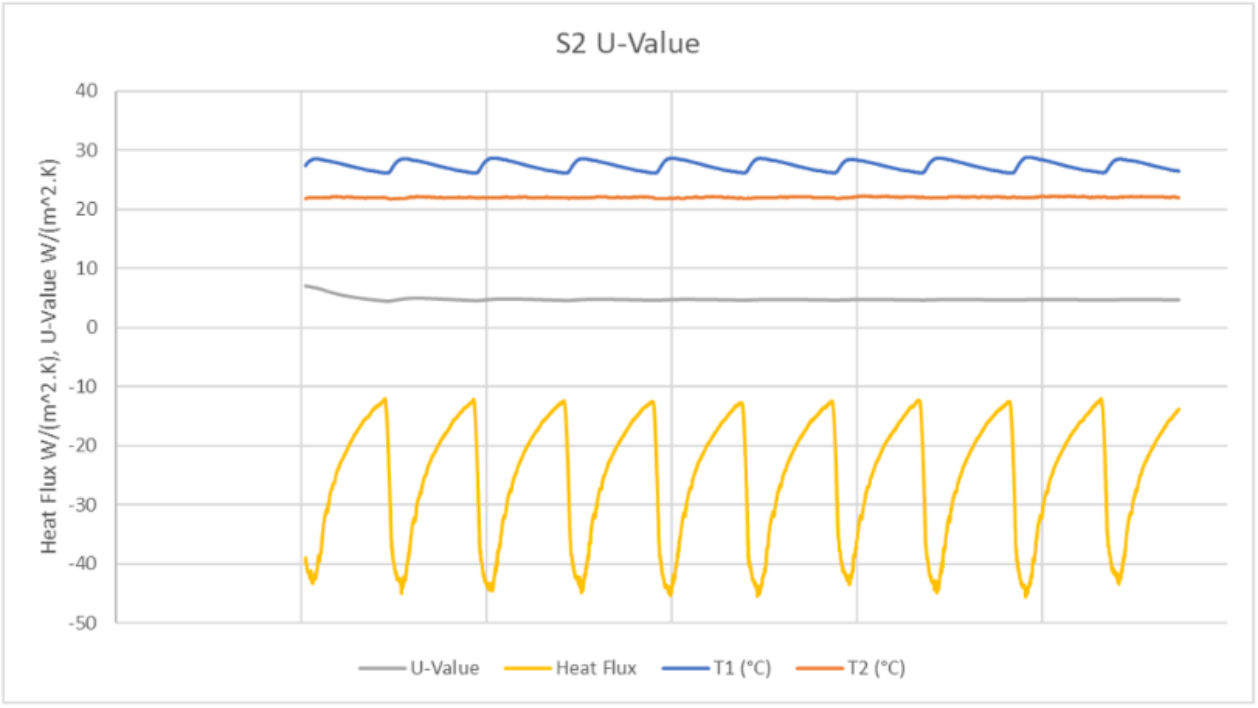

FIGURE 4.19: THE U-VALUE RESULT OF THE S2 SAMPLE

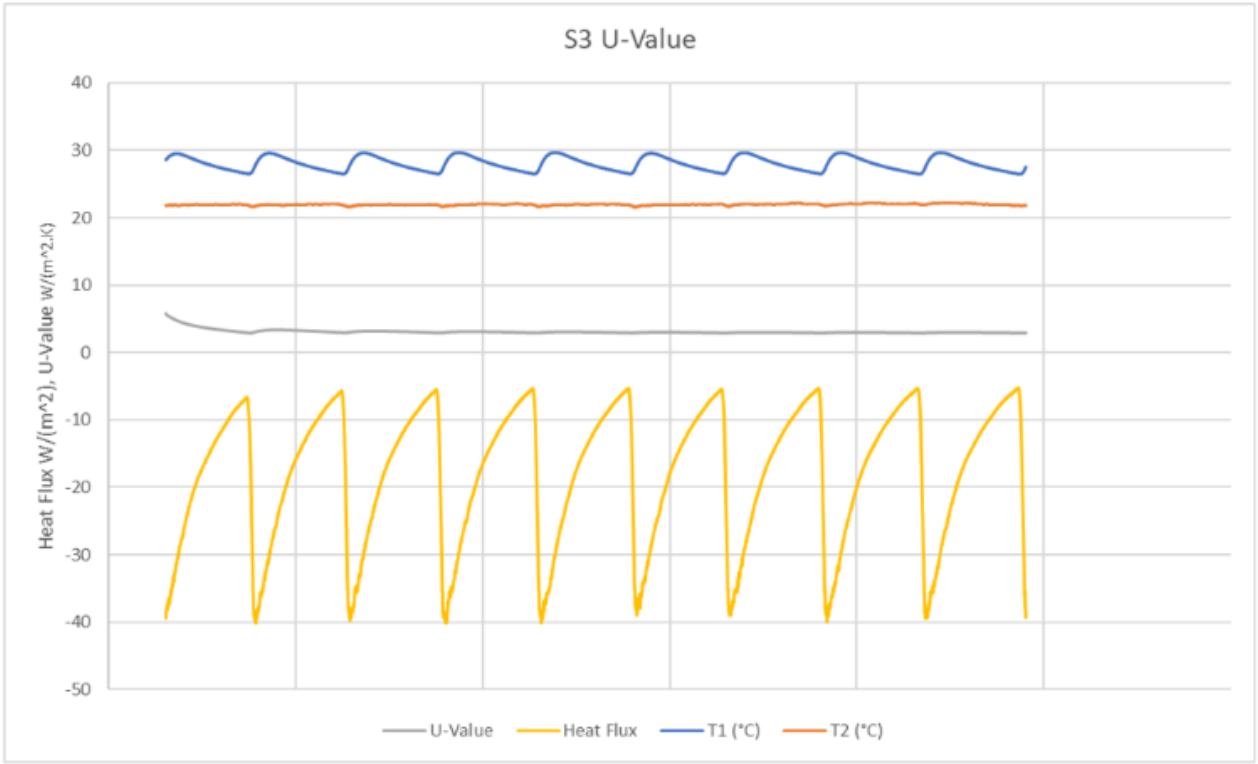

FIGURE 4.20: THE U-VALUE RESULTS OF THE S3 SAMPLE

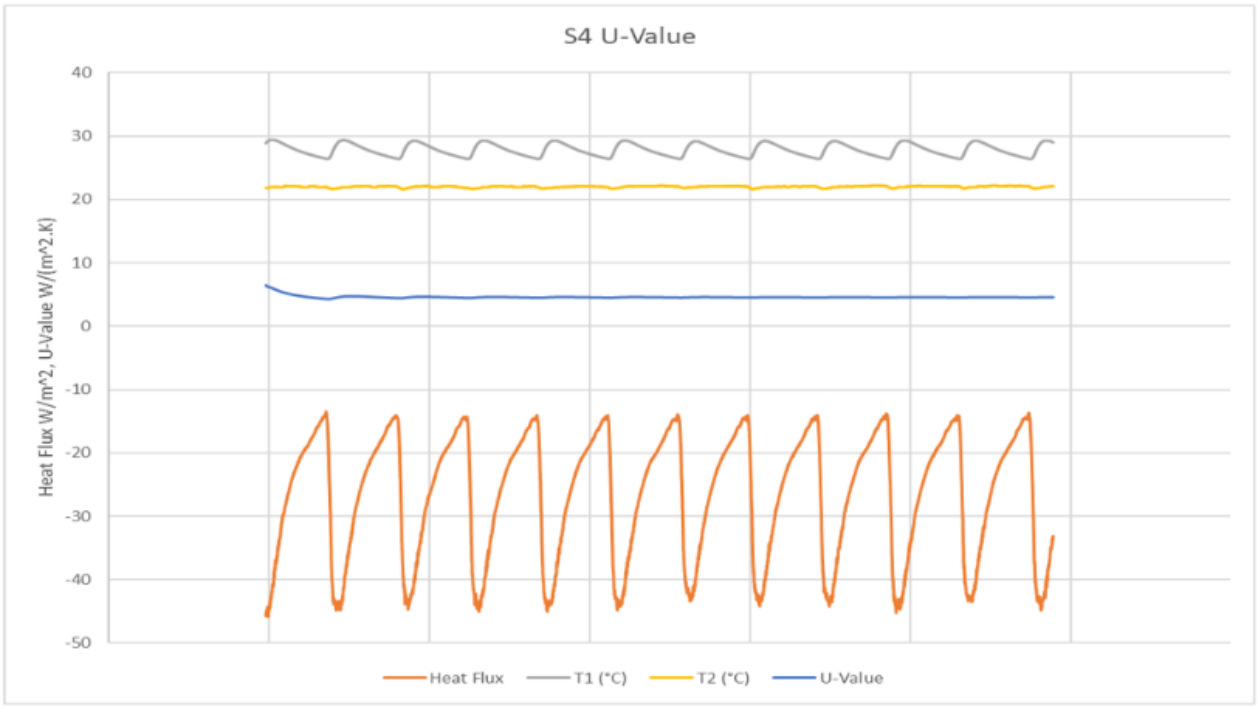

FIGURE 4.21: THE U-VALUE RESULT OF THE S4 SAMPLE

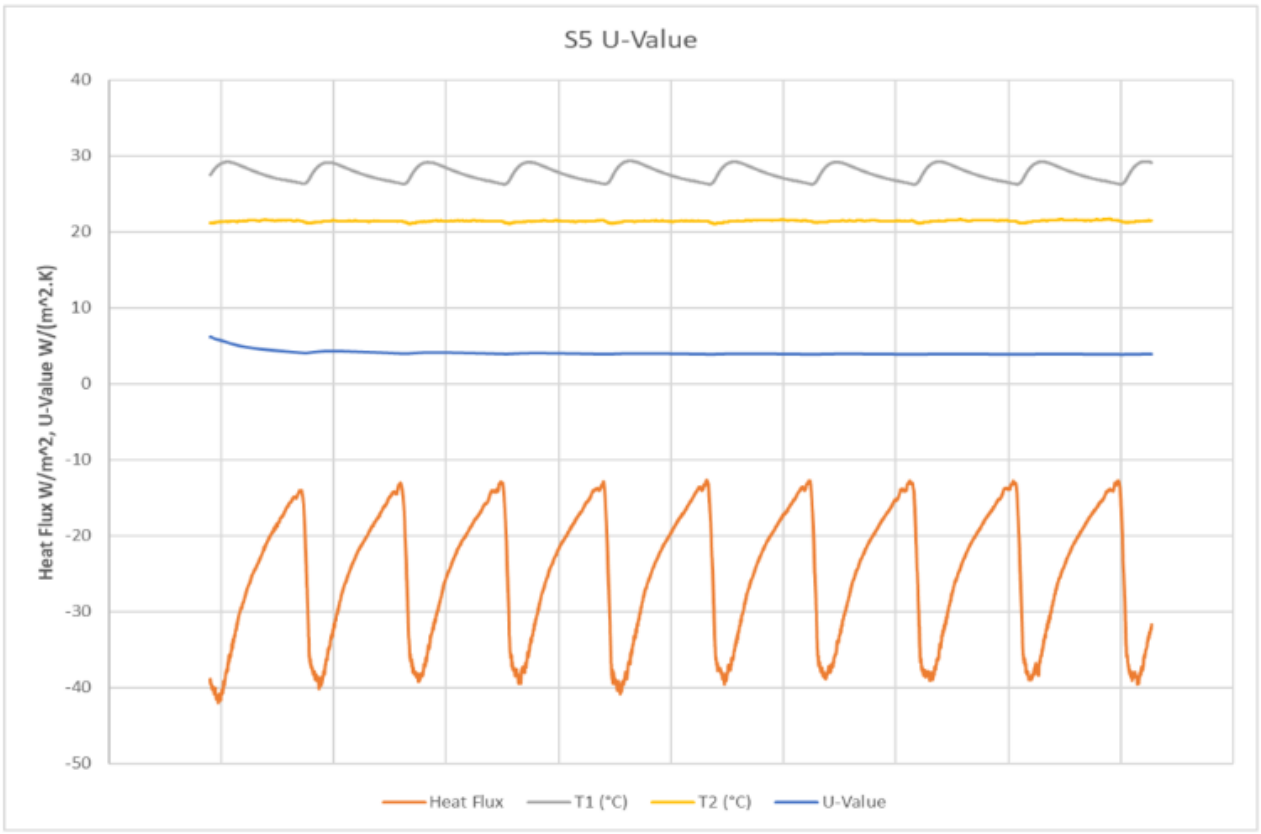

FIGURE 4.22: THE U-VALUE RESULT OF THE S5 SAMPLE

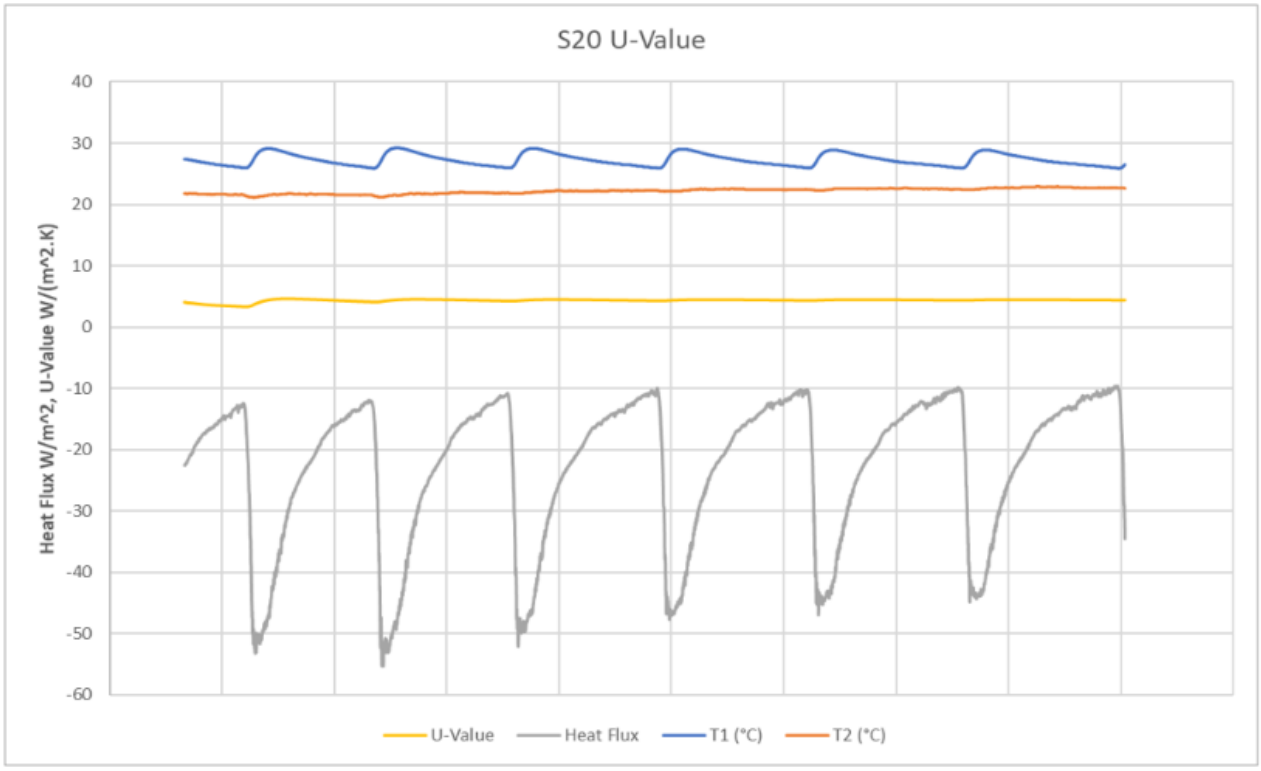

FIGURE 4.23: THE U-VALUE RESULT OF THE S20 SAMPLE

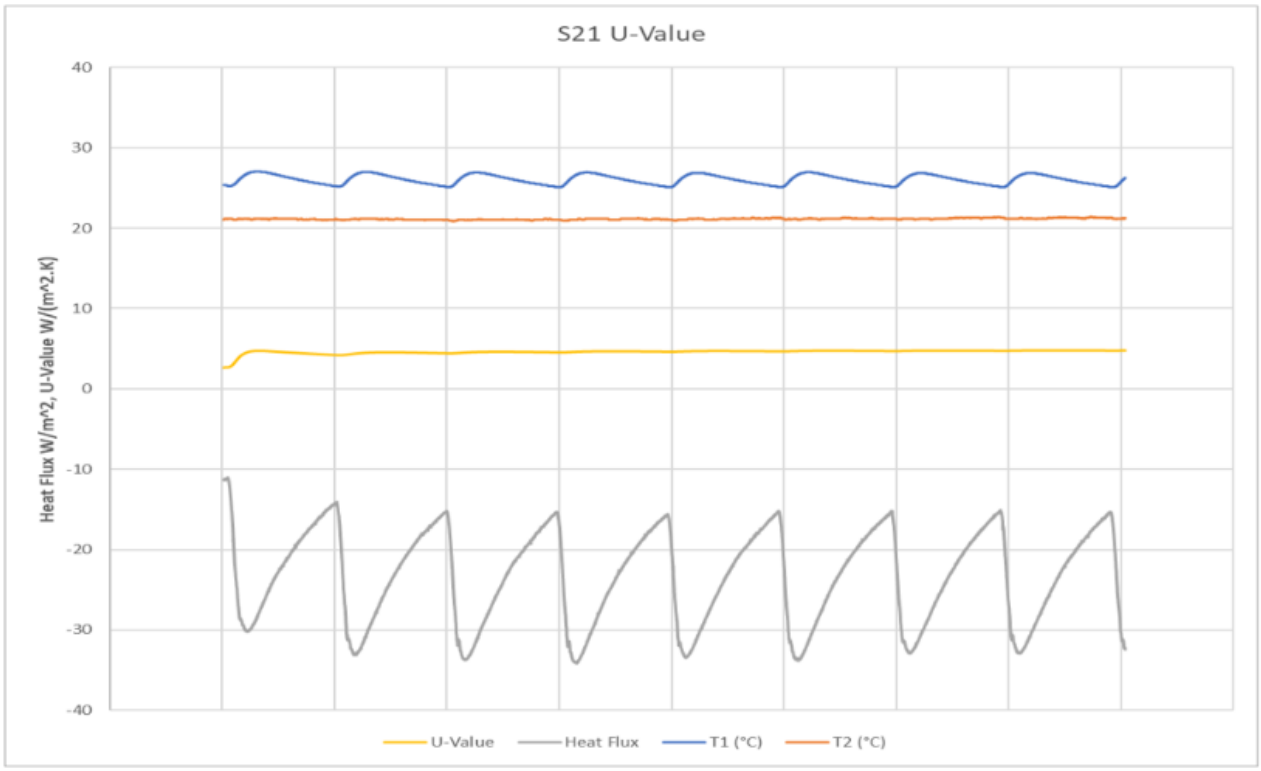

FIGURE 4.24: THE U-VALUE RESULT OF THE S21 SAMPLE

The U-value results for the STPV samples indicate that S3 has the best insulation capability among the STPV samples, with a U-value of 2.93 W/(m^2.K). The U-value result of S3 is similar to DG2 due to the physical structure of the S3 sample. The structure of the S3 sample is a double glazing sample

with a 17mm gap filled with air which would reduce the thermal conductivity hence the lower U-value result.

Analysing the other STPV sample's U-value results, the outcomes highlight that the STPV samples tend to have insulation capabilities DG1 while having comparable physical attributes to SG1. These outcomes imply that CdTe solar cells in the STPV sample improve the thermal insulation ability of the glazing system.

Table 4.5 shows the mean values of the U-value results for the glazing samples.

TABLE 4.5: THE U-VALUE RESULTS FOR THE GLAZING SAMPLES

Sample	U-Value W/(m^2.K)
SG1	6.24
DG1	3.78
DG2	2.46
S1	4.36
S2	4.66
S3	2.93
S4	4.57
S5	3.92
S20	4.40
S21	4.77

4.3. Electrical Characteristics

The Electrical Characterisation Testing Setup aims to identify the electrical characteristics of the CdTe STPV glazing samples. These characteristics are presented by the I-V and P-V curves. These curves help identify the maximum power generated, the efficiency of each sample, and the fill-factor as well, following the testing setup that has been implemented in the section 3.3.3.1.

The I-V and P-V curves for the STPV samples that identify the electrical characteristics for them is shown in Figure 4.25, Figure 4.26, Figure 4.27, Figure 4.28, Figure 4.29, and Figure 4.30 below. Whereas S1 I-V and P-V curves are Shown in Figure 3.16.

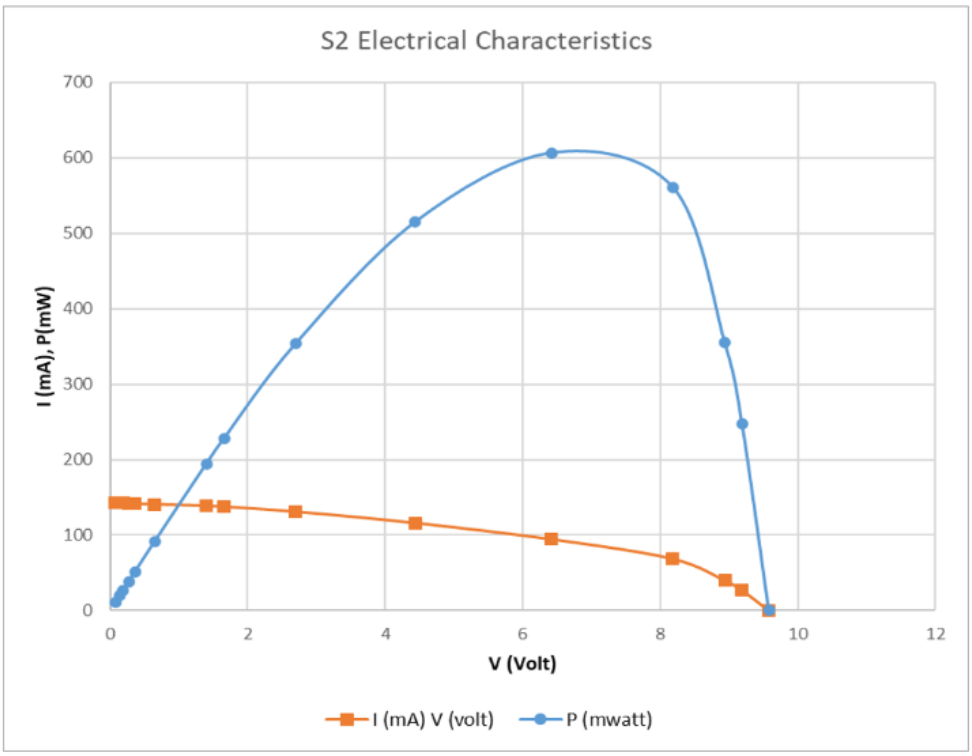

FIGURE 4.25: I-V AND P-V CURVES FOR S2

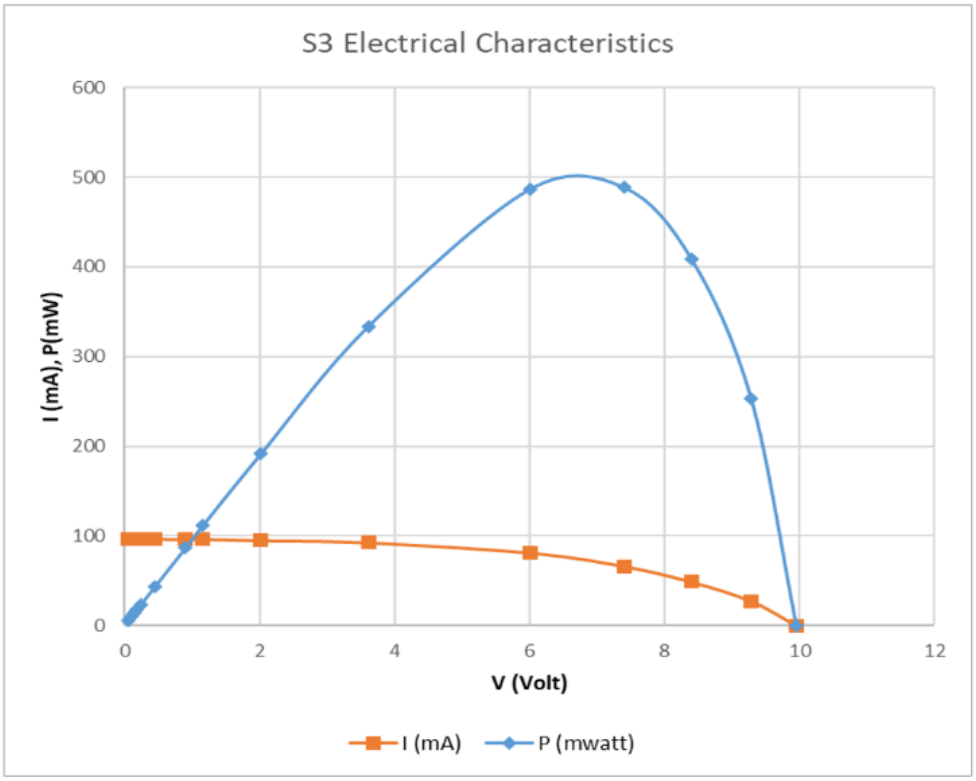

FIGURE 4.26: I-V AND P-V CURVES FOR S3

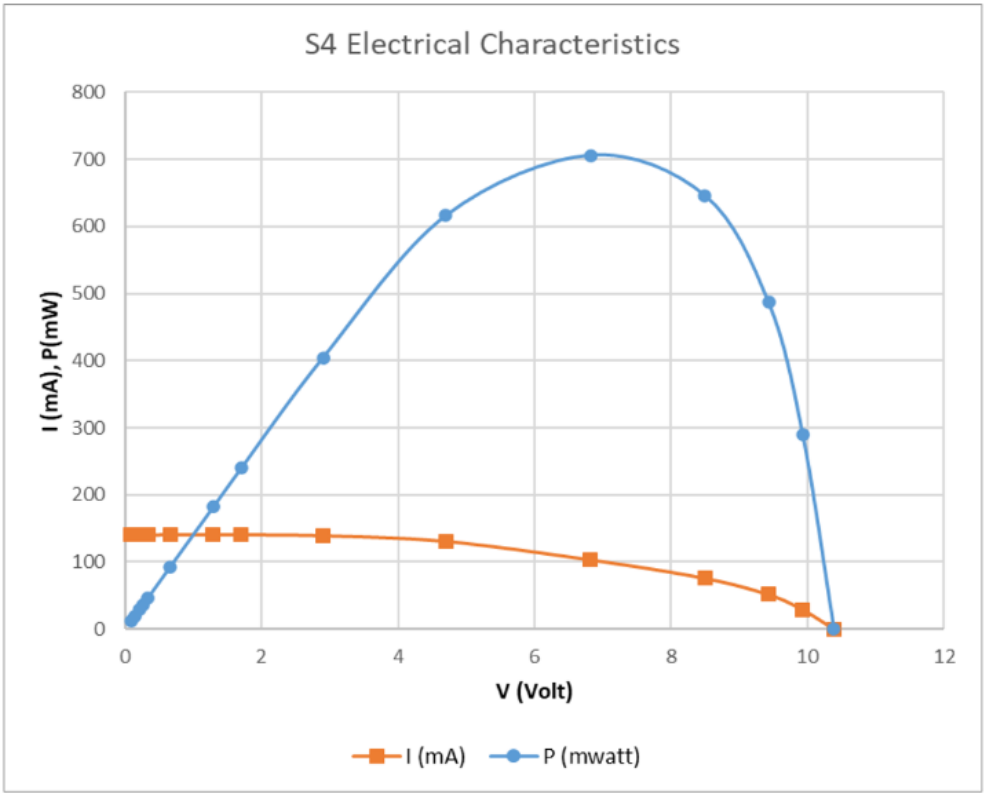

FIGURE 4.27: I-V AND P-V CURVES FOR S4

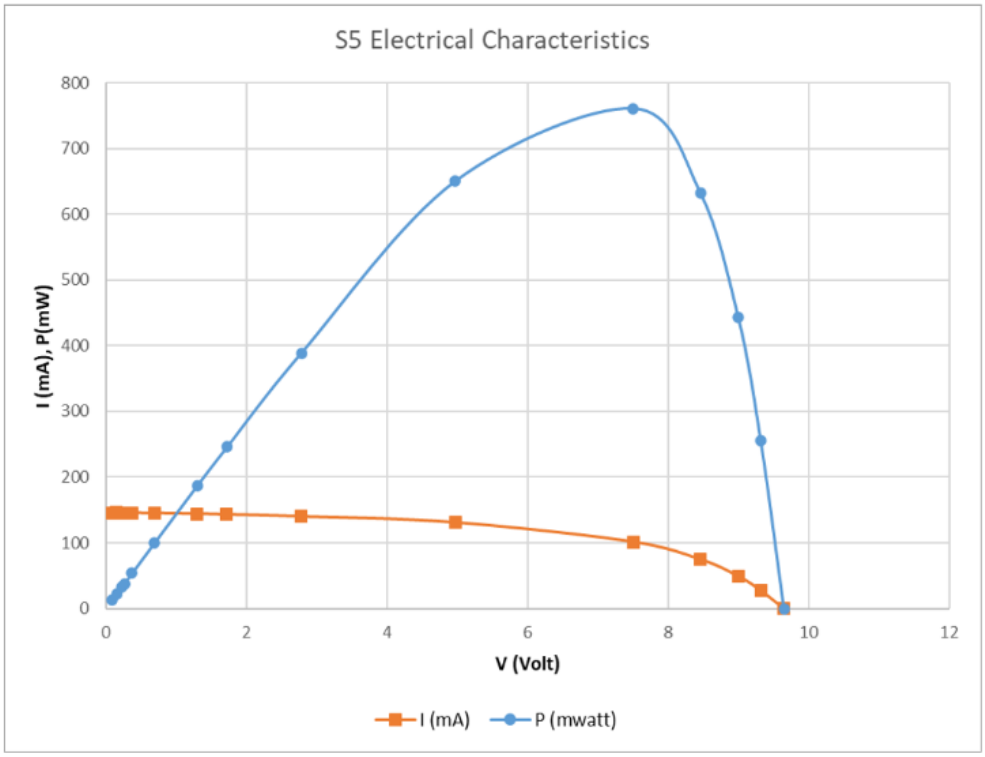

FIGURE 4.28: I-V AND P-V CURVES FOR S5

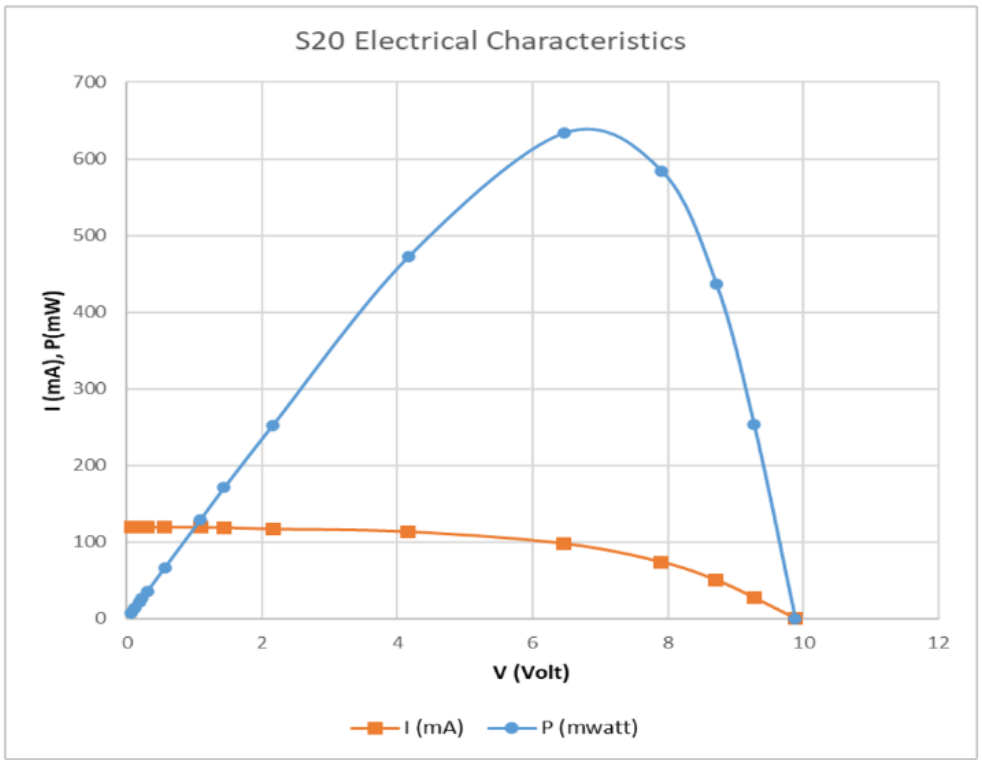

FIGURE 4.29: I-V AND P-V CURVES FOR S20

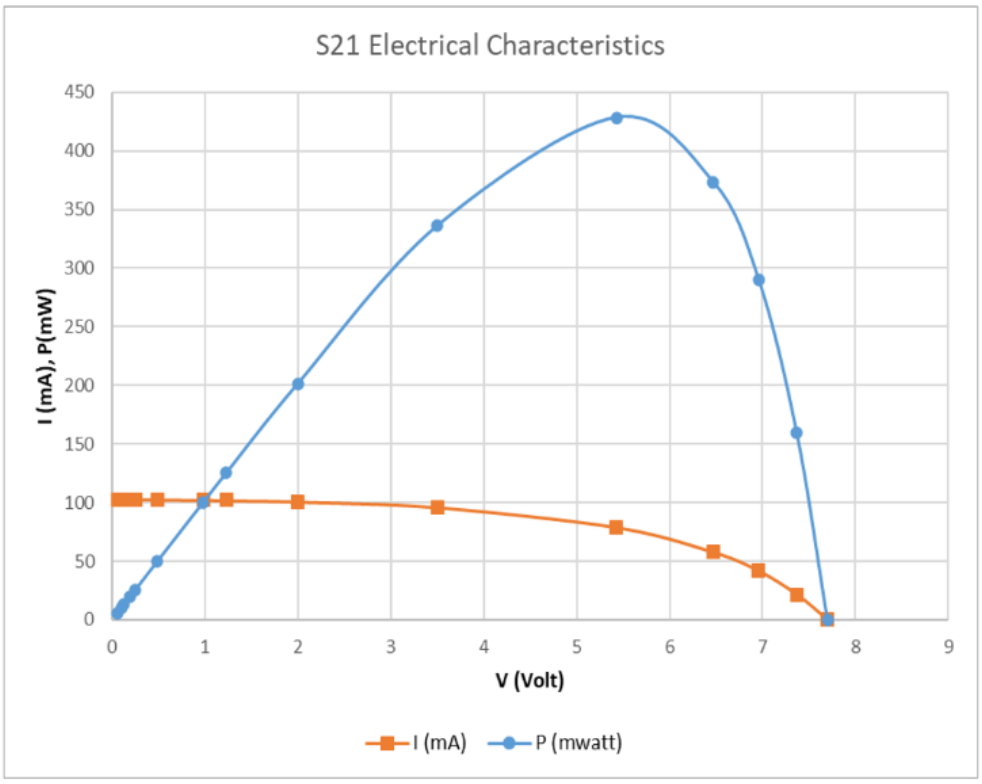

FIGURE 4.30: I-V AND P-V CURVES FOR S21

The outcome results for the electrical characteristics of STPV glazing samples indicate that as the transmittance ability of the STPV sample decreases the electrical efficiency of the sample increases which concurred with the S5 sample. S5 has the highest electrical efficiency with 3.38% as the fenestration of the sample allows the CdTe solar cells to absorb most of the solar irradiance, hence the higher conversion capability.

It is worth mentioning that the least electrically efficient is S21, with electrical efficiency of 1.9%. when compared with the highest performance S5 the difference is around 1.5%. Table 4.6 shows the electrical efficiency of the STPV samples.

TABLE 4.6: THE ELECTRICAL EFFICIENCY OF THE STPV SAMPLES

Sample	η%
S1	2.24
S2	2.69
S3	2.17
S4	3.14
S5	3.38
S20	2.81
S21	1.90

To compute the quality of the STPV samples the Fill-Factor ($FF\%$) is calculated as discussed in Equation 3.3, Chapter 3, section 3.2.1. Table 4.7 shows the current, voltage, and power at the MPP, along the open and short circuit conditions.

TABLE 4.7: STPV SAMPLES $FF\%$ CALCULATIONS

Sample	I_{MPP} (mA)	V_{MPP} (Volt)	P_{MPP} (mW)	$I_{Sh.c}$ (mA)	$V_{o.c}$ (Volt)	$FF\%$
S1	83.34	6.05	504.21	122.10	10.17	40.60
S2	94.44	6.42	606.30	142.47	9.58	44.42
S3	66.00	7.40	488.40	95.70	9.95	51.29
S4	103.50	6.82	705.87	140.55	10.39	48.34
S5	101.40	7.50	760.50	145.50	9.65	54.16
S20	98.04	6.46	633.34	119.1	9.88	53.82
S21	78.90	5.43	428.43	102.3	7.7	54.39

CHAPTER 5
SIMULATION MODELS ANALYSIS

5. Simulation Models Analysis

This chapter can be divided into two parts. The first part will discuss the overall energy performance, while the second part will discuss the possible impact that such a technology could have on the overall electrical system.

The overall energy assessment will be conducted through a numerical model developed by the EnergyPlus software tool embedded within Designbuilder software. This energy assessment will be carried out on the STPV sample profiles that have been built in Chapter 3 and Chapter 4. In the second part of this chapter, a load flow analysis on a grid level will be carried out employing PowerFactory (DIgSILENT) software.

5.1. Overall Energy Assessment

This part is split into two phases, phase one is going to investigate the impact of the STPV glazing samples on an office setting under different WWRs and compare the outcomes with the reference points DG1 and DG2 outcomes. The best-performing STPV sample is going to be utilised in the second phase.

Phase two of this part will be based on scaling up the office set-up into a whole building. While examining the best-performing STPV sample from phase one under different WWRs.

5.1.1. Glazing Systems Profiles

The thermal, optical, and electrical attributes for the glazing samples through a series of tests have been highlighted in Chapter 3 and Chapter 4. For energy assessment, the thermal characteristics SHGC and U-value, alongside the transmittance ability and the electrical efficiency for the glazing samples are required and listed in Table 5.1.

TABLE 5.1: GLAZING SAMPLES PROFILES

Sample	SHGC	U-value	Transmittance%	Electrical Efficiency (η%)
SG1	89%	6.24	74	N/A
DG1	84%	3.78	69.83	N/A
DG2	78%	2.46	65.26	N/A
S1	32%	4.36	26.24	2.24
S2	17%	4.66	13.14	2.69
S3	28%	2.93	23.20	2.17
S4	21%	4.57	17.11	3.14
S5	17%	3.92	13.55	3.38
S20	28%	4.40	23.25	2.81
S21	28%	4.77	22.45	1.90

To avoid repetition in the energy assessment simulations, S3, which has the highest insulation capability, S1, which has the highest visible light transmittance capability, and S5, which has the

highest electrical efficiency, were selected. DG1 and DG2 were chosen as reference points because double-glazing systems are the most commonly used systems in practice.

5.1.2. Simulation Settings

5.1.2.1. Geographical Profile

It was assumed that the numerical model was built in Sheffield, located in the northeast of England, United Kingdom. According to the Köppen climate classification [105], the climate in this area is typically temperate and classified as an oceanic climate. This means that winters tend to be cold and wet, while summers are warm but still wet. It's important to note that it's highly unlikely for extreme weather conditions such as heatwaves, cold snaps, high winds, or droughts to occur. The EnergyPlus weather data profiles were used as the weather profiles for the simulations in this model.

5.1.2.2. Thermal Simulation Settings

Simulations were conducted to evaluate the thermal performance according to the European Commission Joule projects [106]. The HVAC scheme incorporated is a Fan-coil unit, and the conversion factor is 1.67 for both heating and cooling loads. This factor accounts for any losses that may occur due to the distribution or inefficiency of indoor environment control equipment. The indoor environment control setting for heating was set to 20°C, with a setback point of 12°C. For cooling, the setpoint and setback point were 26°C and 28°C, respectively.

5.1.2.3. Daylight simulation settings

The utilisation of CdTe solar cells within the glazing systems reduces the natural light that enters the indoor environment, leading to an increase in lighting demand. Ensuring an adequate daylight performance in the indoor environment, the numerical model has established a knee point of 500 lux that must be achieved during simulations. This would necessitate a lighting power density of 8 W/m^2.

5.1.3. Office Setup Simulations

A numerical model has been created to simulate an office setting and assess the impact of STPV glazing systems on daylight and thermal demands. The model has a width of 5m, a length of 5m, and a height of 3.5m, while the glazing is integrated into the southern wall. This is based on the assumption that the assessment takes place in the United Kingdom, where the most efficient placement for solar systems is on a southern orientation as seen in Figure 5.1 below.

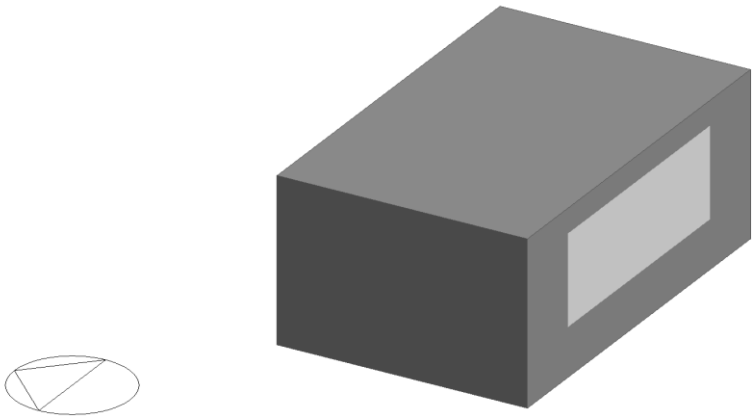

FIGURE 5.1: OFFICE SETTING NUMERICAL MODEL

There are three different frameworks for simulations, each representing a different Window-to-Wall Ratio (WWR) which corresponds to different glazing sizes in practice. If the glazing system covers 30% or less of the wall area, it is classified as small. If it covers more than 40% but less than or equal to 60% of the wall area, it is considered an average-sized glazing. If the glazing covers more than 60% of the wall area, it is categorised as a large glazing system.

5.1.3.1. Small Glazing Systems (WWR=30%)

Figure 5.2 shows the office setting at WWR = 30%, and the glazing sample is integrated into the southern-oriented wall.

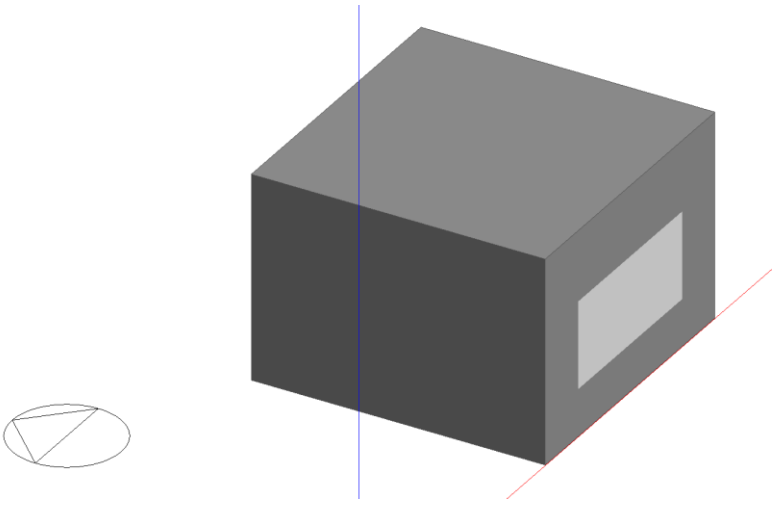

FIGURE 5.2: OFFICE SETTING AT 30% WWR

As for the annual energy assessment results, they are shown in Figure 5.3, Figure 5.4, Figure 5.5, Figure 5.6 and Figure 5.7 which are the outcomes for DG1, DG2, S1, S3 and S5 respectively.

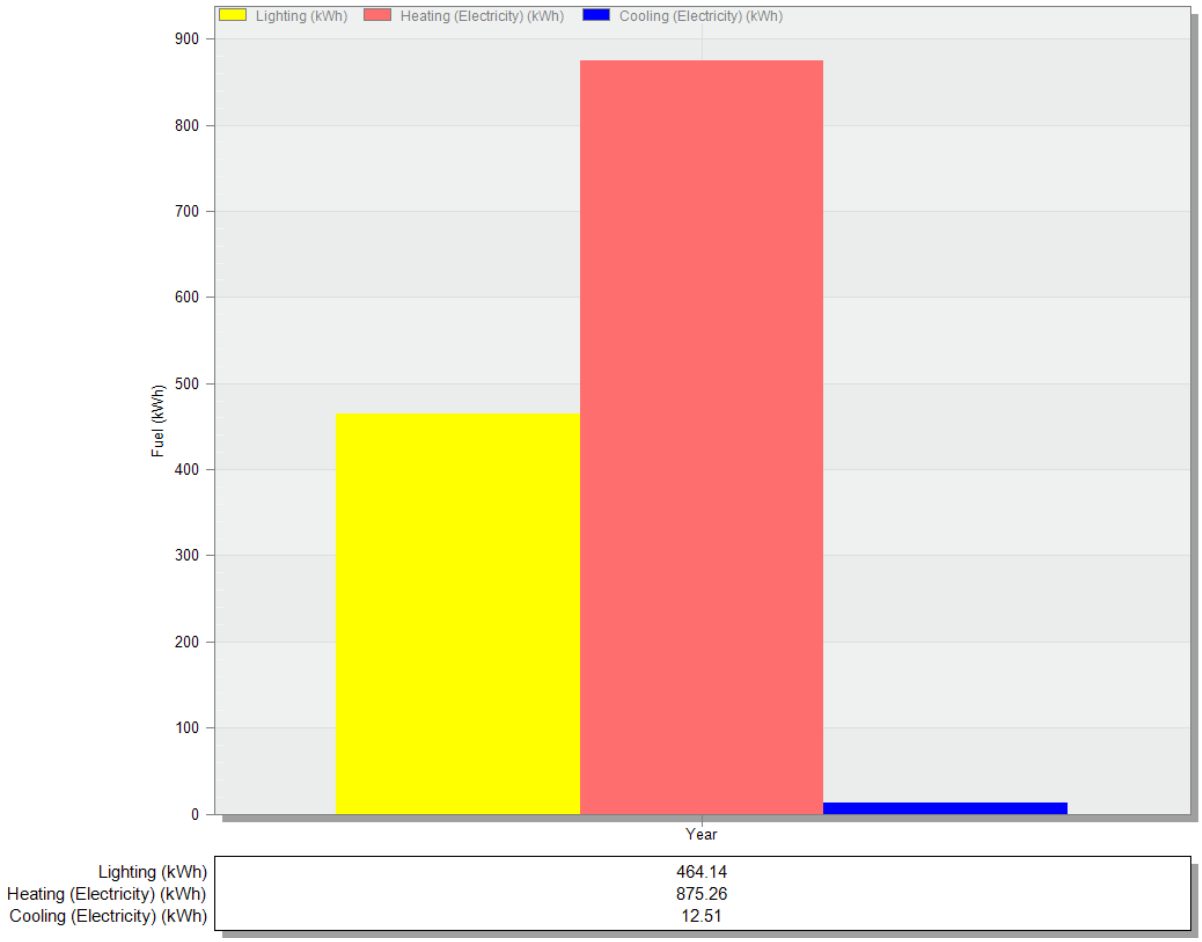

Lighting (kWh)	464.14
Heating (Electricity) (kWh)	875.26
Cooling (Electricity) (kWh)	12.51

FIGURE 5.3: DG1 OUTCOME AT 30% WWR

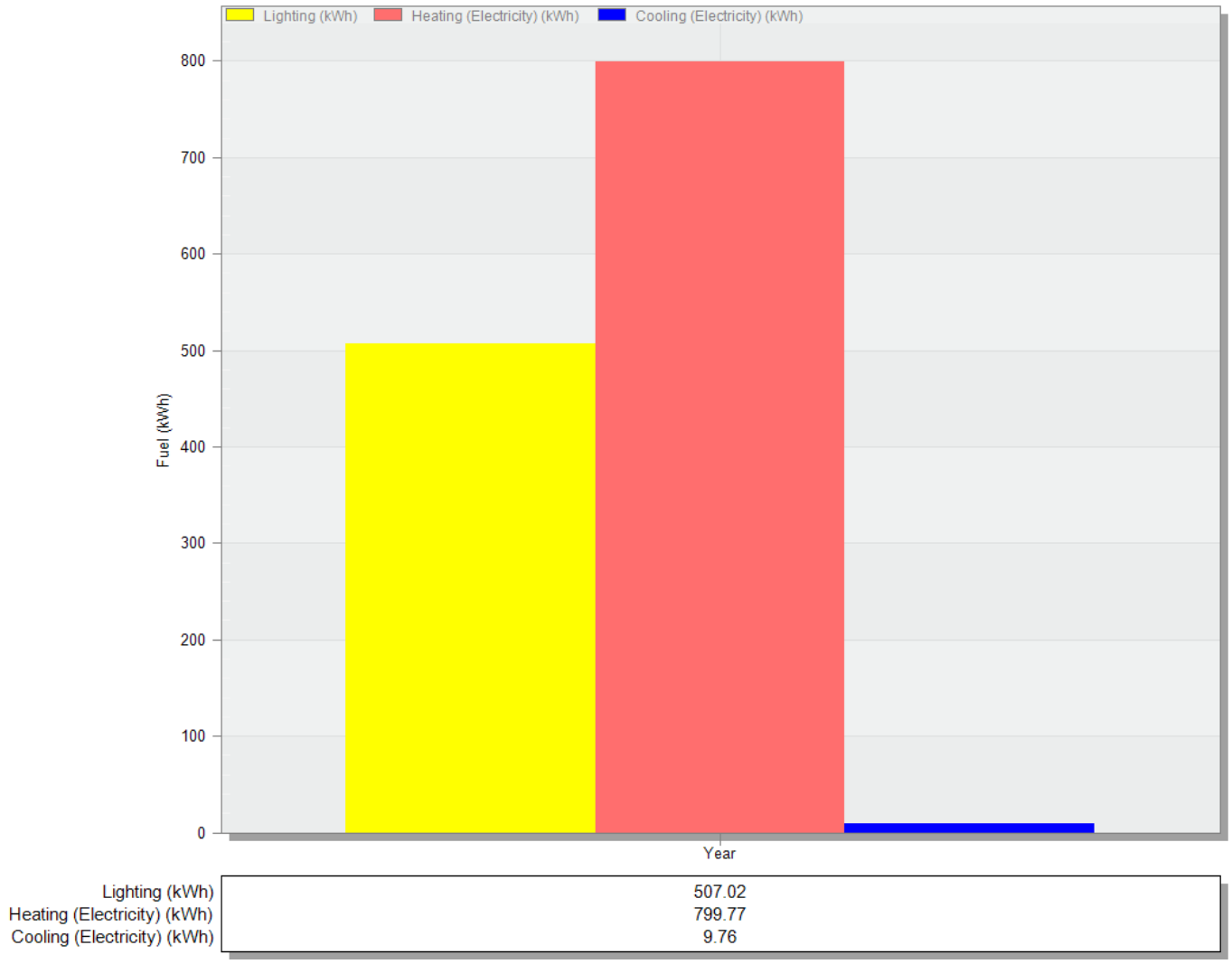

Lighting (kWh)	507.02
Heating (Electricity) (kWh)	799.77
Cooling (Electricity) (kWh)	9.76

FIGURE 5.4: DG2 OUTCOME AT 30% WWR

Lighting (kWh)	719.80
Heating (Electricity) (kWh)	1158.82
Cooling (Electricity) (kWh)	0.76
Generation (Electricity) (kWh)	-70.55

FIGURE 5.5: S1 OUTCOME AT 30% WWR

Lighting (kWh)	766.08
Heating (Electricity) (kWh)	1096.89
Cooling (Electricity) (kWh)	0.18
Generation (Electricity) (kWh)	-69.29

FIGURE 5.6: S3 OUTCOME AT 30% WWR

FIGURE 5.7: S5 OUTCOME AT 30% WWR

The annual energy assessment for the glazing samples at 30% WWR indicates that the overall energy performance for reference points DG1 and DG2 consumes less energy and as a result performance better than the STPV glazing samples S1, S3, and S5 as shown in Table 5.2.

TABLE 5.2: GLAZING SAMPLES OVERALL ENERGY PERFORMANCE AT 30% WWR

Sample	Overall Energy Performance (kWh)
DG1	1351.92
DG2	1316.55
S1	1808.83
S3	1793.86
S5	2028.5

Based on the analysis of the energy consumption, it was found that the STPV S3 sample had the lowest energy consumption with 1793.86 kWh. Following closely was S1 with 1808.83 kWh, and S5

with 2028.5 kWh. These findings suggest that STPV sample S3 is the most energy-efficient among the samples analysed.

Upon analysis, it was determined that meeting the heating demand is the most energy-intensive aspect, irrespective of the type of glazing employed. Notably, the use of STPV samples resulted in a significant increase in heating demand compared to the reference points DG1 and DG2. This is due to the CdTe solar cells restricting the amount of natural light entering the indoor space, thereby reducing passive heating, and resulting in an upsurge in the heating demand.

The utilisation of STPV glazing systems, which incorporate solar cells, leads to a decrease in the transmittance ability of daylight. As a result, the need for daylight increases. Nonetheless, the use of STPV glazing can lead to a significant reduction in cooling needs. It is noteworthy, however, that the United Kingdom's climate profile generally presents a low cooling load.

It's worth noting that the S5 sample produced the highest energy output at 107.09 kWh, followed by S1 at 70.55 kWh and S3 at 69.29 kWh. This is largely attributed to the fenestration used in the STPV samples, which limits the conversion capability to less than 3.40% at its best. Moreover, utilising the STPV samples at 30% WWR results in a reduction of active cells, which ultimately leads to a decrease in the overall energy generated.

5.1.3.2. Averaged-Size Glazing Systems (WWR=60%)

Figure 5.8 shows the office setting at WWR = 60%, and the glazing sample is integrated into the southern-oriented wall.

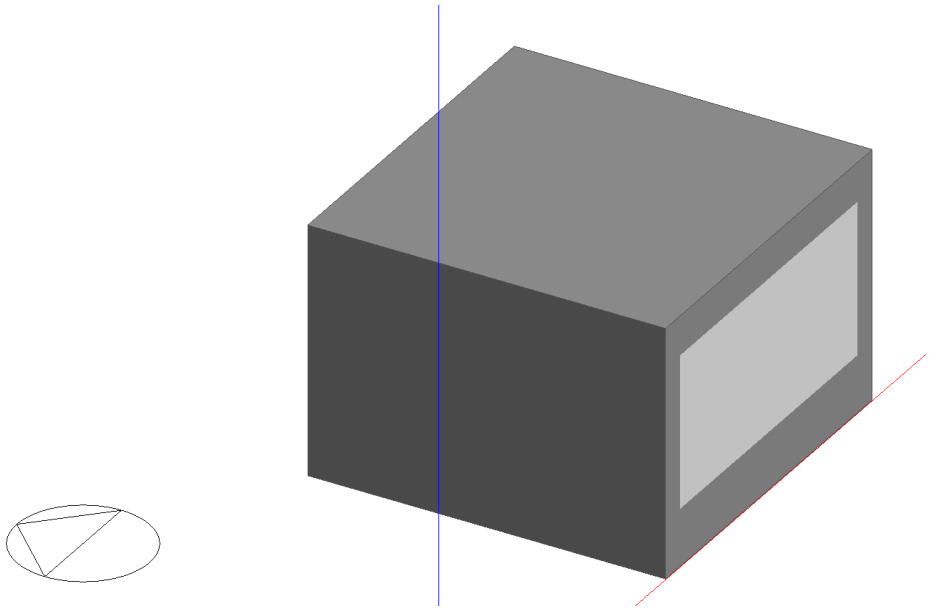

FIGURE 5.8: OFFICE SETTING AT 60% WWR

As for the annual energy assessment results, they are shown in Figure 5.9, Figure 5.10, Figure 5.11, Figure 5.12, and Figure 5.13 which are the outcomes for DG1, DG2, S1, S3 and S5 respectively.

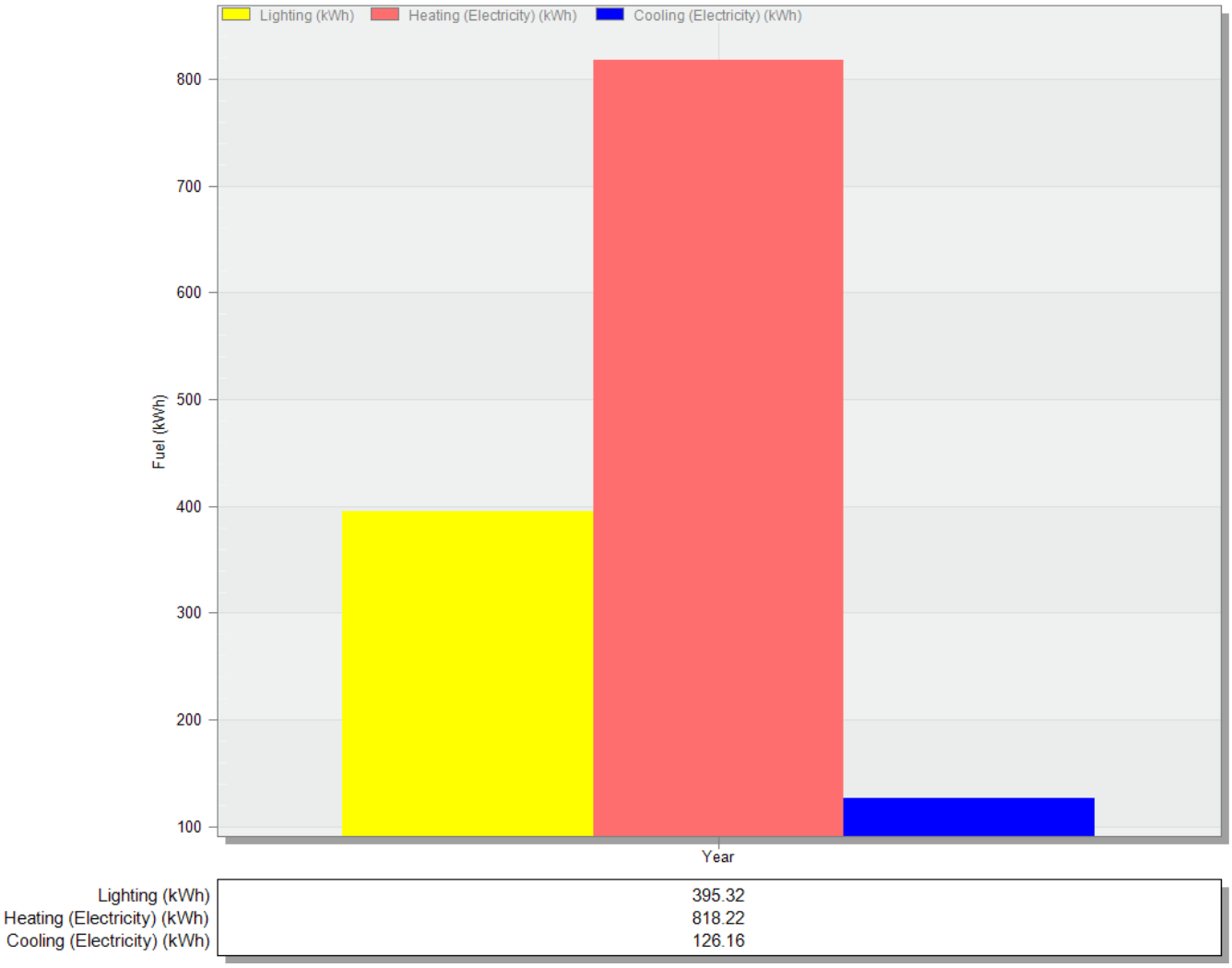

Lighting (kWh)	395.32
Heating (Electricity) (kWh)	818.22
Cooling (Electricity) (kWh)	126.16

FIGURE 5.9: DG1 OUTCOME AT 60% WWR

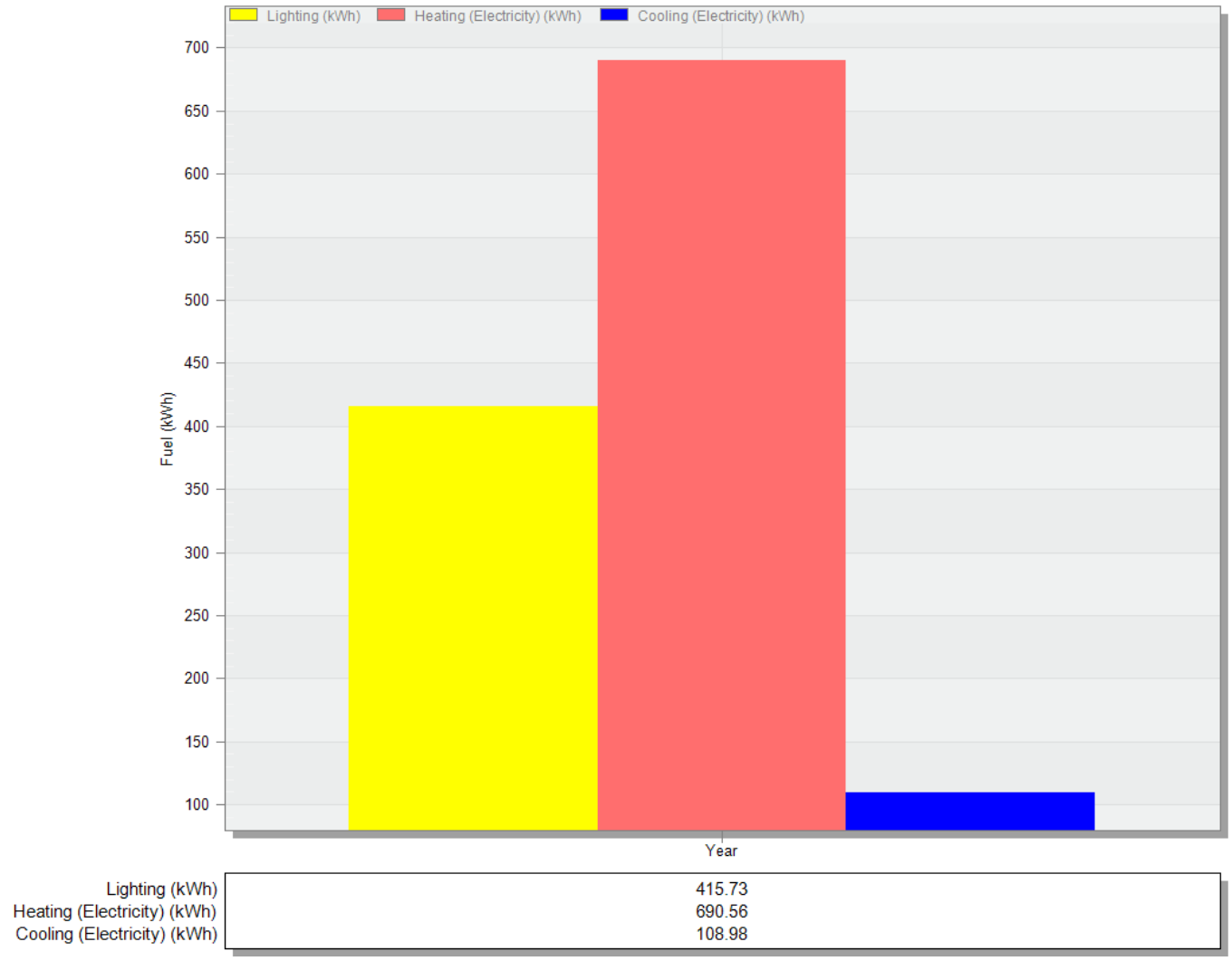

Lighting (kWh)	415.73
Heating (Electricity) (kWh)	690.56
Cooling (Electricity) (kWh)	108.98

FIGURE 5.10: DG2 OUTCOME AT 60% WWR

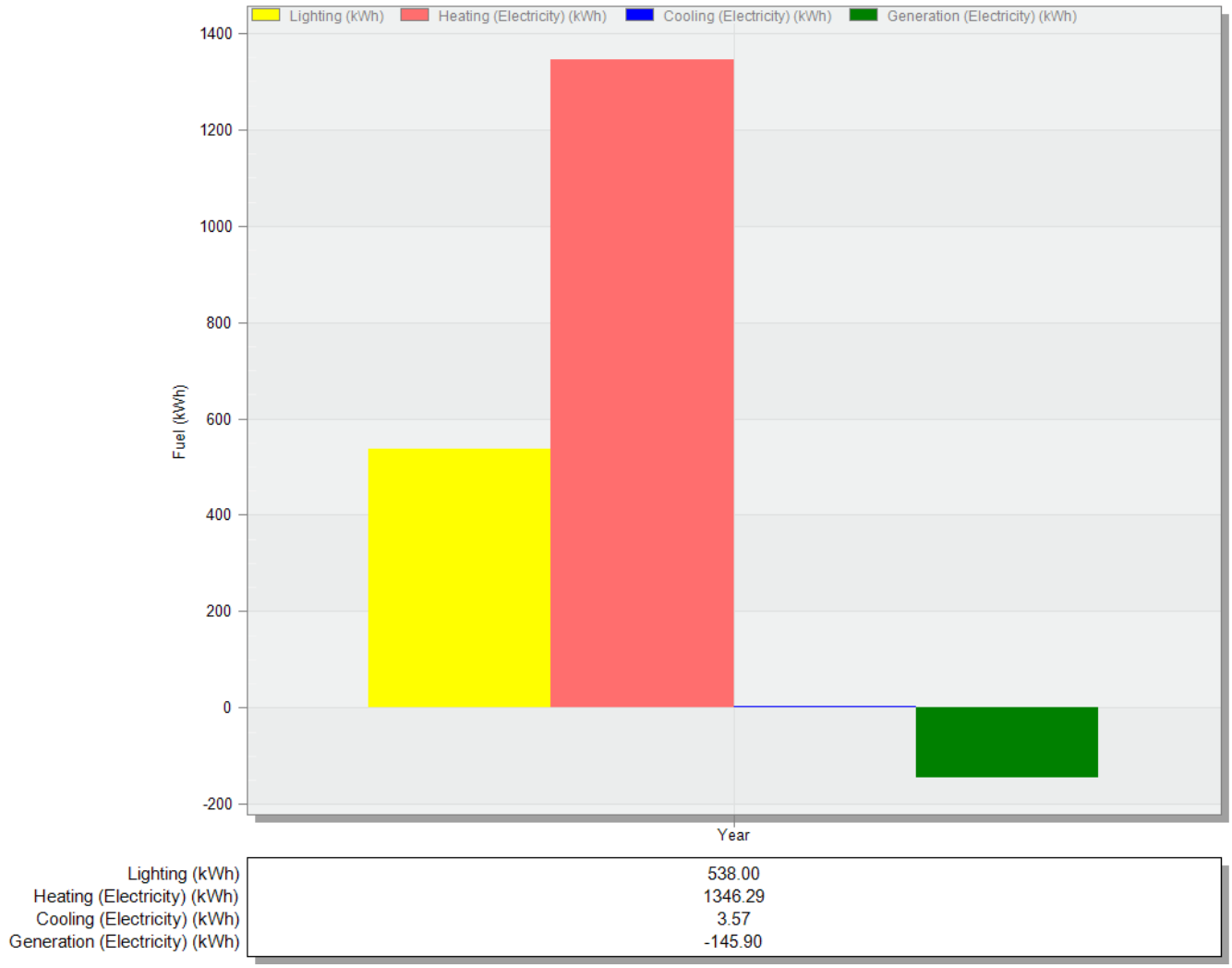

Lighting (kWh)	538.00
Heating (Electricity) (kWh)	1346.29
Cooling (Electricity) (kWh)	3.57
Generation (Electricity) (kWh)	-145.90

FIGURE 5.11: S1 OUTCOME AT 60% WWR

Lighting (kWh)	568.49
Heating (Electricity) (kWh)	1236.97
Cooling (Electricity) (kWh)	0.75
Generation (Electricity) (kWh)	-143.30

FIGURE 5.12: S3 OUTCOME AT 60% WWR

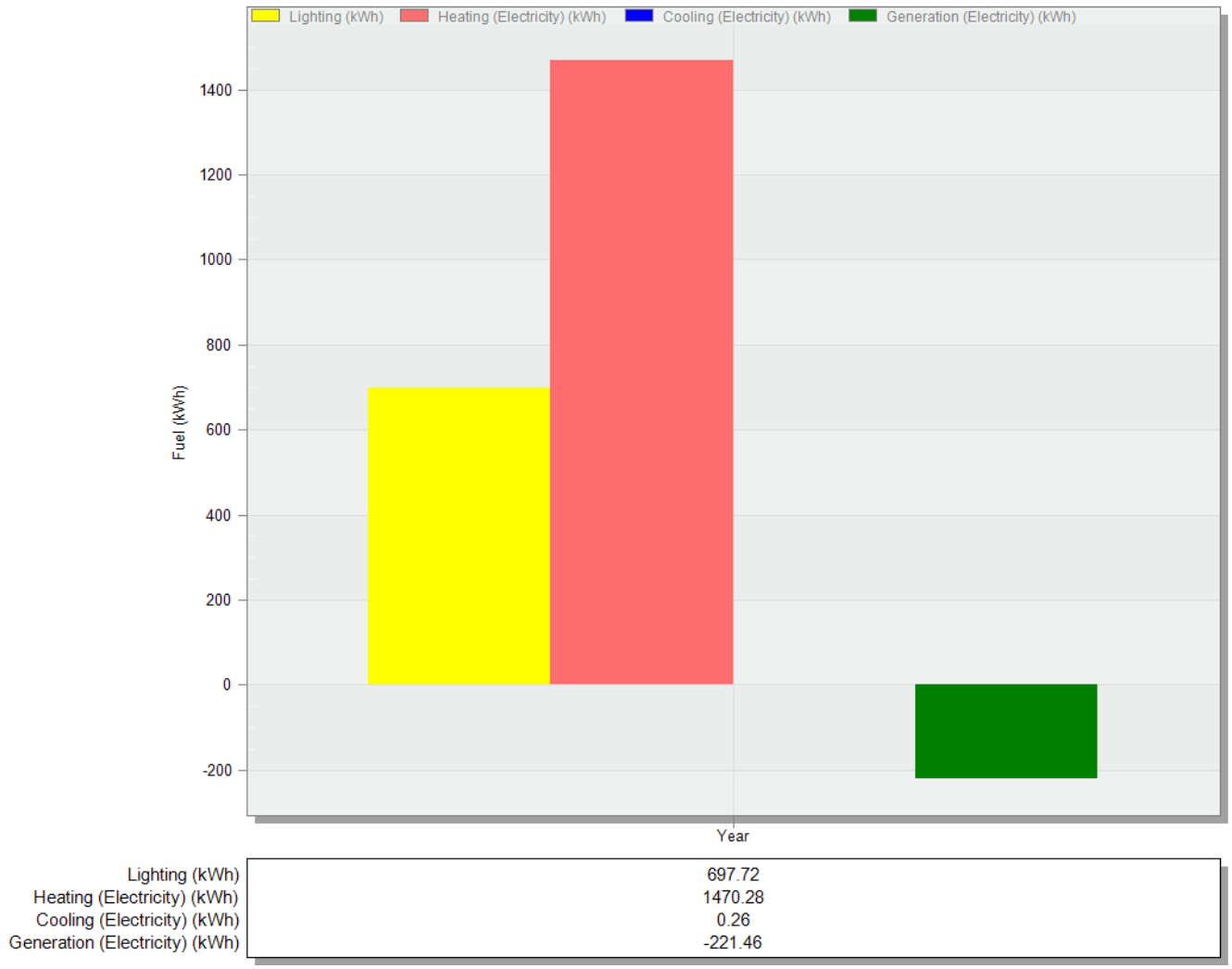

FIGURE 5.13: S5 OUTCOME AT 60% WWR

The annual energy assessment for the glazing samples at 60% WWR indicates that the overall energy performance for reference points DG1 and DG2 consumes less energy and as a result performance better than the STPV glazing samples S1, S3, and S5 as shown in Table 5.3.

TABLE 5.3: GLAZING SAMPLES OVERALL ENERGY PERFORMANCE AT 60% WWR

Sample	Overall Energy Performance (kWh)
DG1	1339.7
DG2	1215.27
S1	1741.96
S3	1662.91
S5	1946.8

Based on the analysis of the energy consumption, it was found that the STPV S3 sample had the lowest energy consumption with 1662.91 kWh. Following closely was S1 with 1741.96 kWh, and S5 with 1946.8 kWh. These findings suggest that STPV sample S3 is the most energy-efficient among the samples analysed.

The results follow the same trends as in the energy assessment in small glazing as the heating demand is the most energy-intensive aspect, irrespective of the type of glazing employed. Notably, the use of STPV samples resulted in a significant increase in heating demand compared to the reference points DG1 and DG2. This is due to the CdTe solar cells restricting the amount of natural light entering the indoor space, thereby reducing passive heating, and resulting in an upsurge in the heating demand.

The utilisation of STPV glazing systems, which incorporate solar cells, leads to a decrease in the transmittance ability of daylight. As a result, the need for daylight increases. Nonetheless, the use of STPV glazing can lead to a significant reduction in cooling needs. It is noteworthy, however, that the United Kingdom's climate profile generally presents a low cooling load.

Simairlly to section 5.1.3.1, S5 sample produced the highest energy output at 221.46 kWh, followed by S1 at 145.9 kWh and S3 at 143.3 kWh. This is largely attributed to the fenestration used in the STPV samples, which limits the conversion capability to less than 3.40% at its best. Additionally, as the STPV samples cover larger areas of the wall, the overall energy consumption decreases. This is due to the increase in active cells increasing overall generated energy.

5.1.3.3. Large Glazing Systems (WWR=100%)

Figure 5.14 shows the office setting at WWR = 100%, and the glazing sample is integrated into the southern-oriented wall.

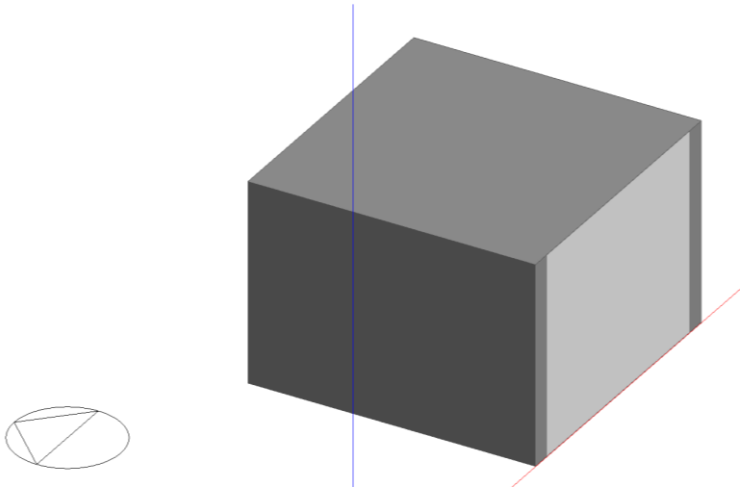

FIGURE 5.14: OFFICE SETTING AT 100% WWR

As for the annual energy assessment results, they are shown in Figure 5.15, Figure 5.16, Figure 5.17, Figure 5.18 and Figure 5.19 which are the outcomes for DG1, DG2, S1, S3 and S5 respectively.

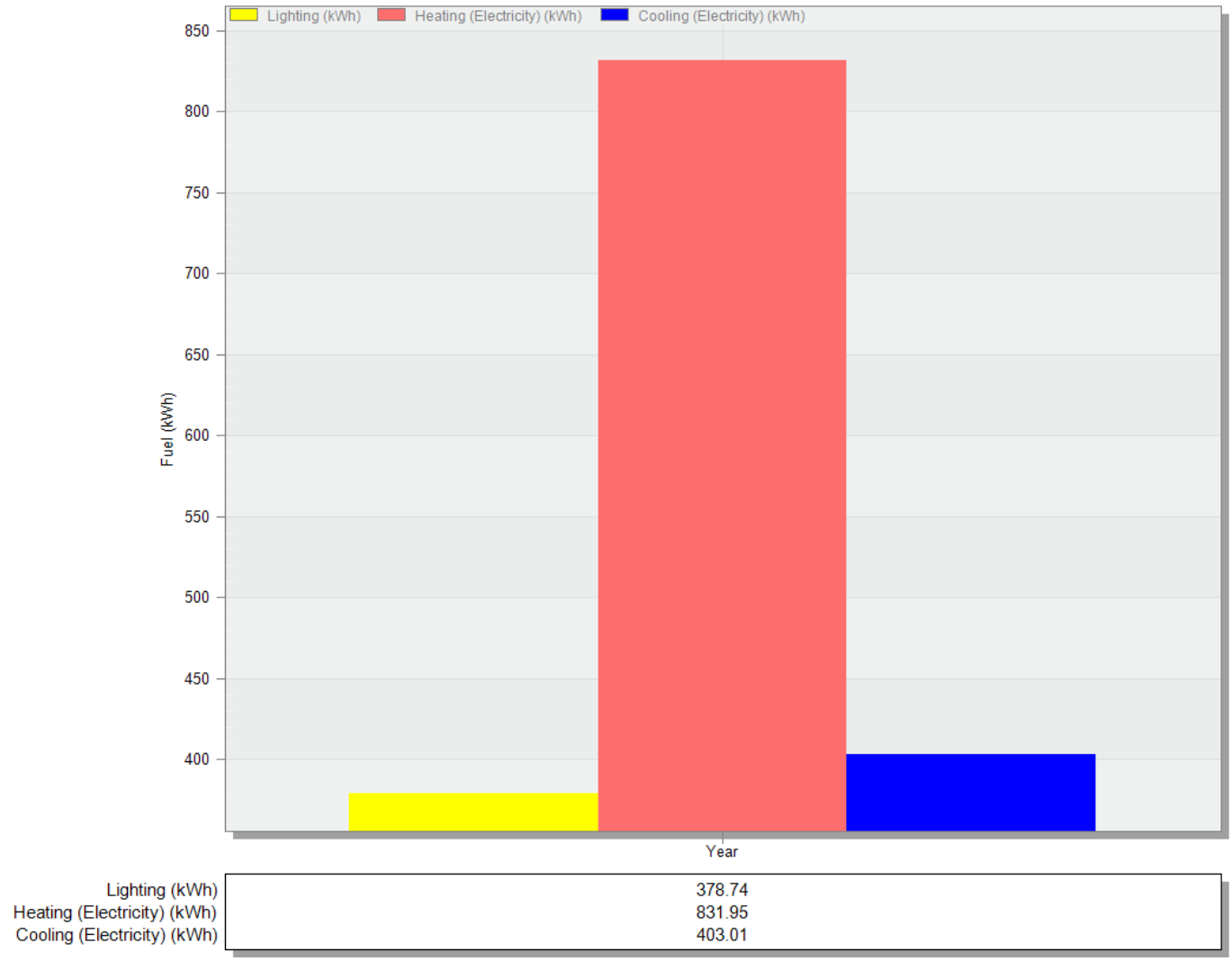

Lighting (kWh)	378.74
Heating (Electricity) (kWh)	831.95
Cooling (Electricity) (kWh)	403.01

FIGURE 5.15: DG1 OUTCOME AT 100% WWR

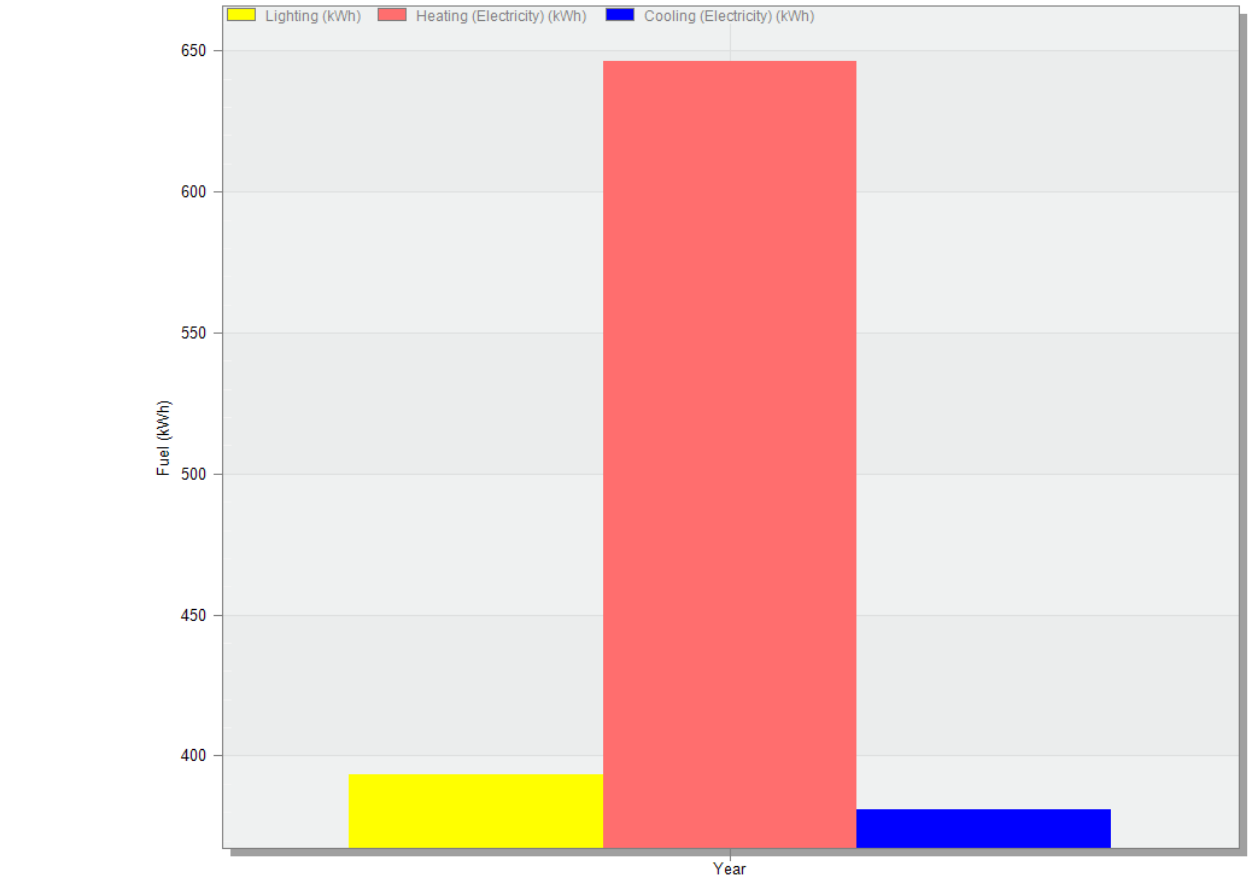

Lighting (kWh)	393.39
Heating (Electricity) (kWh)	646.50
Cooling (Electricity) (kWh)	380.73

FIGURE 5.16: DG2 OUTCOME AT 100% WWR

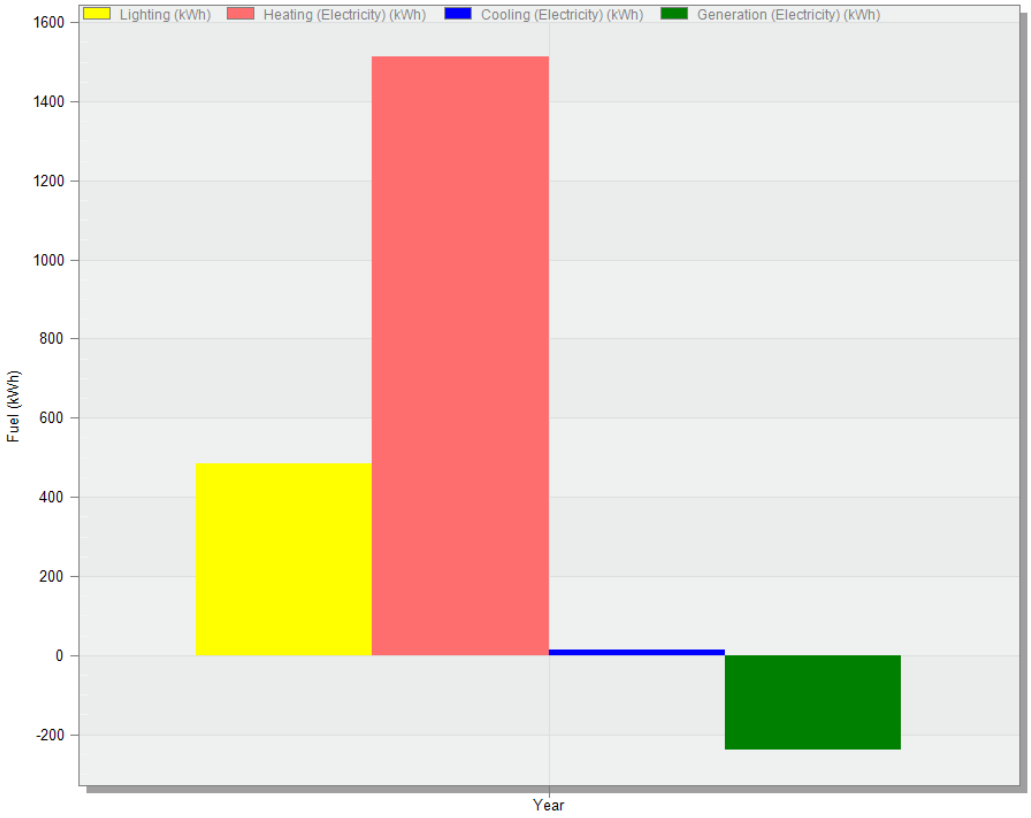

Lighting (kWh)	484.01
Heating (Electricity) (kWh)	1514.02
Cooling (Electricity) (kWh)	14.01
Generation (Electricity) (kWh)	-239.88

FIGURE 5.17: S1 OUTCOME AT 100% WWR

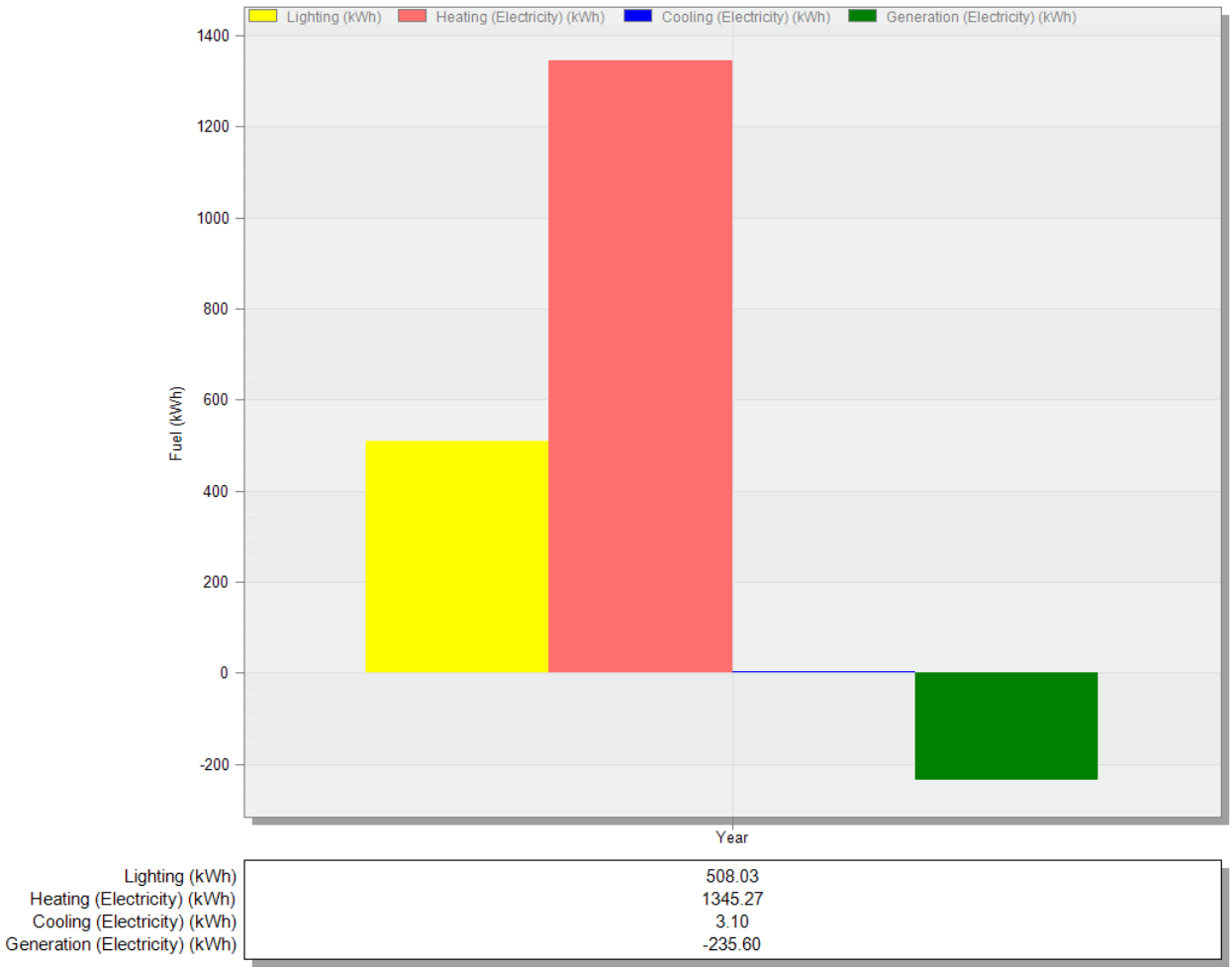

Lighting (kWh)	508.03
Heating (Electricity) (kWh)	1345.27
Cooling (Electricity) (kWh)	3.10
Generation (Electricity) (kWh)	-235.60

FIGURE 5.18: S3 OUTCOME AT 100% WWR

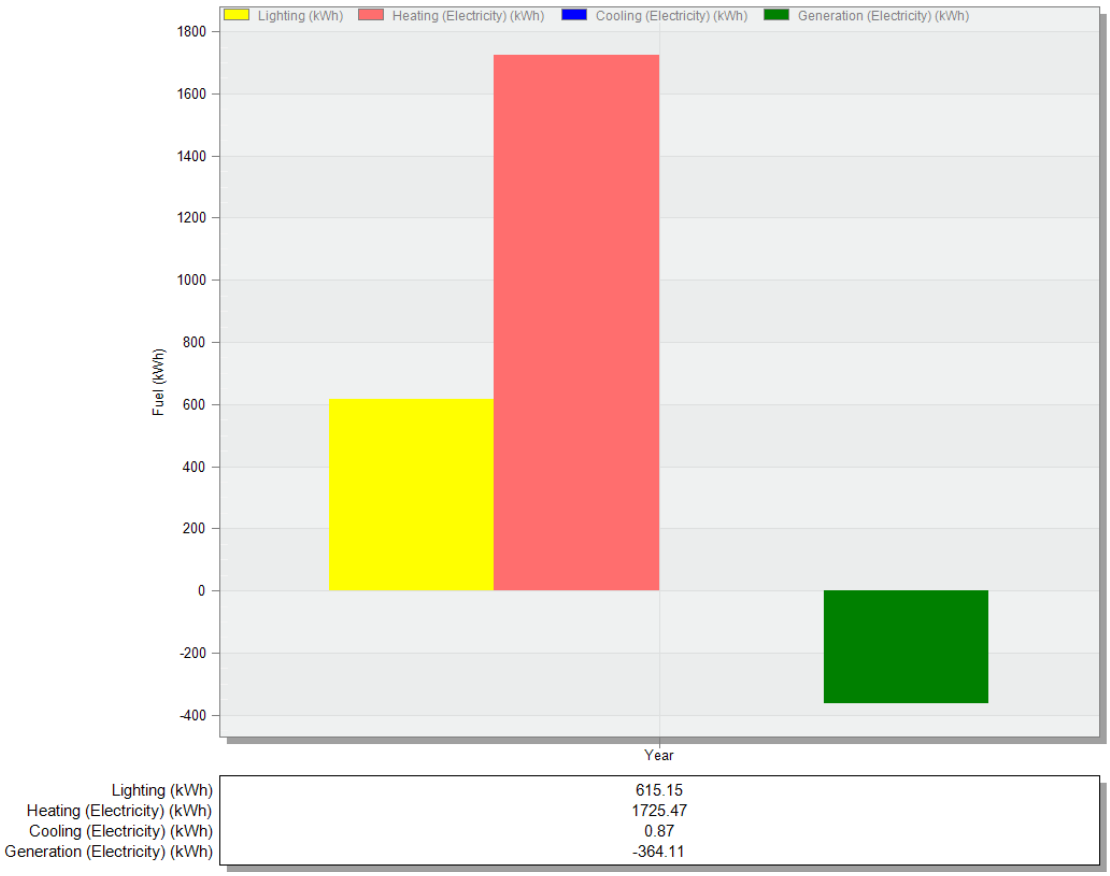

FIGURE 5.19: S5 OUTCOME AT 100% WWR

The annual energy assessment for the glazing samples at 100% WWR indicates that the overall energy performance for reference points DG1 and DG2 consumes less energy and as a result performance better than the STPV glazing samples S1, S3, and S5 as shown in Table 5.4.

TABLE 5.4: GLAZING SAMPLES OVERALL ENERGY PERFORMANCE AT 100% WWR

Sample	Overall Energy Performance (kWh)
DG1	1613.7
DG2	1420.63
S1	1772.17
S3	1620.81
S5	1946.8

Based on the analysis of the energy consumption, it was found that the STPV S3 sample had the lowest energy consumption with 1620.81 kWh. Following closely was S1 with 1772.17 kWh, and S5 with 1977.38 kWh. These findings suggest that STPV sample S3 is the most energy-efficient among the samples analysed.

The results follow the same trends as in the energy assessment in small glazing as the heating demand is the most energy-intensive aspect, irrespective of the type of glazing employed. Notably, the use of STPV samples resulted in a significant increase in heating demand compared to the

reference points DG1 and DG2. This is due to the CdTe solar cells restricting the amount of natural light entering the indoor space, thereby reducing passive heating, and resulting in an upsurge in the heating demand.

The utilisation of STPV glazing systems, which incorporate solar cells, leads to a decrease in the transmittance ability of daylight. As a result, the need for daylight increases. Nonetheless, the use of STPV glazing can lead to a significant reduction in cooling needs. It is noteworthy, however, that the United Kingdom's climate profile generally presents a low cooling load.

As in sections 5.1.3.1 and 5.1.3.2, S5 sample produced the highest energy output at 364.11 kWh, followed by S1 at 239.88 kWh and S3 at 235.6 kWh. This is largely attributed to the fenestration used in the STPV samples, which limits the conversion capability to less than 3.40% at its best. Additionally, as the STPV samples cover larger areas of the wall, the overall energy consumption decreases. This is due to the increase in active cells increasing overall generated energy.

5.1.4. Scaled-up Simulations

As stated in the literature review, most researchers have investigated the impact of integrating STPV glazing systems when utilised in Office settings, to gain a better understanding of the effect that a possible integration of STPV glazing systems would have on the whole building, a numerical model represents a scaled-up building has been developed and will be used to investigate the overall energy performance for the best-performing reference point and STPV sample which are DG2, and S3.

The simulations are going to occur under three different WWRs similar to the section 5.1.3 which are 30% WWR, 60% WWR, and 100% WWR as shown in Figure 5.20.

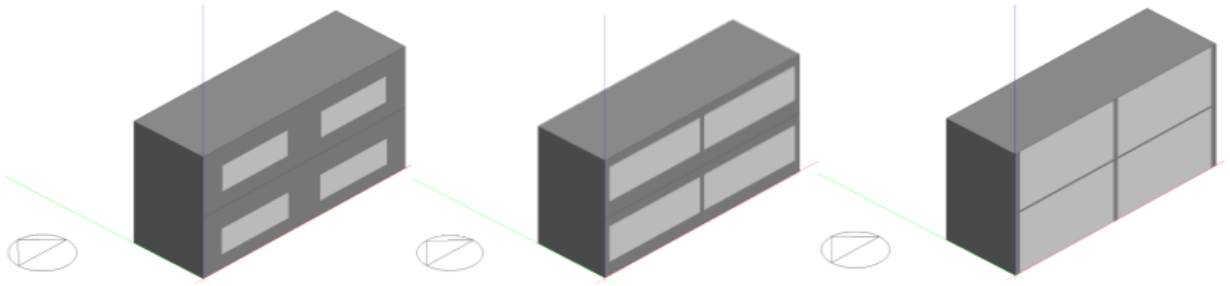

FIGURE 5.20: SCALE-UP MODEL UNDER DIFFERENT WWR, 30%, 60% AND 100%

5.1.4.1. Reference Point (DG2)

The annual energy assessment results for DG2 at different WWRs are shown in Figure 5.21, Figure 5.22 and Figure 5.23.

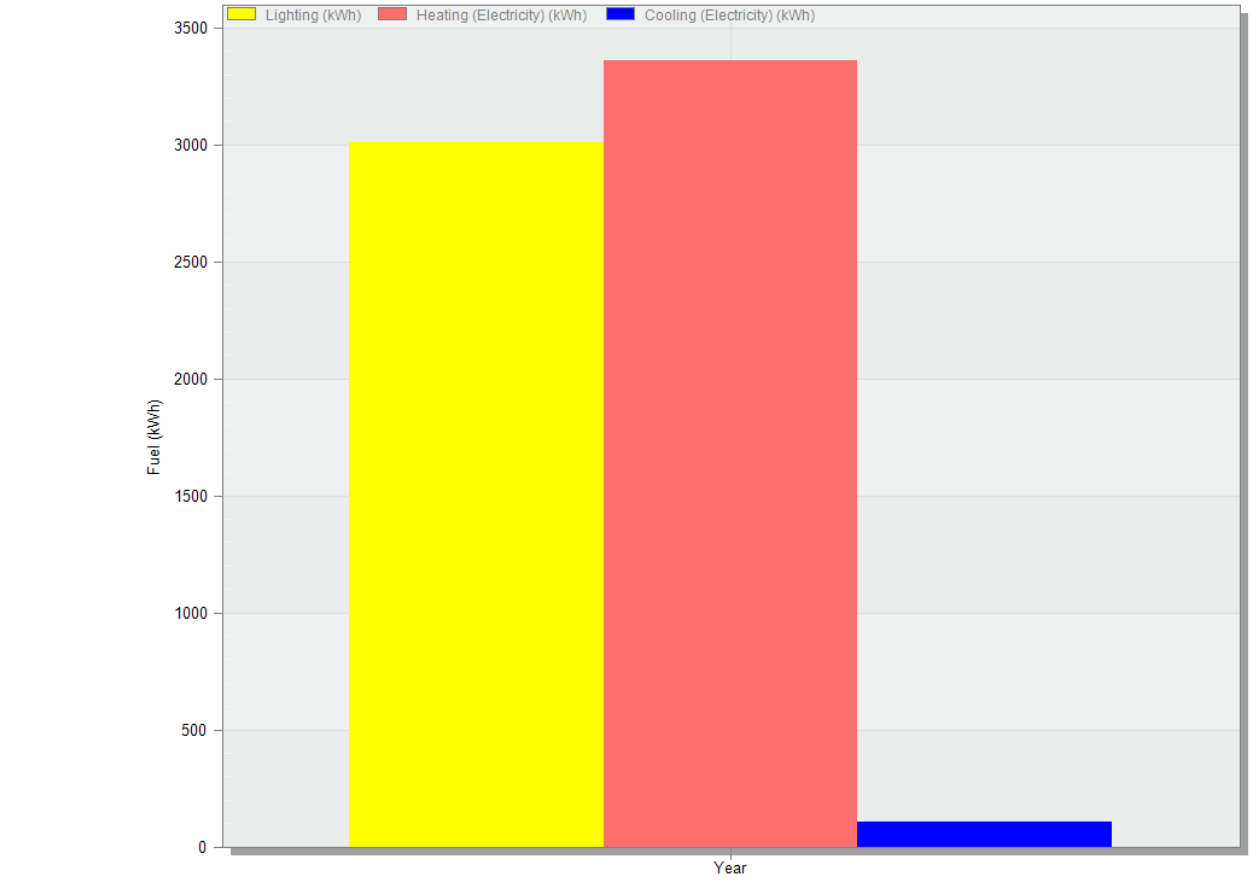

Lighting (kWh)	3011.81
Heating (Electricity) (kWh)	3359.89
Cooling (Electricity) (kWh)	105.64

FIGURE 5.21: DG2 OUTCOMES AT 30% WWR

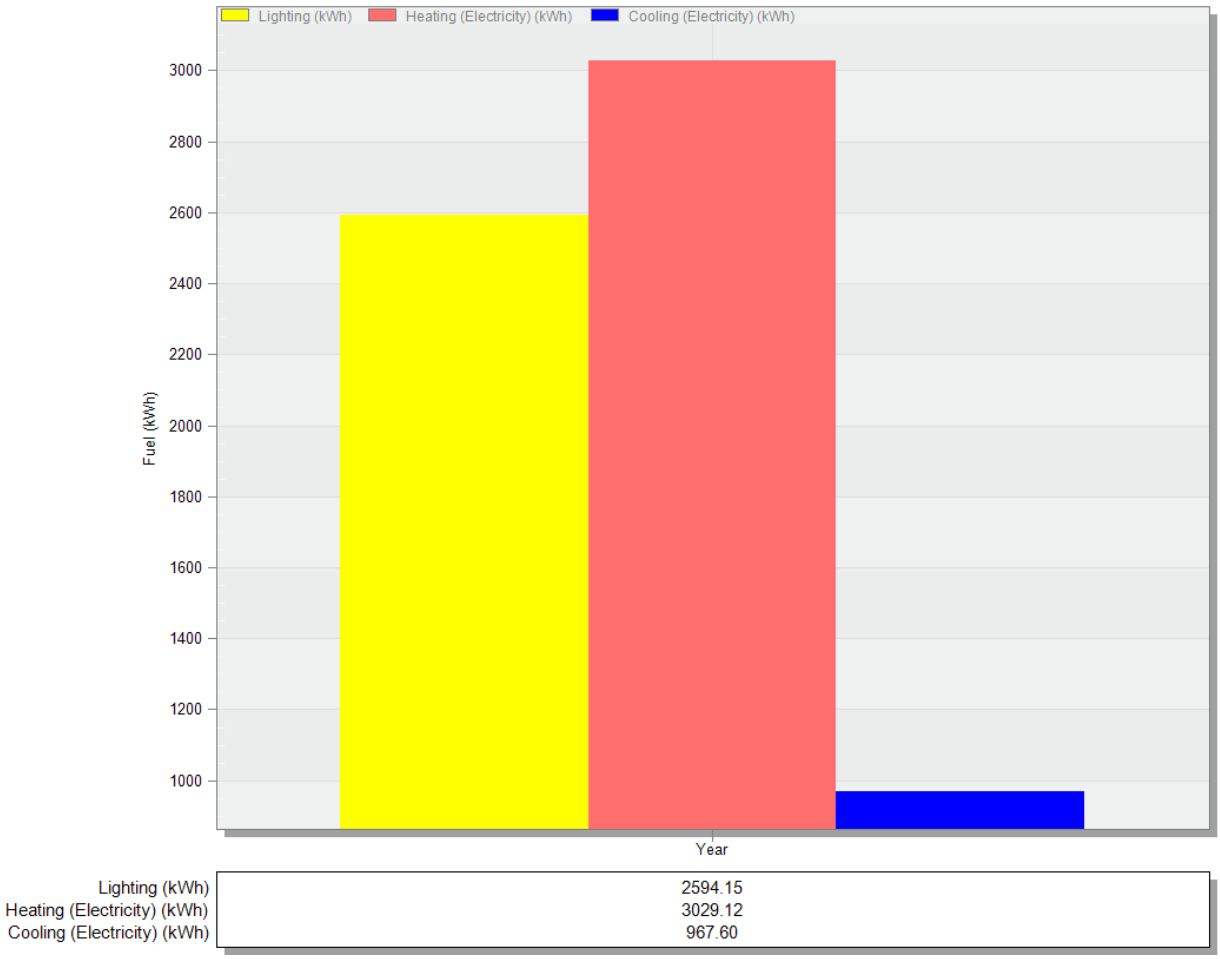

FIGURE 5.22: DG2 OUTCOMES AT 60% WWR

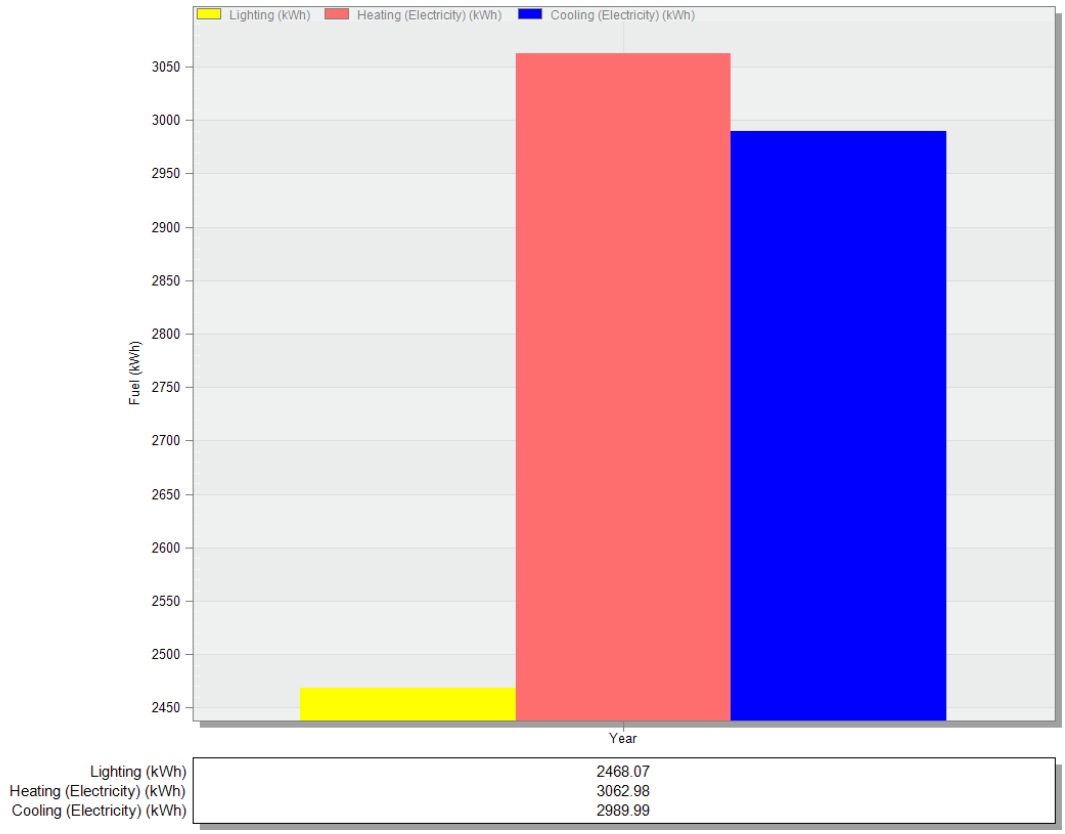

FIGURE 5.23: DG2 OUTCOMES AT 100% WWR

The overall energy consumption levels for DG2 at different WWRs are shown in Table 5.5 below.

TABLE 5.5: OVERALL ENERGY PERFORMANCE FOR DG2

WWR%	Overall Energy (kWh)
30%	6477.34
60%	6590.8
100%	8521.04

5.1.4.2. STPV Sample (S3)

The annual energy assessment results for S3 at different WWRs are shown in Figure 5.21, Figure 5.22, and Figure 5.23.

Lighting (kWh)	4390.15
Heating (Electricity) (kWh)	5218.81
Cooling (Electricity) (kWh)	0.74
Generation (Electricity) (kWh)	-442.87

FIGURE 5.24: S3 OUTCOME AT 30% WWR

Lighting (kWh)	3418.03
Heating (Electricity) (kWh)	6151.94
Cooling (Electricity) (kWh)	5.48
Generation (Electricity) (kWh)	-911.75

FIGURE 5.25: S3 OUTCOME AT 60% WWR

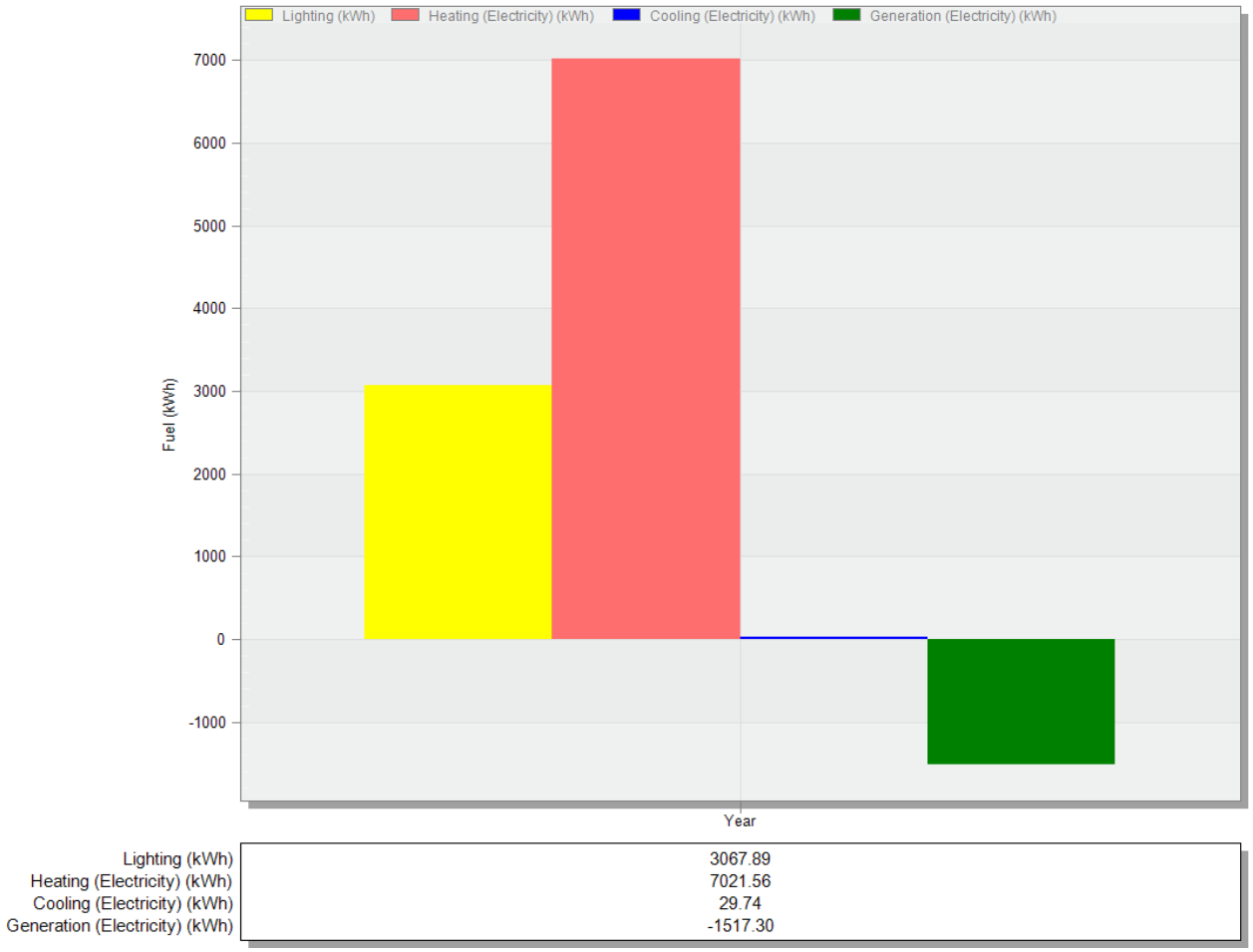

FIGURE 5.26: S3 OUTCOME AT 100% WWR

The overall energy consumption levels for S3 at different WWRs are shown in Table 5.6 below.

TABLE 5.6: OVERALL ENERGY PERFORMANCE FOR S3

WWR%	Overall Energy (kWh)
30%	9163.83
60%	8663.69
100%	8601.9

5.1.4.3. Results Analysis

The results of the scaled-up numerical model follow similar trends to the office setting numerical model. The reference point DG2 glazing outperformed the S3 STPV glazing sample in all simulation cases of studies.

It is important to acknowledge that as the DG2 glazing sample covers more surface area of the wall, the cooling requirements increase. This is due to the greater amount of solar radiation that penetrates the glazing sample, increasing the cooling load. Conversely, the heating and daylight loads decrease as the DG2 sample covers more of the wall.

In relation to the S3 STPV sample, it appears that energy consumption is enhanced when the glazing area is increased. This can be attributed to the fact that a greater glazing area allows for more active solar cells, thereby generating more energy. Another benefit of using STPV glazing systems is that they help to minimise a building's cooling requirements by limiting the amount of solar irradiance that enters the indoor environment via the solar cells.

5.2. Load Flow Analysis

For this part of the research PowerFactory 2023 SP4 version has been used to develop an aggregate dynamic numerical model that integrates the reference point DG2 and S3 STPV glazing samples. This model utilises the Nine-Bus template within the software. The 9-bus system is a network model of an electrical system comprising three big power plants one Hydro-power station (G1) and two Coal power stations (G2 & G3) while 230kV transmission lines are used to connect the system, as shown in Figure 5.27.

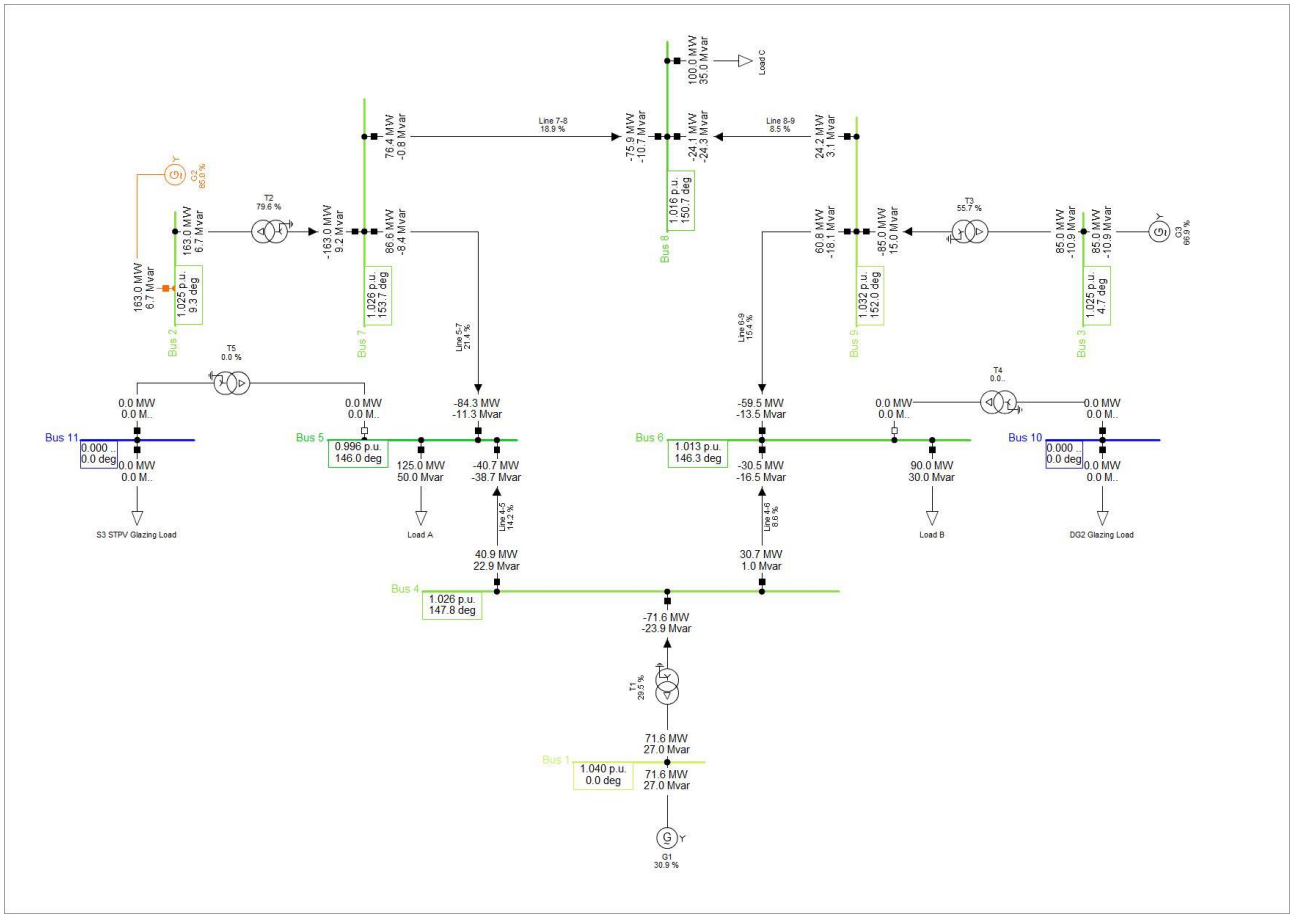

FIGURE 5.27: SINGLE LINE DIAGRAM FOR THE DYNAMIC MODEL

The simulation investigated the impact of the loads resulting by integrating the S3 STPV glazing system, and DG2 reference glazing sample into the grid through Busbars 11 and 10 respectively.

These simulations were carried out when the glazing samples covered 30% WWR, 60% WWR, and 100% WWR as shown in Table 5.7.

TABLE 5.7: THE DG2 AND S3 LOADS (MW) AT DIFFERENT WWR%

WWR%	DG2 (MW)	S3 (MW)
30%	73.94	104.61
60%	75.24	98.9
100%	97.27	98.2

The dynamic model outcomes indicate that the impact of installing the DG2 and S3 loads at different locations in the system are shown in Figure 5.28, Figure 5.29, and Figure 5.30 below.

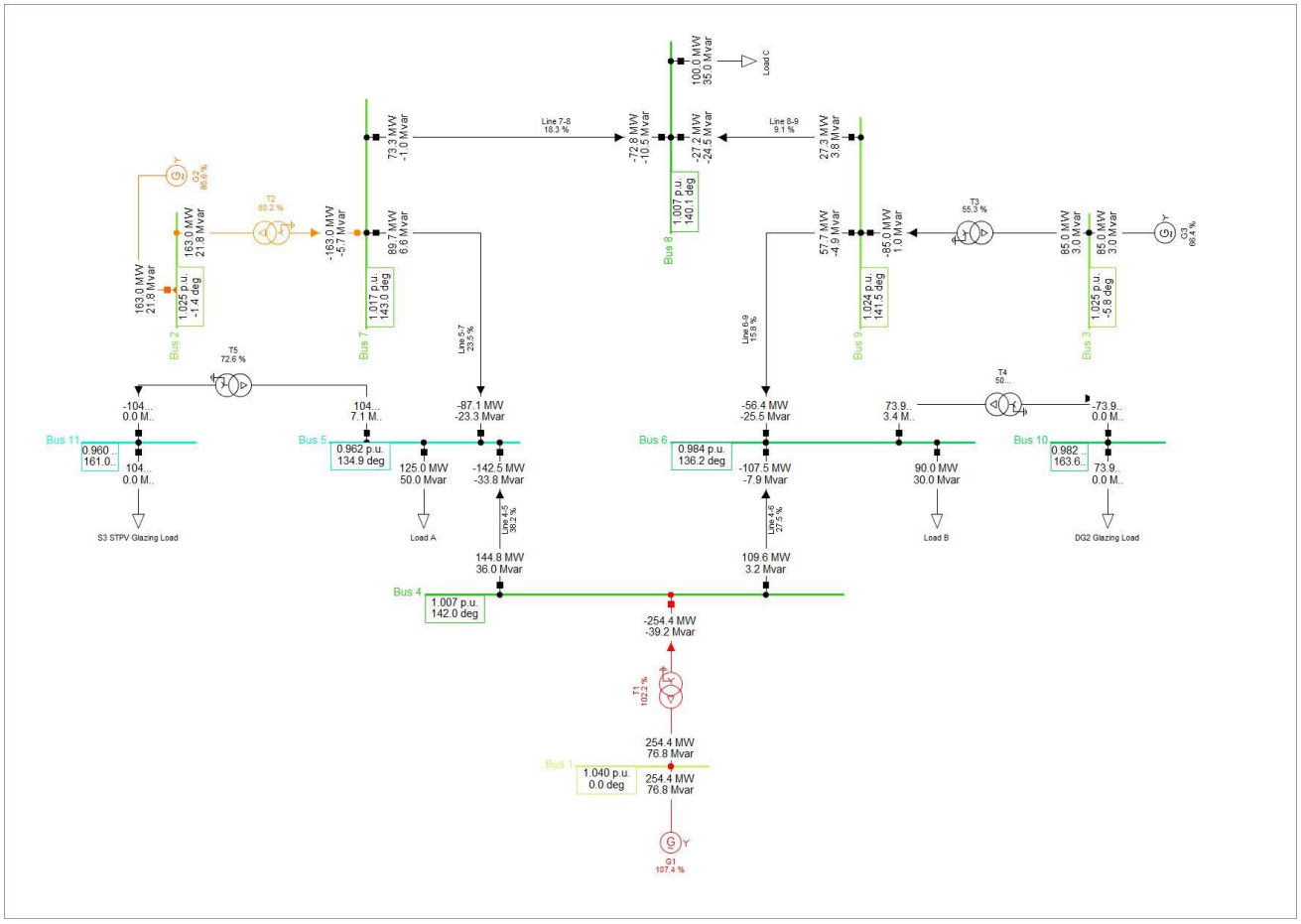

FIGURE 5.28: LOAD FLOW FOR THE LOADS AT 30% WWR

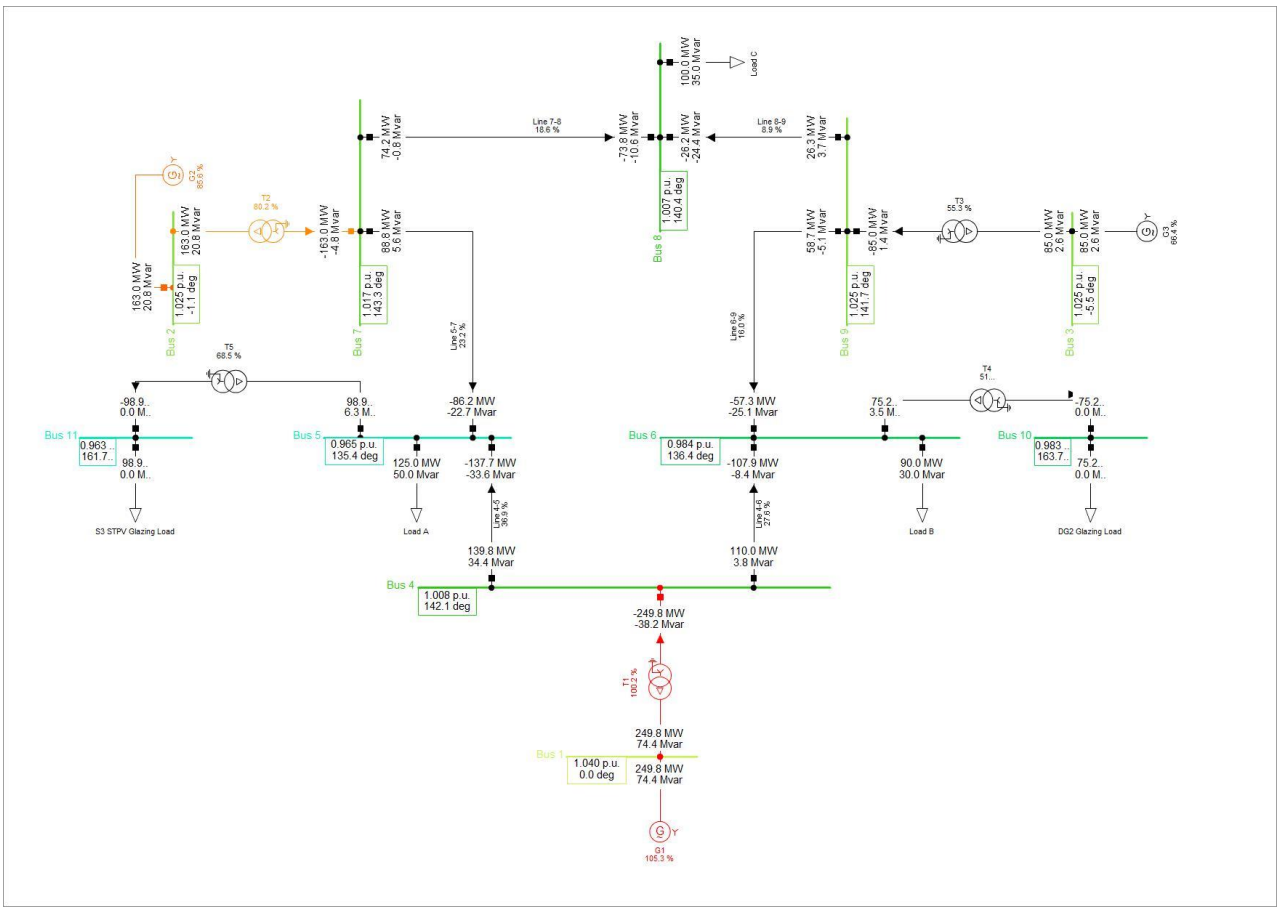

FIGURE 5.29: LOAD FLOW FOR THE LOADS AT 60% WWR

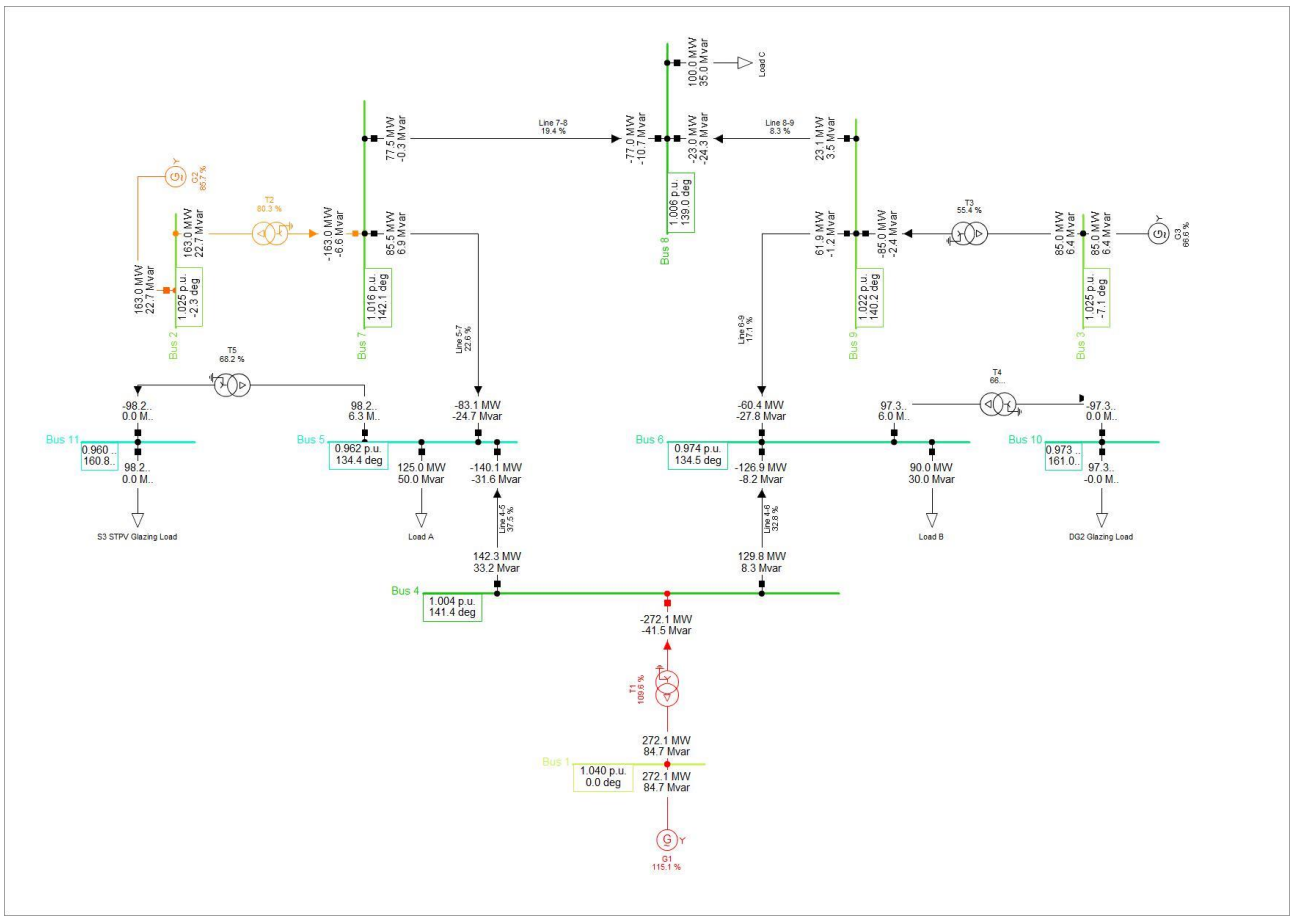

FIGURE 5.30: LOAD FLOW FOR THE LOADS AT 100% WWR

The simulation results indicate that the addition of both loads does not lead to overloading in any of the lines with line 4-5 having the highest loading at all seniors. The highest loading that line 4-5 achieved was 38.2% when the DG2 and S3 were operating at WWR = 30%.

As for the transformers, the T1 tends to overload in all seniors with the highest overloading achieved was 109.5% when DG2 and S3 were operating at WWR = 100%. Furthermore, the hydro-power station (G1) is overloading in each scenario, with the highest loading achieved was 115.1% when DG2 and S3 were operating at WWR = 100%.

CHAPTER 6
CONCLUSION & FURTHER WORK

6. Conclusion and Future Work

In this research, a methodology was presented for assessing the overall energy performance of semi-transparent PV technologies using both experimental and software simulations. This chapter reviews the approaches and most significant results of the research will be presented and concludes with recommendations for potential future research.

6.1. Conclusion

The most important results that this research has attained are listed below:

- This research presented a lab-based approach to characterise and quantify the different glazing sample's optical, thermal, and electrical attributes. The optical characteristics describe the glazing's ability to transmit, absorb, and reflect solar irradiance. The transmittance test results for the reference point glazing systems indicate that SG1 has the highest transmittance ability with 74%, followed by DG1 with 69.83%, followed by DG2 with 65.26%.
- As for the STPV samples, S1 has the highest transmittance ability with 26.24%, followed by S20 with 23.25%, followed by S3 with 23.2%, whereas S2 has the lowest transmittance ability with 13.14%.
- The SHGC results for the reference points indicate that SG1 has the highest SHGC with 89%, followed by DG1 with 84% and then DG2 with 78%.
- The SHGC results for the STPV glazing samples indicate that S1 has the highest SHGC with 32%, followed by S3, S20 and S21 with 28%. Whereas S2 and S5 have recorded the lowest SHGC metric result with 17%.
- As for the U-value results conducted on the reference points, the SG1 sample has the highest U-value of 6.24 W/(m^2.K). DG2 has the lowest U-value by 2.46 W/(m^2.K) ,and DG1 is around 3.78 W/(m^2.K).
- Based on the U-value results of the STPV samples, it is evident that S3 has the highest insulation capability among all the samples, with a U-value of 2.93 W/(m^2.K). Upon analysing the U-value results of the other STPV samples, it was observed that they tend to have insulation capabilities similar to DG1 while having comparable physical attributes to SG1. This suggests that CdTe solar cells in the STPV sample enhance the glazing system's thermal insulation ability.
- S5 has the highest electrical efficiency with 3.38%, while the least electrically efficient is S21, with electrical efficiency of 1.9%.
- The annual energy assessment for the glazing samples at all WWR indicates that the overall energy performance for reference points DG1 and DG2 consumes less energy and, as a result, performance better than the STPV glazing samples S1, S3, and S5.
- The dynamic model outcomes indicate that the impact of installing the DG2 and S3 loads at different locations in the system does not affect the transmission network, where no line is overloaded. Whereas transformer (T1) and generator (G1) are overloaded in each case study.

6.2. Further Work

On the other hand, this research provides opportunities for future work. Potential areas for further exploration include:

- The results of the overall energy assessment indicated that further research is needed regarding the fenestration process for the CdTe STPV glazing samples to produce a more electrically efficient glazing system.
- Further research is needed regarding the overall energy performance of STPV glazing systems utilising solar cells for organic and synthesise materials is needed.
- To obtain more accurate and practical outcomes, it is imperative to undertake a comprehensive cost analysis that incorporates not only the initial capital expenses but also the long-term benefits of reduced operating costs.
- Further research is necessary to improve the wiring and frame structure of STPV glazing systems. Additionally, more investigation is needed to determine the required inverter specifications.
- Further research is needed to investigate the impact of utilising CdTe STPV glazing on the whole electrical system. The results outlined that connecting the CdTe STPV glazing systems would lead to overloading at the main supplier generator and transformers.

References

[1] S. Zhang *et al*, "Scenarios of the energy reduction potential of zero energy building promotion in the Asia-Pacific region to year 2050," *Energy (Oxf.),* vol. 213, pp. 118792, 2020. DOI: 10.1016/j.energy.2020.118792.

[2] J. Peng *et al*, "Study on the overall energy performance of a novel c-Si based semitransparent solar photovoltaic window," *Appl. Energy,* vol. 242, pp. 854-872, 2019. . DOI: 10.1016/j.apenergy.2019.03.107.

[3] Y. Cheng *et al*, "Investigation on the daylight and overall energy performance of semi-transparent photovoltaic facades in cold climatic regions of China," *Appl. Energy,* vol. 232, pp. 517-526, 2018. . DOI: 10.1016/j.apenergy.2018.10.006.

[4] N. Skandalos *et al*, "Overall energy assessment and integration optimization process of semitransparent PV glazing technologies," *Prog Photovoltaics Res Appl,* vol. 26, *(7),* pp. 473-490, 2018. DOI: 10.1002/pip.3008.

[5] J. Peng *et al*, "Numerical investigation of the energy saving potential of a semi-transparent photovoltaic double-skin facade in a cool-summer Mediterranean climate," *Appl. Energy,* vol. 165, pp. 345-356, 2016. . DOI: 10.1016/j.apenergy.2015.12.074.

[6] T. Miyazaki, A. Akisawa and T. Kashiwagi, "Energy savings of office buildings by the use of semi-transparent solar cells for windows," *Renewable Energy,* vol. 30, *(3),* pp. 281-304, 2005. DOI: 10.1016/j.renene.2004.05.010.

[7] A. K. Shukla, K. Sudhakar, and P. Baredar, "Recent advancement in BIPV product technologies: A review," *Energy & Buildings,* vol. 140, pp. 188-195, 2017. DOI: 10.1016/j.enbuild.2017.02.015.

[8] M. Wang *et al*, "Assessment of energy performance of semi-transparent PV insulating glass units using a validated simulation model," *Energy,* vol. 112, pp. 538-548, 2016. DOI: 10.1016/j.energy.2016.06.120.

[9] M. Wang *et al*, "Comparison of energy performance between PV double skin facades and PV insulating glass units," *Appl. Energy,* vol. 194, pp. 148-160, 2017. . DOI: 10.1016/j.apenergy.2017.03.019.

[10] J. Song *et al*, "Power output analysis of transparent thin-film module in building integrated photovoltaic system (BIPV)," *Energy & Buildings,* vol. 40, *(11),* pp. 2067-2075, 2008. DOI: 10.1016/j.enbuild.2008.05.013.

[11] S. Barman *et al*, "Assessment of the efficiency of window integrated CdTe based semi-transparent photovoltaic module," *Sustainable Cities and Society,* vol. 37, pp. 250-262, 2018. DOI: 10.1016/j.scs.2017.09.036.

[12] Y. Sun *et al*, "Integrated semi-transparent cadmium telluride photovoltaic glazing into windows: Energy and daylight performance for different architecture designs," *Appl. Energy,* vol. 231, pp. 972-984, 2018. . DOI: 10.1016/j.apenergy.2018.09.133.

[13] L. Olivieri *et al*, "Energy saving potential of semi-transparent photovoltaic elements for building integration," *Energy,* vol. 76, pp. 572-583, 2014. DOI: 10.1016/j.energy.2014.08.054.

[14] Y. H. Sabry *et al*, "Measurement-Based Modeling of a Semitransparent CdTe Thin-Film PV Module Based on a Custom Neural Network," *IEEE Access,* vol. 6, pp. 34934-34947, 2018. DOI: 10.1109/ACCESS.2018.2848903.

[15] P. W. Wong *et al*, "Semi-transparent PV: Thermal performance, power generation, daylight modelling and energy saving potential in a residential application," *Renewable Energy,* vol. 33, *(5),* pp. 1024-1036, 2008. DOI: 10.1016/j.renene.2007.06.016.

[16] J. Peng *et al*, "Comparative study of the thermal and power performances of a semi-transparent photovoltaic façade under different ventilation modes," *Appl. Energy,* vol. 138, pp. 572-583, 2015. . DOI: 10.1016/j.apenergy.2014.10.003.

[17] E. M. Saber *et al*, "PV (photovoltaics) performance evaluation and simulation-based energy yield prediction for tropical buildings," *Energy,* vol. 71, pp. 588-595, 2014. DOI: 10.1016/j.energy.2014.04.115.

[18] S. Xu *et al*, "Optimal PV cell coverage ratio for semi-transparent photovoltaics on office building façades in central China," *Energy & Buildings,* vol. 77, pp. 130-138, 2014. DOI: 10.1016/j.enbuild.2014.03.052.

[19] S. Roaf, L. Brotas and F. Nicol, "Counting the costs of comfort," *Building Research and Information: The International Journal of Research, Development and Demonstration,* vol. 43, *(3),* pp. 269-273, 2015. DOI: 10.1080/09613218.2014.998948.

[20] A. Eljojo, *Effect of Windows Size, Position and Orientation on the Amount of Energy Needed for Winter Heating and Summer Cooling.* 2017. DOI: 10.13140/RG.2.2.32424.47361.

[21] Siddhartha and Maya Yeshwanth Pai, "Effect of Building Orientation and Window Glazing on the Energy Consumption of HVAC System of an Office Building for Different Climate Zones," *International Journal of Engineering Research & Technology (Ahmedabad),* vol. 4, *(9),* 2015. DOI: 10.17577/IJERTV4IS090754.

[22] A. M. A. Youssef, Z. J. Zhai, and R. M. Reffat, "Design of optimal building envelopes with integrated photovoltaics," *Build. Simul,* vol. 8, *(3),* pp. 353-366, 2015. . DOI: 10.1007/s12273-015-0214-y.

[23] A. Cannavale, U. Ayr, and F. Martellotta, "Energetic and visual comfort implications of using perovskite-based building-integrated photovoltaic glazings," *Energy Procedia,* vol. 126, pp. 636-643, 2017. DOI: 10.1016/j.egypro.2017.08.256.

[24] S. Saridar and H. Elkadi, "The impact of applying recent façade technology on daylighting performance in buildings in eastern Mediterranean," *Build. Environ.,* vol. 37, *(11),* pp. 1205-1212, 2002. . DOI: 10.1016/S0360-1323(01)00095-6.

[25] K. J. Chua and S. K. Chou, "Evaluating the performance of shading devices and glazing types to promote energy efficiency of residential buildings," *Build. Simul,* vol. 3, *(3),* pp. 181-194, 2010. . DOI: 10.1007/s12273-010-0007-2.

[26] O. Aydin, "Conjugate heat transfer analysis of double pane windows," *Build. Environ.,* vol. 41, *(2),* pp. 109-116, 2006. . DOI: 10.1016/j.buildenv.2005.01.011.

[27] B. P. Jelle *et al*, "Fenestration of today and tomorrow: A state-of-the-art review and future research opportunities," *Solar Energy Mater. Solar Cells,* vol. 96, *(1),* pp. 1-28, 2012. DOI: 10.1016/j.solmat.2011.08.010.

[28] T. Chow, C. Li, and Z. Lin, "Innovative solar windows for cooling-demand climate," *Sol Energ Mat Sol C,* vol. 94, *(2),* pp. 212-220, 2010. DOI: 10.1016/j.solmat.2009.09.004.

[29] S. Forughian and M. Taheri Shahr Aiini, "Comparative Study of Single-glazed and Double-glazed Windows in Terms of Energy Efficiency and Economic Expenses," *Tarih Kültür Ve Sanat Araştırmalari Dergisi,* vol. 6, *(3),* pp. 879-893, 2017. DOI: 10.7596/taksad.v6i3.884.

[30] S. Ghoshal and S. Neogi, "Advance Glazing System – Energy Efficiency Approach for Buildings a Review," *Energy Procedia,* vol. 54, pp. 352-358, 2014. DOI: 10.1016/j.egypro.2014.07.278.

[31] A. Ghosh and B. Norton, "Advances in switchable and highly insulating autonomous (self-powered) glazing systems for adaptive low energy buildings," *Renewable Energy,* vol. 126, pp. 1003-1031, 2018. DOI: 10.1016/j.renene.2018.04.038.

[32] K. A. R. Ismail, C. T. Salinas, and J. R. Henriquez, "A comparative study of naturally ventilated and gas filled windows for hot climates," *Energy Conversion and Management,* vol. 50, *(7),* pp. 1691-1703, 2009. DOI: 10.1016/j.enconman.2009.03.026.

[33] K. A. R. Ismail and C. Salinas S., "Non-gray radiative convective conductive modeling of a double glass window with a cavity filled with a mixture of absorbing gases," *Int. J. Heat Mass Transfer,* vol. 49, *(17),* pp. 2972-2983, 2006. DOI: 10.1016/j.ijheatmasstransfer.2006.01.051.

[34] K. A. R. Ismail and J. R. Henríquez, "Two-dimensional model for the double glass naturally ventilated window," *Int. J. Heat Mass Transfer,* vol. 48, *(3),* pp. 461-475, 2005. DOI: 10.1016/j.ijheatmasstransfer.2004.09.022.

[35] M. Arıcı and H. Karabay, "Determination of optimum thickness of double-glazed windows for the climatic regions of Turkey," *Energy Build.,* vol. 42, *(10),* pp. 1773-1778, 2010. DOI: 10.1016/j.enbuild.2010.05.013.

[36] B. Norton *et al*, "Enhancing the performance of building integrated photovoltaics," *Solar Energy,* vol. 85, *(8),* pp. 1629-1664, 2011. DOI: 10.1016/j.solener.2009.10.004.

[37] M. D. Archer and R. (. Hill, *Clean Electricity from Photovoltaics.* 2001.

[38] H. M. Lee *et al*, "Operational power performance of south-facing vertical BIPV window system applied in office building," *Solar Energy,* vol. 145, pp. 66-77, 2017. DOI: 10.1016/j.solener.2016.07.056.

[39] P. Selvaraj *et al*, "Investigation of semi-transparent dye-sensitized solar cells for fenestration integration," *Renewable Energy,* vol. 141, pp. 516-525, 2019. DOI: 10.1016/j.renene.2019.03.146.

[40] J. Bambara and A. K. Athienitis, "Energy and economic analysis for the design of greenhouses with semi-transparent photovoltaic cladding," *Renewable Energy,* vol. 131, pp. 1274-1287, 2019. Available: https://dx.doi.org/10.1016/j.renene.2018.08.020. DOI: 10.1016/j.renene.2018.08.020.

[41] L. Lu and K. M. Law, "Overall energy performance of semi-transparent single-glazed photovoltaic (PV) window for a typical office in Hong Kong," *Renewable Energy,* vol. 49, pp. 250-254, 2013. DOI: 10.1016/j.renene.2012.01.021.

[42] G. Y. Yun, M. McEvoy, and K. Steemers, "Design and overall energy performance of a ventilated photovoltaic façade," *Solar Energy,* vol. 81, *(3),* pp. 383-394, 2007. Available: https://dx.doi.org/10.1016/j.solener.2006.06.016. DOI: 10.1016/j.solener.2006.06.016.

[43] K. H. Refat and R. N. Sajjad, "Prospect of achieving net-zero energy building with semi-transparent photovoltaics: A device to system level perspective," *Applied Energy,* vol. 279, pp. 115790, 2020. Available: https://dx.doi.org/10.1016/j.apenergy.2020.115790. DOI: 10.1016/j.apenergy.2020.115790.

[44] J. Wu *et al*, "Coupled optical-electrical-thermal analysis of a semi-transparent photovoltaic glazing façade under building shadow," *Appl. Energy,* vol. 292, pp. 116884, 2021. . DOI: 10.1016/j.apenergy.2021.116884.

[45] W. Xiong *et al*, "Investigation of the effect of Inter-Building Effect on the performance of semi-transparent PV glazing system," *Energy (Oxf.),* vol. 245, pp. 1, 2022. DOI: 10.1016/j.energy.2022.123160.

[46] T. Saga, "Advances in crystalline silicon solar cell technology for industrial mass production," *NPG Asia Materials,* vol. 2, *(3),* pp. 96-102, 2010. DOI: 10.1038/asiamat.2010.82.

[47] T. Y. Y. Fung and H. Yang, "Study on thermal performance of semi-transparent building-integrated photovoltaic glazings," *Energy & Buildings,* vol. 40, *(3),* pp. 341-350, 2008. DOI: 10.1016/j.enbuild.2007.03.002.

[48] K. E. Park *et al*, "Analysis of thermal and electrical performance of semi-transparent photovoltaic (PV) module," *Energy (Oxf.),* vol. 35, *(6),* pp. 2681-2687, 2010. DOI: 10.1016/j.energy.2009.07.019.

[49] W. Zhang *et al*, "Study of the Application Characteristics of Photovoltaic-Thermoelectric Radiant Windows," *Energies (Basel),* vol. 14, *(20),* pp. 6645, 2021. Available: https://search.proquest.com/docview/2584392392. DOI: 10.3390/en14206645.

[50] A. Karthick, K. Kalidasa Murugavel and L. Kalaivani, "Performance analysis of semitransparent photovoltaic module for skylights," *Energy (Oxford),* vol. 162, pp. 798-812, 2018. Available: https://dx.doi.org/10.1016/j.energy.2018.08.043. DOI: 10.1016/j.energy.2018.08.043.

[51] A. Karthick *et al*, "Investigation of Inorganic Phase Change Material for a Semi-Transparent Photovoltaic (STPV) Module," *Energies (Basel),* vol. 13, *(14),* pp. 3582, 2020. Available: https://search.proquest.com/docview/2423992691. DOI: 10.3390/en13143582.

[52] Y. Cheng *et al*, "Investigation on the daylight and overall energy performance of semi-transparent photovoltaic facades in cold climatic regions of China," *Appl. Energy,* vol. 232, pp. 517-526, 2018. . DOI: 10.1016/j.apenergy.2018.10.006.

[53] J. Peng, L. Lu, and H. Yang, "An experimental study of the thermal performance of a novel photovoltaic double-skin facade in Hong Kong," *Solar Energy,* vol. 97, pp. 293-304, 2013. DOI: 10.1016/j.solener.2013.08.031.

[54] J. Yoon *et al*, "An experimental study on the annual surface temperature characteristics of amorphous silicon BIPV window.(Report)," *Energy & Buildings,* vol. 62, pp. 166, 2013. . DOI: 10.1016/j.enbuild.2013.01.020.

[55] W. He *et al*, "Experimental and numerical investigation on the performance of amorphous silicon photovoltaics window in East China," *Build. Environ.,* vol. 46, *(2),* pp. 363-369, 2011. . DOI: 10.1016/j.buildenv.2010.07.030.

[56] T. Chow, Z. Qiu, and C. Li, "Potential application of “see-through” solar cells in ventilated glazing in Hong Kong," *Solar Energy Mater. Solar Cells,* vol. 93, *(2),* pp. 230-238, 2009. DOI: 10.1016/j.solmat.2008.10.002.

[57] J. Peng *et al*, "Developing a method and simulation model for evaluating the overall energy performance of a ventilated semi-transparent photovoltaic double-skin facade. (Report)," *Prog Photovoltaics Res Appl,* vol. 24, *(6),* pp. 781, 2016. DOI: 10.1002/pip.2727.

[58] E. Leite Didoné and A. Wagner, "Semi-transparent PV windows: A study for office buildings in Brazil," *Energy & Buildings,* vol. 67, pp. 136-142, 2013. DOI: 10.1016/j.enbuild.2013.08.002.

[59] W. Zhang *et al*, "Comparison of the overall energy performance of semi-transparent photovoltaic windows and common energy-efficient windows in Hong Kong," *Energy Build.,* vol. 128, pp. 511-518, 2016. DOI: 10.1016/j.enbuild.2016.07.016.

[60] F. Chen *et al*, "Solar heat gain coefficient measurement of semi-transparent photovoltaic modules with indoor calorimetric hot box and solar simulator," *Energy Build.,* vol. 53, pp. 74-84, 2012. DOI: 10.1016/j.enbuild.2012.06.005.

[61] E. Cuce, C. Young and S. B. Riffat, "Thermal performance investigation of heat insulation solar glass: A comparative experimental study," *Energy Build.,* vol. 86, pp. 595-600, 2015. DOI: 10.1016/j.enbuild.2014.10.063.

[62] J. Peng *et al*, "Validation of the Sandia model with indoor and outdoor measurements for semi-transparent amorphous silicon PV modules," *Renewable Energy,* vol. 80, pp. 316-323, 2015. DOI: 10.1016/j.renene.2015.02.017.

[63] Y. T. Chae *et al*, "Building energy performance evaluation of building integrated photovoltaic (BIPV) window with semi-transparent solar cells," *Applied Energy,* vol. 129, pp. 217-227, 2014. Available: https://dx.doi.org/10.1016/j.apenergy.2014.04.106. DOI: 10.1016/j.apenergy.2014.04.106.

[64] W. Wang *et al*, "Experimental Assessment of the Energy Performance of a Double-Skin Semi-Transparent PV Window in the Hot-Summer and Cold-Winter Zone of China," *Energies (Basel),* vol. 11, *(7),* pp. 1700, 2018. Available: https://search.proquest.com/docview/2108514504. DOI: 10.3390/en11071700.

[65] H. Tian *et al*, "Thermal Comfort Evaluation of Rooms Installed with STPV Windows," *Energies (Basel),* vol. 12, *(5),* pp. 808, 2019. Available: https://search.proquest.com/docview/2316650955. DOI: 10.3390/en12050808.

[66] H. Tian *et al*, "Study on Lighting -Heating-Electricity Coupled Energy Saving Potential for STPV Window in Southwest China," *IOP Conference Series. Materials Science and Engineering,* vol. 556, *(1),* pp. 12008, 2019. Available: https://iopscience.iop.org/article/10.1088/1757-899X/556/1/012008. DOI: 10.1088/1757-899X/556/1/012008.

[67] H. Tian *et al*, "Study on the Energy Saving Potential for Semi-Transparent PV Window in Southwest China," *Energies (Basel),* vol. 11, *(11),* pp. 3239, 2018. Available: https://search.proquest.com/docview/2316359291. DOI: 10.3390/en11113239.

[68] Y. Cheng *et al*, "An optimal and comparison study on daylight and overall energy performance of double-glazed photovoltaics windows in cold region of China," *Energy (Oxford),* vol. 170, pp. 356-

366, 2019. Available: https://dx.doi.org/10.1016/j.energy.2018.12.097. DOI: 10.1016/j.energy.2018.12.097.

[69] N. Skandalos and D. Karamanis, "Investigation of thermal performance of semi-transparent PV technologies," *Energy and Buildings,* vol. 124, pp. 19-34, 2016. Available: https://dx.doi.org/10.1016/j.enbuild.2016.04.072. DOI: 10.1016/j.enbuild.2016.04.072.

[70] K. Kapsis and A. K. Athienitis, "A study of the potential benefits of semi-transparent photovoltaics in commercial buildings," *Solar Energy,* vol. 115, pp. 120-132, 2015. DOI: 10.1016/j.solener.2015.02.016.

[71] T. Hwang, S. Kang, and J. T. Kim, "Optimization of the building integrated photovoltaic system in office buildings—Focus on the orientation, inclined angle, and installed area," *Energy and Buildings,* vol. 46, pp. 92-104, 2012. Available: https://dx.doi.org/10.1016/j.enbuild.2011.10.041. DOI: 10.1016/j.enbuild.2011.10.041.

[72] A. Mesloub *et al*, "Performance Analysis of Photovoltaic Integrated Shading Devices (PVSDs) and Semi-Transparent Photovoltaic (STPV) Devices Retrofitted to a Prototype Office Building in a Hot Desert Climate," *Sustainability (Basel, Switzerland),* vol. 12, *(23),* pp. 10145, 2020. DOI: 10.3390/su122310145.

[73] Y. Zhu *et al*, "An analysis of cadmium telluride and amorphous silicon PV cells," in 2022. DOI: 10.1109/CGEE55282.2022.9976880.

[74] H. Alrashidi *et al*, "Thermal performance of semitransparent CdTe BIPV window at temperate climate," *Solar Energy,* vol. 195, pp. 536-543, 2020. DOI: 10.1016/j.solener.2019.11.084.

[75] Y. Sun *et al*, "Analysis of the daylight performance of window integrated photovoltaics systems," *Renewable Energy,* vol. 145, pp. 153-163, 2020. DOI: 10.1016/j.renene.2019.05.061.

[76] Y. Sun *et al*, "Integrated CdTe PV glazing into windows: energy and daylight performance for different window-to-wall ratio," *Energy Procedia,* vol. 158, pp. 3014-3019, 2019. DOI: 10.1016/j.egypro.2019.01.976.

[77] D. Liu *et al*, "Comprehensive evaluation of window-integrated semi-transparent PV for building daylight performance," *Renewable Energy,* vol. 145, pp. 1399-1411, 2020. DOI: 10.1016/j.renene.2019.04.167.

[78] D. Liu *et al*, "Evaluation of the colour properties of CdTe PV windows," *Energy Procedia,* vol. 158, pp. 3088-3093, 2019. DOI: 10.1016/j.egypro.2019.01.1000.

[79] S. Preet *et al*, "Analytical model of semi-transparent photovoltaic double-skin façade system (STPV-DSF) for natural and forced ventilation modes," *The International Journal of Ventilation,* pp. 1-30, 2021. DOI: 10.1080/14733315.2021.1971873.

[80] A. Ghosh *et al*, "Visual Comfort Analysis of Semi-Transparent Perovskite Based Building Integrated Photovoltaic Window for Hot Desert Climate (Riyadh, Saudi Arabia)," *Energies (Basel),* vol. 14, *(4),* pp. 1043, 2021. Available: https://doaj.org/article/74f8ed0fbfd347a48224c14dd23145c0. DOI: 10.3390/en14041043.

[81] N. Skandalos and D. Karamanis, "PV glazing technologies," *Renewable & Sustainable Energy Reviews,* vol. 49, pp. 306-322, 2015. DOI: 10.1016/j.rser.2015.04.145.

[82] S. A. Afghan, H. Almusawi and H. Geza, "Simulating the electrical characteristics of a photovoltaic cell based on a single-diode equivalent circuit model," *MATEC Web of Conferences,* vol. 126, pp. 3002, 2017. Available: https://search.proquest.com/docview/2039336858. DOI: 10.1051/matecconf/201712603002.

[83] M. H. El-Ahmar, A. M. El-Sayed and A. M. Hemeida, "Mathematical modeling of photovoltaic module and evalute the effect of varoius paramenters on its performance," in Dec 2016, Available: https://ieeexplore.ieee.org/document/7836976. DOI: 10.1109/MEPCON.2016.7836976.

[84] N. Asim *et al*, "A review on the role of materials science in solar cells," *Renewable & Sustainable Energy Reviews,* vol. 16, *(8),* pp. 5834-5847, 2012. DOI: 10.1016/j.rser.2012.06.004.

[85] W. Shockley, "The behavior of holes and electrons in semiconductors," in 1950. DOI: 10.1109/CEI.1950.7513613.

[86] A. M. Aly *et al*, "Design of microgrid with flywheel energy storage system using HOMER software for case study," in Feb 2019, Available: https://ieeexplore.ieee.org/document/8646441. DOI: 10.1109/ITCE.2019.8646441.

[87] J. A. Gow and C. D. Manning, "Development of a model for photovoltaic arrays suitable for use in simulation studies of solar energy conversion systems," in 1996, DOI: 10.1049/cp:19960890.

[88] W. De Soto, S. A. Klein, and W. A. Beckman, "Improvement and validation of a model for photovoltaic array performance," *Solar Energy,* vol. 80, *(1),* pp. 78-88, 2006. DOI: 10.1016/j.solener.2005.06.010.

[89] S. Lu *et al*, "Modified calculation of solar heat gain coefficient in glazing façade buildings," *Energy Procedia,* vol. 122, pp. 151-156, 2017. DOI: 10.1016/j.egypro.2017.07.335.

[90] R. McCluney and F. S. E. Center, "Fenestration solar gain analysis," 1996.

[91] T. J. Kim *et al*, "Development and evaluation of a measurement method and system for solar heat gain coefficient and thermal transmittance," vol. 19, *(sup5),* pp. S5-964-964, 2015. Available: https://www.tandfonline.com/doi/abs/10.1179/1432891714Z.0000000001230. DOI: 10.1179/1432891714Z.0000000001230.

[92] American Society of Heating, Refrigerating and Air-Conditioning Engineers and Ashrae, *2013 ASHRAE Handbook: Fundamentals.* 2013Available: https://books.google.co.uk/books?id=b6rYnAEACAAJ.

[93] M. Tamm *et al*, "Development of a Reduced Order Model of Solar Heat Gains Prediction," vol. 13, *(23),* pp. 6316, 2020. Available: https://search.proquest.com/docview/2467260197. DOI: 10.3390/en13236316.

[94] J. S. Carlos and H. Corvacho, "Evaluation of the performance indices of a ventilated double window through experimental and analytical procedures: SHGC-values," vol. 86, pp. 886-897, 2015. Available: https://dx.doi.org/10.1016/j.enbuild.2014.11.002. DOI: 10.1016/j.enbuild.2014.11.002.

[95] The British Standards Institution, "BS ISO 9869-1:2014: Thermal insulation. Building elements. 7IIn-situ7R measurement of thermal resistance and thermal transmittance: Heat flow meter method," 2014.

[96] The British Standards Institution, "BS ISO 19916-3:2021: Glass in building. Vacuum insulating glass: Test methods for evaluation of performance under temperature differences," 2022.

[97] The British Standards Institution, "BS ISO 19916-1:2018: Glass in building. Vacuum insulating glass: Basic specification of products and evaluation methods for thermal and sound insulating performance," 2018.

[98] The British Standards Institution, "BS EN ISO 52022-3:2017: Energy performance of buildings. Thermal, solar and daylight properties of building components and elements: Detailed calculation method of the solar and daylight characteristics for solar protection devices combined with glazing," 2017.

[99] Y. Fang *et al*, "Experimental validation of a numerical model for heat transfer in vacuum glazing," vol. 80, *(5),* pp. 564-577, 2006. DOI: 10.1016/j.solener.2005.04.002.

[100] P. Robinson and J. Littler, "Advanced glazing: Outdoor test room measurements, performance prediction and building thermal simulation," *Build.Environ.,* vol. 28, *(2),* pp. 145-152, 1993. Available: https://www.sciencedirect.com/science/article/pii/0360132393900488. DOI: 10.1016/0360-1323(93)90048-8.

[101] T. T. Chow *et al*, "A Comparative Study of PV Glazing Performance in Warm Climate," vol. 18, *(1),* pp. 32-40, 2009. DOI: 10.1177/1420326X08100323.

[102] D. P. Grimmer, R. D. McFarland, and J. D. Balcomb, "Initial experimental tests on the use of small passive-solar test-boxes to model the thermal performance of passively solar-heated building designs," vol. 22, *(4),* pp. 351-354, 1979. Available: https://www.sciencedirect.com/science/article/pii/0038092X79901889. DOI: 10.1016/0038-092X(79)90188-9.

[103] P. Wouters *et al*, "The use of outdoor test cells for thermal and solar building research within the PASSYS project," *Build.Environ.,* vol. 28, *(2),* pp. 107-113, 1993. Available: https://www.sciencedirect.com/science/article/pii/0360132393900444. DOI: 10.1016/0360-1323(93)90044-4.

[104] M. R. Collins and S. J. Harrison, "The effects of calorimeter tilt on the inward-flowing fraction of absorbed solar radiation in a venetian blind," in 2001, .

[105] M. C. Peel, B. L. Finlayson, and T. A. McMahon, "Updated world map of the Köppen-Geiger climate classification," vol. 11, *(5),* pp. 1633-1644, 2007. DOI: 10.5194/hess-11-1633-2007.

[106] D. Van Dijk and W. J. Platzer, "Reference office for thermal, solar and lighting calculations," vol. 27, 2001.